Final Report

Assessment of Structural Degradation for Bridges and Culverts

Sponsoring Agencies:

South Carolina Department of Transportation

Federal Highway Administration

Principal Investigators:

Dr. Paul Ziehl
Professor, Civil and Environmental Engineering
University of South Carolina

Dr. Tommy Cousins
Professor, Civil Engineering
Clemson University

Dr. Brandon Ross
Associate Professor, Civil Engineering
Clemson University

Dr. Nathan Huynh
Professor, Civil and Environmental Engineering
University of South Carolina

June 2020

Technical Report Documentation Page

1. Report No FHWA-SC-20-03	2. Government Accession No.	3. Recipient's Catalog No.
4. Title and Subtitle *Assessment of Structural Degradation for Bridges and Culverts*		5. Report Date *June 2020* 6. Performing Organization Code
7. Author/s *Drs. Paul Ziehl, Tommy Cousins, Brandon Ross, and Nathan Huynh*		8. Performing Organization Report No.
9. Performing Organization Name and Address *University of South Carolina* *Dept. of Civil and Environmental Engineering* *300 Main Street, Columbia, SC 29208*		10. Work Unit No. (TRAIS) 11. Contract or Grant No. SPR No. 739
12. Sponsoring Organization Name and Address South Carolina Department of Transportation Office of Materials and Research 1406 Shop Road Columbia, SC 29201		13. Type of Report and Period Covered *Final Report* 14. Sponsoring Agency Code

15. Supplementary Notes

16. Abstract

Degradation of bridge components is an ongoing challenge facing the South Carolina Department of Transportation (SCDOT). This report addresses current and evolving technologies to assist with condition assessment of bridges and culverts while increasing worker safety. Technologies investigated include aerial drones, robotic crawlers, and jetyaks. In addition to demonstration and field evaluation of these technologies, live load testing of two bridges was carried out. This approach provided insight into joint efficiency. Acoustic emission data was investigated and found to be a potentially promising technique for shear regions and for long term assessment under ambient loading conditions. Benefit cost analysis indicated that the widespread adoption of aerial drones could significantly benefit the SCDOT for bridge inspections, particularly if SCDOT personnel were trained to operate the devices. It is recommended that aerial drones be implemented immediately and utilized in parallel with visual and tactile inspection of bridges.

17. Key Words	18. Distribution Statement		
Bridge inspection; robotics; aerial drones; live load testing; acoustic emission; autonomy	No restrictions. This document is available to the public through the National Technical Information Service, Springfield, VA 22161.		
19. Security Classification (of this report) Unclassified	20. Security Classification (of this page) Unclassified	21. No. Of Pages *137*	22. Price *$252.00*

Form DOT F 1700.7 (8-72) Reproduction of form and completed page is authorized

Disclaimer

The contents of this report reflect the views of the authors who are responsible for the facts and the accuracy of the data presented herein. The contents do not necessarily reflect the official views or policies of the South Carolina Department of Transportation or the Federal Highway Administration. This report does not constitute a standard, specification, or regulation.

The State of South Carolina and the United States Government do not endorse products or manufacturers. Trade or manufacturer's names appear herein solely because they are considered essential to the object of this report.

Acknowledgments

The authors wish to acknowledge the Steering Committee, particularly the timely and helpful input of Rodrick Tucker (Chair) and Mark Hunter, and all members: William Russell Aikens, Tsemin 'Billy' Chao, and Blake Gerken (FHWA), as well as Merrill Zwanka, Terry Swygert, Meredith Heaps, and Judy Hundley.

We would also like to acknowledge the support of Will Munnerlyn who was instrumental to the demonstration and field evaluation portions of the project, and Russell Inglett and Robert Moore and the technical staff at the University of South Carolina Structures and Materials Laboratory.

This report and others would not be possible without the continuous effort and input of the postdoctoral fellows, graduate research assistants and undergraduate researchers who work diligently on all aspects of the effort including laboratory, numerical, and field investigations in addition to drafting of the report and providing useful comments on the research approach. In alphabetical order these include Li Ai (PhD candidate), Rafal Anay (while at U. South Carolina as a PhD candidate), Mahmoud Bayat (Postdoctoral Fellow), David Bianco (MS graduate), and Vafa Soltangharaei (PhD candidate).

Executive Summary

Degradation of bridge components is an ongoing challenge facing the South Carolina Department of Transportation (SCDOT). Both visual and tactile inspection of bridges across South Carolina has yielded reasonable results. However, current inspection approaches require considerable time to access the more remote locations of bridges and in some cases require traffic control to be completed in a safe manner. In addition to these considerations, many maintenance activities will need to be conducted by a reduced workforce in the future. Therefore, efficient evaluation methods will become increasingly critical.

A wide variety of robotic techniques are available to save money and time while potentially increasing worker safety. These include aerial drones, crawlers, and other means for condition assessment of bridges and culverts, and jetyaks or similar means for assessment of scour. Selecting the most promising technique for different applications is best approached through experience and an understanding of the physical principles of interest.

In addition to the robotic technologies, a focus of the research work was live load evaluation of in-service bridges. The live load evaluations provided insight into the effectiveness of joints between slabs in one case and the beneficial restraint of boundary conditions in another. Acoustic emission was investigated and found to be a potentially promising technique where behavior is difficult to address through displacement-based approaches, such as shear regions, and for semi-autonomous evaluation of distress under ambient loading conditions.

A benefit cost analysis indicated that the widespread adoption of aerial drones could significantly benefit the SCDOT for bridge inspections, particularly if SCDOT personnel were trained to operate the devices. A similar finding was true for the case of jetyaks for scour evaluation on a case by case basis. For culvert inspection, robotic approaches may also provide benefit on a case by case basis.

It is recommended that aerial drones be implemented immediately and utilized in parallel with visual and tactile inspection of bridges. The cost of such devices is low and operation is not difficult. It is recommended that inspection report photographs taken by hand-held cameras be supplemented with images captured by aerial drones where feasible. In this way a data base of images will be assembled for later interpretation and evaluation as automated image processing techniques evolve.

Live load testing is in progress throughout the state and this is valuable to better understand the behavior of bridges and bridge types, particularly with regard to boundary conditions and joint efficiency. It is recommended that acoustic emission be further evaluated to supplement live load testing with an emphasis on assessing distress in shear regions.

Table of Contents

List of Figures

List of Tables

1. Introduction

Visual and tactile inspection are used in the United States to evaluate the condition of bridges and have yielded reasonable results. However, these approaches are time consuming and can be inadequate for identification of hidden defects or defects located in areas that are not easily accessible. Informed decisions for retrofit, rehabilitation, or replacement strategies will take on increased importance in the future as degradation continues and traffic demands increase. Compounding this situation, many maintenance activities will need to be conducted by a reduced workforce in the future. Therefore, efficient evaluation methods will be increasingly critical.

A wide variety of evaluation techniques are available to save both money and time. Selecting the most promising technique for a given application, or applications, is determined by experience and an understanding of the physical principles underlying such techniques.

Based on discussions with SCDOT personnel, a few of the primary issues facing inspection and assessment crews include a) cracking and related corrosion with emphasis on girder end regions (often caused by leakage of joints, leading to issues with bearings); b) over height vehicle damage to superstructure components; c) cracking and corrosion in culverts, sometimes associated with leaching and in other cases simply related to age; d) scour at inlets and outlets of culverts; and e) corrosion of piles and other components in coastal regions.

Chapter 2 of this report presents a literature review and results of surveys with other state DOTs. The results of this chapter were used to guide the selection of methodologies for the laboratory investigations, which are presented in Chapter 3. Laboratory investigations guided the selection of technologies for field demonstrations which included both aerial drone technologies for superstructure and substructure investigations and autonomous kayak systems for subsurface evaluation. Field demonstrations are described in Chapter 4. Chapter 5 provides an overview of live load testing performed on two bridges in South Carolina and Chapter 6 describes the findings of those live load tests. Chapter 7 discusses the costs and benefits of the systems investigated. Chapter 8 summarizes the findings while providing clear recommendations for implementation.

2. Literature Review

The University of South Carolina and Clemson University are assisting the South Carolina Department of Transportation with the selection and implementation of evaluation approaches for bridges components and culverts, with the exception of bridge decks which have been investigated under a separate project. Multiple technologies have been investigated and recommendations made.

This chapter presents a review of the state of the practice, and is divided into to the following sub-sections:

1. Aerial Drones and Robots for Bridge Inspection
2. Approaches for Scour Evaluation
3. Approaches for Culvert Inspection
4. State DOT (Department of Transportation) Survey Results

2.1. Aerial Drones and Robots for Bridge Inspection

Bridge inspections have traditionally been conducted with tactile techniques, using a boom truck, climbing equipment, ladders, and other methods to allow technicians to gain physical access to areas of interest on the bridge (Sash et al., 2000; Melo et al., 2017). An example of traditional tactile inspection is National Bridge Inventory (NBI) condition ratings. Drones, or Unmanned Aerial Vehicles (UAVs), are increasingly investigated and utilized by infrastructure maintenance entities for remotely monitoring and assessing civil structural systems (e.g. solar panels, buildings). Equipped with powerful cameras, UAVs allow an engineer to analyze images and videos for defects. Drones can also be equipped with thermal cameras and processing software to provide further information with the aim of ensuring the safe operation of civil structures. Several state DOTs have begun using UAVs to monitor bridge degradation, thereby reducing hazards associated with manual inspection such as traffic redirection, inspector access, and others (AASHTOnews, 2019).

Some desired characteristics of drones to be used in bridge inspections are powerful cameras that can look directly overhead and the ability to maintain control in GPS (Global Positioning System) deprived environments such as under a large structure.

Drones have the potential to be a viable alternative to manual bridge inspection because they move freely and rapidly with little interference to surroundings. A potential drawback of these aerial systems is the inability to conduct tactile inspections with current hardware, however, these systems may be deployed to identify areas which require further investigation.

2.1.1. Consumer Drones

Consumer drones refer to drones that are marketed toward the amateur videographer and hobbyist market. These drones typically cost below approximate $2,000 and are readily available. Consumer drones are typically small (weighing in most cases less than 1 kg), allow for convenient storage, and are capable of fitting into tight spaces during flight. Consumer drones rely heavily on GPS for stability and lack the redundancies built into more expensive, industrial drone solutions. They do however, present a cost-effective option for bridge inspection.

In this report, Parrot Anafi and DJI Mavic Pro were chosen as consumer drones. They were chosen because they are available, easy to operate, and cost effective.

Parrot Anafi: The Parrot Anafi is a 320 gram (0.71 lbs.) foldable drone with the unique ability to pan from below to directly above during flight (**Figure 2.1**). This capability lends it a distinct advantage for bridge inspection as no other drone in this segment has the capability to do so. The drone features a 4k resolution HDR (High Dynamic Range), 21 MP (Megapixels) camera that is gimbal stabilized on two axes and digitally stabilized on the third. It also offers a 2.8 X "lossless" digital zoom in 1080P (resolution in pixels) due to the oversized optical sensor. The system has an impressive operating range of 2.4 miles (3.9 kilometers) and can fly for approximately 25 minutes (Parrot, 2019). It has the lowest cost risk of any of the drone options here at approximate $699 from the manufacturer and other venders. Additional batteries can be purchased and charged during flight for continuous operation with battery changes. These features combined with a wind resistance of 50 km/hour (31.1 miles/hour) (make the system a capable option for bridge inspection.

Figure 2.1. Parrot Anafi (Parrot, 2019)

Table 2.1. Benefits, limitations, and options for Parrot Anafi

Apparent Benefits	Apparent Limitations	Options
• **180 degree pivoting camera (below to above)** • **Smart phone control** • **Good range** • **4k video, 21 MP camera** • **Lossless digital zoom** • **Affordable**	• No collision avoidance • Single camera limits ability to view surroundings during image capture	• Propeller guards

DJI Mavic Pro: DJI is the most successful entity in the consumer drone industry with over 70% market share and one of their most popular products is the Mavic Pro. The Mavic Pro has a reputation for user-friendly flying and high-quality imagery.

The system weighs 734 grams (1.6 lbs.) and has a 27-minute flight time, with a single 18 MP bottom mounted camera that is 3-axis stabilized handheld system (DJI, 2019a). The camera being mounted on the bottom of the craft limits its ability to capture images overhead. The camera can be deflected upward by approximately 30 degrees which enables some overhead inspection but with increased offset. The drone has a vision-based stabilization system which aids in stable hovering and during the "return to home" function. It also has collision avoidance sensors on the front of the drone to reduce the potential for contact with structures. The system is advertised at approximate $999 from the DJI website and other distributers. DJI is shown in **Figure 2.2**.

Figure 2.2. DJI Mavic Pro (DJI, 2019a)

Table 2.2. Benefits, limitations, and options for the DJI Mavic Pro

Apparent Benefits	Apparent Limitations	Options
• **Proven in consumer market to be a reliable, stable platform** • **Reliable product support** • **Ease of use** • **Affordable**	• Limited flight range and flight time • Camera only deflects upward 30 degrees, limiting overhead use	• Propeller guards

2.1.2. Custom Drones

Custom drones allow for flexibility to create a system which is tailored to a specific task. Custom drone systems support a wide variety of tasks for hobbyists and businesses. Many of the shortcomings of available consumer and industrial drones could be addressed through designing a custom drone. However, designing and building a custom drone requires skill and experience, and customer support and troubleshooting assistance are minimal or non-existent. Still, the flexibility that a custom drone system supplies is worth the difficulties in some cases.

In this report, McNAIR Center/TIG Hitco and DJI Matrice 100were chosen as custom drones. They were chosen because they are available for the research group.

McNAIR Center/TIG Hitco: The researchers at the McNAIR Center for Aerospace Innovation and Research, partnering with TIG Hitco, designed and produced a large hexa-copter drone which utilizes the continuous fiber 3d printing technology they developed to serve as the primary structure for the system (**Figure 2.3**). The system demonstrates the option for building a custom drone for visual inspection. Custom drones allow for more flexibility and can be tailored to the specific needs of the SCDOT and can be improved over time with emerging technologies and hardware upgrades.

This system boasts an impressive payload of 26 lbs. (11.8 kg)., a maximum flight time of 45 minutes without payload, and 18 minutes with maximum payload. The system can be modified to accept an array of different cameras and sensors to meet the needs of the inspector.

Figure 2.3. McNair/TIG Hitco drone (Photo credit: Wout De Backer)

Table 2.3. Benefits, limitations, and options for the McNair/TIG HItco drone

Apparent Benefits	Apparent Limitations	Options
• **High payload rating** • **High stability** • **High flight time**	• Costly • No product supports • Requires in depth knowledge to modify and upkeep	• Extensive

DJI Matrice 100: The DJI Matrice 100 is a customizable and programmable flight platform, with modular frame, expansion bays, universal power and communication ports, dual battery compartments and an optional guidance package that operates as a collision avoidance suite (**Figure 2.4**). The system allows for

extensive customization with DJI reliability and customer support. The system also allows for integration with other DJI hardware such as cameras and navigation equipment.

The maximum takeoff weight of the system is 3.6 kg (7.9 lbs.), which allows for approximately 1.2 kg (2.65 lbs.) of payload. Hovering time depends on the battery selection and payload - ranging from 22 minutes with no payload and one TB47D battery to 40 minutes with no payload and two TB48D batteries (DJI, 2019b).

The system also supports dual users and an operating range of 3.5 – 5.0 km (2.2-3.1 miles). Flights can be pre-programmed which allows the operator to pay attention to camera control and recording. The system does not come with a camera, however all DJI cameras are adaptable to the system. For bridge inspection the preferred configuration would be a Zenmuse Z30 camera with two TB48D batteries and collision avoidance hardware.

The system has an approximate price of $3,299 without extra options. The price of system with options such as Guidance; two TB48D batteries, and Zenmuse Z30 is estimated to be close to approximate price of $8,000, which is still more affordable than industrial drone options.

Figure 2.4. DJI Matrice 100 (DJI, 2019b)

Table 2.4. Benefits, limitations, and options for the DJI M100

Apparent Benefits	Apparent Limitations	Options
• **Adaptable to many testing needs** • **Multiple battery options** • **Multiple camera mount options** • **Can be outfitted with collision avoidance hardware** • **Camera can be mounted on top** • **DJI Support**	• Limited flight range and flight time • Requires technical knowledge to adapt for bridge inspection	• Guidance (collision avoidance) • Multiple cameras and mounts • Nearly limitless

2.1.3. Industrial Drones

Industrial grade drone systems are classified as drones for which the manufacturer intends to cater directly to industrial needs, such as inspection, site mapping, search and rescue, and data capture. These systems typically have higher quality hardware and redundancies to improve operational reliability and performance. Drones in this category are typically larger than consumer drones and accommodate higher payloads in some cases.

In this report, senseFly Albris, FreeFly ALTA 6&8, Digital Aerolus Aertos 120, and DJI Matrice 210 were chosen as industrial drones. They were chosen because they have redundant hardware options, high payloads, and good performance.

senseFly Albris: This drone is equipped with a camera that can shoot HD (High Definition) video, captures 38 MP still images, and has an infrared mode (**Figure 2.5**). The drone camera can be switched between IR and visible spectrum observation mid-flight. It has an advertised flight time of 14-22 minutes, depending on payload, and it can operate in winds up to 32 km/hr. (20 Mile/hour). Most importantly, this UAV has a camera which can be pivoted 180 degrees from below to above the system and can operate without a GPS signal if a predetermined flight path is programmed (senseFly, 2018). The drone also has navcams and ultrasonic sensors that allow it to fly near structures of interest.

As a small drone, it does not have a payload rating and is designed to operate only with the manufactured weight. Although this prevents the system from being adapted with additional sensors, it is already fitted with most of the sensors that would be needed for visual inspection of bridges.

The flight data manager allows for geotagging of images and, using image processing software, geo-referenced maps and models of the inspected area can be generated. This capability would aid in tracking the precise location of potential defects and how they progress over time.

This is the same drone system (senseFly) that was featured in a Minnesota Department of Transportation drone inspection study. However, the system is anticipated to be discontinued. Prices for the system vary with values averaging around approximate cost of $11,000.

Figure 2.5. senseFly Albris (senseFly, 2018)

Table 2.5. Benefits, limitations, and options for the senseFly Albris

Apparent Benefits	Apparent Limitations	Options
• **Portability and ease of operation** • **Camera can capture video, still, and thermal imagery** • **Autonomous (pre-programmed) or remote-guided (eMotion 3 software)** • **Demonstrated in Minnesota DOT study**	• Limited flight range and flight time • Costly	• Pix4Dmapper • Pix4Dbim

FreeFly ALTA 8: This drone has an advertised 15-35-minute flight time, depending on payload and battery type (**Figure 2.6**), and it can operate in extreme weather due to built-in GPS, IMU (Inertial Measurement Unit), and barometer. This UAV has a top-mounted gimbal that allows for the use of many different camera systems (FreeFly, 2019a).

The ALTA Application for smartphones allows the pilot to monitor satellite connectivity and quantity, vibration levels, etc. during flight. The ALTA 8 is shown below in Figure . It features a weather resistant enclosure for the flight control systems to prevent damage during the onset of adverse weather conditions and comes with an optional first-person view (FPV) camera mount for navigation. The system has an approximate cost of $17,495. The system will require a camera for inspection, a recommended FPV mount and associated camera, and a controller.

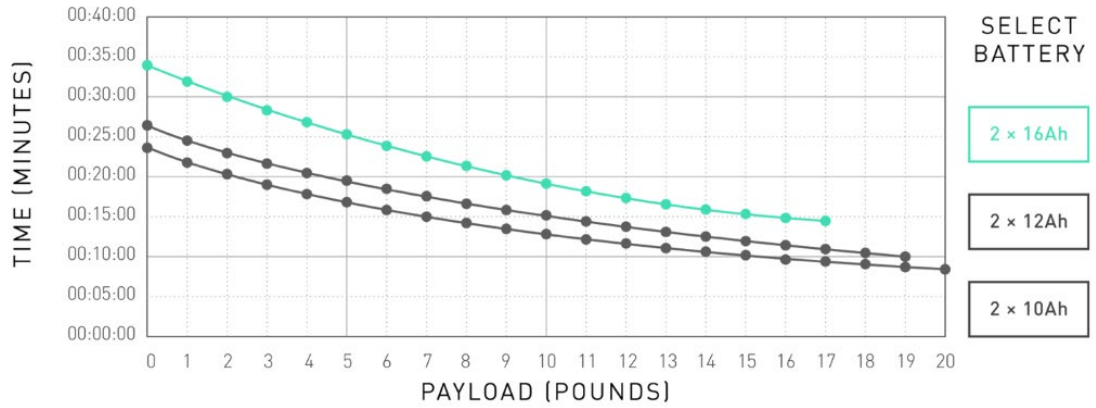

Figure 2.6. FreeFly ALTA 8 flight time vs. payload plot (FreeFly, 2019a)

Figure 2.7. FreeFly ALTA 8 (FreeFly, 2019a)

Table 2.6. Benefits, limitations, and options for the FreeFly ALTA 8

Apparent Benefits	Apparent Limitations	Options
• **Portability (folds to 50% of operating size) and ease of operation** • **Demonstrated in Minnesota DOT study** • **Stability in poor weather conditions** • **"Height hold" allows for stable shooting** • **Can select safe height and will return to home if it veers past**	• Limited flight range and time • Camera and stabilizer not included • Costly • Not tested in industrial setting (to our knowledge)	• ALTA App

FreeFly ALTA 6: The ALTA 6 is another FreeFly drone that may be a good candidate for bridge inspections. It is similar in design to the ALTA 8 platform, with six rotors instead of eight. It is smaller, less complex, lighter, and less costly than its larger counterpart. The system has a maximum payload of 15 lbs. (6.8 kg), which allows for a wide range of camera, sensory, and battery options. Flight time for the ALTA 6 is dependent on the batteries selected and the payload and ranges from 10-45 minutes (FreeFly, 2019b). The drone is shown in **Figure 2.9**.

There is an optional top and bottom-mount gimbal configuration to meet a wide range of needs, and a FPV camera mount to accommodate dual operators. This allows the pilot to focus on navigation tasks, while the second operator collects footage with the payload cameras. It also features a weather resistant enclosure for the flight control systems to prevent damage during adverse weather conditions. The system is listed for an approximate price of $11,995 from the manufacturer before extras.

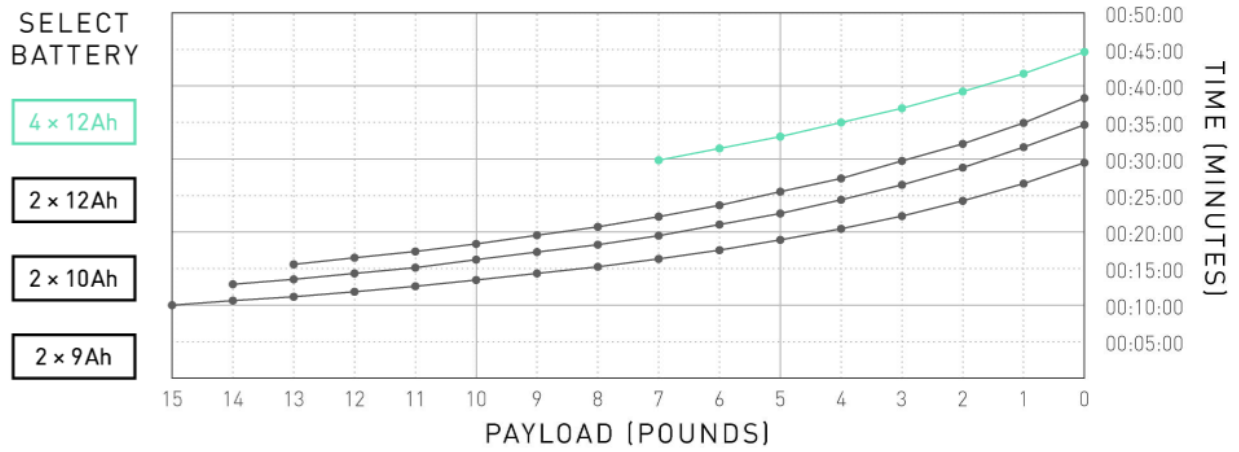

Figure 2.8. Payload vs. flight time for various battery configurations (FreeFly, 2019b)

Figure 2.9. FreeFly ALTA 6 (FreeFly, 2019b)

Table 2.7. Benefits, limitations, and options for the FreeFly ALTA 6

Apparent Benefits	Apparent Limitations	Options
• **Portability (folds to 30% of operating size) and ease of operation** • **Stability in poor weather conditions** • **"Height hold" allows for stable shooting** • **Can select safe height and will return to home if it veers past**	• Limited flight range and flight time • Camera and stabilizer not included • Costly • Not tested in industrial setting (to our knowledge)	• ALTA App

Digital Aerolus Aertos 120: The Aertos 120 is a drone system intended to be used for inspection in tight spaces and without the use of a GPS signal for stability and navigation (**Figure 2.10**). Instead of GPS, the drone uses onboard inertial measurement units to regulate movement. There are no collision avoidance provisions on the drone, instead the drone is designed to withstand impacts and regain stability. The propellers are ducted, and the system uses a stiff carbon fiber frame. The robustness comes at a cost, as the ducts limit the size and efficiency of the propellers, and the structure is heavy (approximately 6 lbs.) which, with the small propellers, limits the flight time to eight minutes.

Like the Parrot Anafi, the Aertos 120 can rotate the primary camera from viewing below to viewing directly above the drone. The camera is a 12 MP unit that is gimbal stabilized on two axes and the setup supports dual displays for tandem-user operations. The FPV flight camera is useful during operation as flying while facing upward can be difficult. The Aertos is advertised for use in small culverts, tunnels, electrical vaults, manholes, sewers, small tanks, and towers. The system is sold for an approximate price of $20,000 and training is offered for a fee (Digital Aerolus, 2019).

Figure 2.10. Aertos 120 (Digital Aerolus, 2019)

Table 2.8. Benefits, limitations, and options for the DA Aertos 120

Apparent Benefits	Apparent Limitations	Options
• **No need for collision avoidance, as is designed to resist contact damage** • **Dual operator capable** • **Does not use GPS signal for stability or navigation**	• Extremely short flight time • Costly • Stability and ease of use are questionable	• Training

DJI Matrice 210: DJI offers drones for industrial applications such as inspection, mapping, search and rescue, agriculture, and film (**Figure 2.11**). The Matrice 210 is a platform with a great deal of flexibility in configuration and payload. The system is designed so that a pilot can control the drone, while another operator manages the payload, collecting images, video, and data as needed. All functions can also be performed by a single operator. There are provisions to aid the pilot in collision avoidance using seven sensors which identify obstacles in front and above the drone. According to the manufacturer "A downward facing vision positioning system enables precision hovering and landing" (DJI, 2019c).

The Matrice has configurations that support a single lower camera, two lower mounted cameras, and a single upward mounted camera. The upward mounted camera can be oriented directly overhead allowing a better view of the underside of bridges. Available cameras for the drone are the Zenmuse X4S, X5S, Z30, XT, XT2, the SLANTRANGE 3PX, and the Sentera AGX710. These cameras all come attached to a 3-axis gimbal allowing stable image and video capture.

Another configuration option is the battery model, which impacts the flight time and the payload capacity. Available batteries are the TB50 and the TB55. The TB50 offers a payload of 2.34 kg (5.16 lbs.) with a maximum flight time of 13 minutes with a full payload. The TB55 allows the drone to handle a payload of 1.61 kg (3.5 lbs.) and a maximum flight time of 24 minutes with a full payload. For an empty flight, the TB50 will allow for 27 minutes of flight and the TB55 will allow for 38 minutes of flight (DJI, 2019c).

The system can cost approximately $25,000 for the dual camera setup, and $15,000 for the top mounted camera setup, which presents a significant investment. Compounding this is the lack of collision avoidance hardware on the sides and top making a potential pilot error a costly prospect. The camera hardware comprises a large portion of the cost (Zenmuse Z30 approx. $3,000; Zenmuse XT approx. $10,000).

Figure 2.11. DJI Matrice 210 (DJI, 2019c)

Table 2.9. Benefits, limitations, and options for the DJI M210

Apparent Benefits	Apparent Limitations	Options
• **Multiple camera configuration options** • **Dual operator capability** • **Multiple battery options** • **Readily available and industry proven** • **Some collision avoidance provisions**	• Camera and stabilizer not included • Costly	• Multiple camera options • Top or bottom mount for camera • Dual-gps receivers • Dual operators

Table 2.10. Summary of drones

Drone System	Anafi	Mavic Pro	McNair/ TIGHITCO	Matrice 100	Albris	ALTA 8	ALTA 6	Aertos 120	Matrice 210
Nav	GPS	GPS	GPS	GPS	GPS	GPS	GPS	Non-GPS	GPS
Collision Avoidance	None	Forward	None	Full	Full	None	None	-	Semi-Full
Payload lbs. (N)	0	0	26 (115.6)	2.5 (11.1)	0	20 (88.9)	15 (66.7)	0	5 (22.2)
Upward View (Degree)	90	30	90	90	90	90	90	90	90
Flight Time (min.)	25	27	15 to 45	22 to 40	14 to 22	8 to 35	10 to 45	8	13 to 38
Wind resistance mph (kph)	31 (50)	22 (35.4)	NA	22 (35.4)	22 (35.4)	NA	NA	NA	27 (43.5)
Dual Operator	No	No	No	Yes	No	Yes	Yes	Yes	Yes
Cost	$699	$759	-	$8,000	$11,000	$17,995	$11,995	$20,000	$15,000
	CONSUMER		CUSTOM		INDUSTRY				

Summary

There are many viable drone options for visual inspection of bridges. Two stand out candidates for bridge inspection are the Parrot Anafi and the Matrice 210. The Anafi offers a cost effective, compact, and high-

quality camera option. The Matrice 210 offers a more robust and customizable solution for more industrial applications. The summary of drones is presented in **Table 2.10**.

2.1.4. Robotic Inspection Systems and Crawlers

Robotic systems are being used for inspection of civil structures and can provide more quantitative feedback than human inspection in some cases (Infrastructure PC, 2018). Robotic inspection systems are available to modify crane trucks with robotic arms, platforms, and control systems (Infrastructure PC, 2018). Additionally, machine vision systems are available for automatic detection of cracks and other damage. Allowing robotic inspection of bridges reduces human risks while improving data reliability and efficiency.

In this report, MRIS-MN1, Versatrax VT450 Crawler, and MRIS were chosen as robotic inspection systems and crawlers to study. They were chosen because they are reliable and they have strong camera.

Robotic Technologies of Tennessee (RTT) - MRIS-MN1: Robotic Technologies of Tennessee (RTT) designs and produces a magnetic tethered robot capable of climbing and maneuvering on ferrous surfaces (**Figure 2.12**). The crawler uses four magnetized wheels to attach and allow the system to move on any ferromagnetic surface without falling off due to its weight, provided that the operator does not drive off a ledge. The system comes with a 25-foot tether (7.6 m) allowing the operator a considerable offset during inspections. Longer tethers are also available. The system has two onboard navigation cameras as well as a five-pound payload capacity for additional sensory equipment (RTT, 2019a).

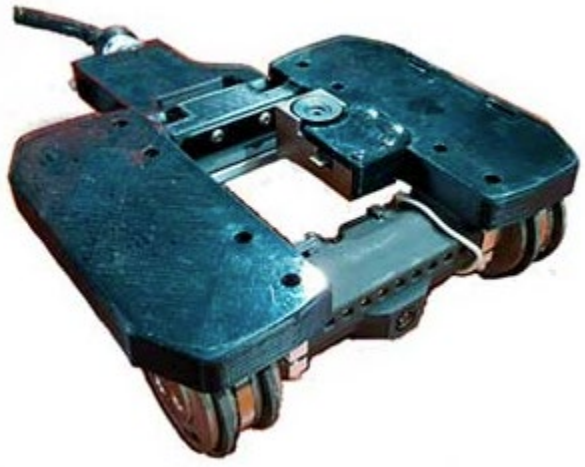

Figure 2.12. MRIS-MN1 (RTT, 2019a)

Table 2.11. Benefits, limitations, and options for the MRIS-MNI

Apparent Benefits	Apparent Limitations	Options
• **Portable inspection capability** • **FPV Camera** • **High strength** • **Ability to add sensors**	• Tethered • Limited to use on ferrous materials • Surface quality • Edge concerns	

Versatrax VT450 Crawler, Nexxis: The Versatrax 450™ is suited for a wide range of applications where remote handling and inspection are required (**Figure 2.13**). This robot allows for inspection, capture, and safe removal of dangerous materials faster than by conventional means. The Versatrax 450™ showcases a wide variety of new Inuktun technologies in a modular system. The 6000 series extended Minitracs™ provide 4 in. (10 cm) of clearance to allow for improved maneuverability over a wide range of obstacles. The main camera, a Spectrum 90™, can be lowered to navigate through tight spaces and then raised to an upright position to gain a 360 degree view from an intuitive position. The four-function manipulator arm unfolds from the crawler for remote handling of articles and debris, and includes a second integrated camera, allowing the user to closely monitor items during handling operations. Forward and rear facing high output LED auxiliary lights allow for high visibility in low light situations (Nexxis, 2019a, Nexxis 2019b)).

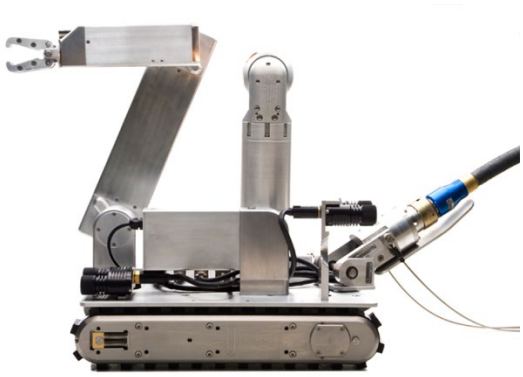

Figure 2.13. VT450 Crawler (Nexxis, 2019a)

Table 2.12. Benefits, limitations, and options for VT450 crawler

Apparent Benefits	Apparent Limitations	Options
• **Portable inspection capability** • **Two color cameras; one for 360 views** • **Scalable framework** • **Built in camera lights and auxiliary lights for visibility in dark environments** • **Multi-joystick controller for ease of operation**	• Tethered	• 10.2" monitor • Digital video recorder • Inclinometer • Directional compass monitor • Chronometer • Laser site lines • Laser profiler

Mobile Robotic Inspection System, Robotic Technologies of Tennessee: The crawler has a mobile climbing platform with an ultrasonic wheel transducer inspection device and pneumatic needle scalars for surface preparation. The system breaks down into four primary components: tractor platform, transducer unit, scalar unit, and interface/controller. In this robot, the operation of the user has real-time control of the travel speed and direction via an intuitive twin joystick control pendant. Positioning of the remote attachments (transducer and scalers) can be remotely adjusted via the control pendant. The powerful permanent magnet pads in the crawler platform enable the unit to work in a wide variety of positions, including horizontal and vertical inspection scans. Data is automatically collected by a simple Windows based program running on a laptop. The software logs the real-time vertical position of the transducer and the thickness readings retrieved automatically from the flaw detector (RTT, 2019b). The device is shown in **Figure 2.14**.

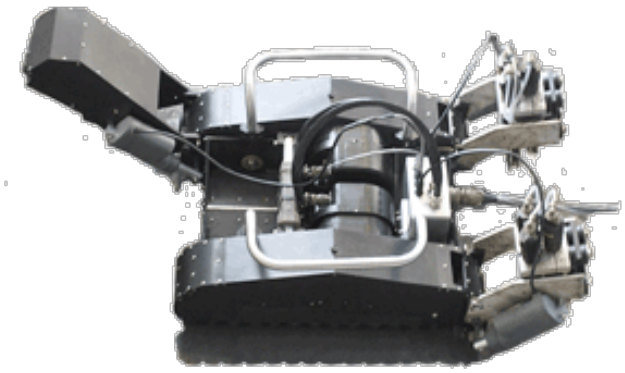

Figure 2.14. Mobile robotic inspection system (RTT, 2019b)

Table 2.13. Benefits, limitations, and options for mobile robotic inspection system

Apparent Benefits	Apparent Limitations	Options
• **Provides greater data collection at less cost** • **Increased coverage** • **Increased notification of damaged areas** • **Perform current inspections in less time and with less manpower** • **Enables new inspection capabilities and techniques**	• Does not have high resolution	• Self-contained power and control system • 100 ft. tether included (additional length available) • Joystick operator interface • Ultrasonic transducer system • Data logging/report generation software • Onboard cameras, controller mounted video display • Coolant system

Table 2.14. Comparison of robotic systems

Robotic System	RTT MRIS-MN1	Versatrax VT450 Crawler	RTT MRIS
Bonding Method	Magnetic	None	Magnetic
Available Payload	5lb (22.25N)	200lb (890N)	N/A
View	FPV	Dual FPV, 360 deg	90 deg
Tethered Length	25ft (7.62 m)	500ft (152.4m)	100ft (30.5m)
Clamping Force	31lb (137N)	None	Not Advertised
Payload Options	Other	Other	Standard UT Probe
	Industrial		

Summary

The MRIS of Robotic Technologies of Tennessee shows promise for NDE of bridges, however, the tethered nature of the systems can be a hindrance for deployment in many situations. A wireless controlled solution would be better suited to the task of bridge inspection. Comparison of the various robot technologies is shown in Table 2.14.

2.2. Approaches for Scour Evaluation

Sonar is a well-developed underwater acoustic imaging approach that can be used for portable, hands-off scour monitoring. These devices, also called acoustic transducers, use sound waves to "ping" the bottom of the waterway and the corresponding echo informs the user of the depth to the bottom. The transducers can be angled toward potential scour areas to determine the amount of erosion. Most sonar for scour monitoring systems are mounted directly to a bridge pier or other portion of a bridge. It is also possible to evaluate scour using boat-mounted sonar. Boat-mounted sonar has the advantage of being portable and able to evaluate different bridges, but with the trade-off of only providing scour data at the time of evaluation. Scour detection sonars are increasing in popularity because they can continuously monitor changes in the stream bed profile and can be connected to a telemetry station which will transmit real time data.

In this report, Teledyne SeaBat 7130, SeaBat IDH Sonar Head, Teledyne MotionScan, 3D Multibeam Scanning Sonar, M3 Sonar Multibeam Echo Sounder, GeoSwath 4R, EM 2040C, EdgeTech 2000, EdgeTech 2205, EdgeTech 2400, EdgeTech 3100, EdgeTech 3200, EdgeTech 3300, MS 1171, Dual Axis Sonar, Micro Electro-Mechanical Systems (MEMS), and fish finders (commensal sonar) were chosen to study the sonar evaluation methods. They were chosen because of their high resolution, a high depth operability, different range of frequency, and 3D scanning.

Teledyne SeaBat 7130: This product is a high-resolution sonar system specifically designed for Autonomous Underwater Vehicles (AUVs) but can also operate on Remotely Operated Underwater Vehicles (ROVs) and small submarines. The SeaBat can go up to a depth of 3,000 meters and operates with a wide range of frequencies. The higher frequency allows for high resolution while the low frequency allows for long range detections. The sonar can process data into real time which allows the information collected to be delivered immediately to a computer without delay. Equipment for the SeaBat is shown in **Figure 2.15** and a data image is shown in **Figure 2.16** (TeledyneMarine, 2019a).

Figure 2.15. SeaBat 7130 sonar emitter (Teledyne Marine, 2019a)

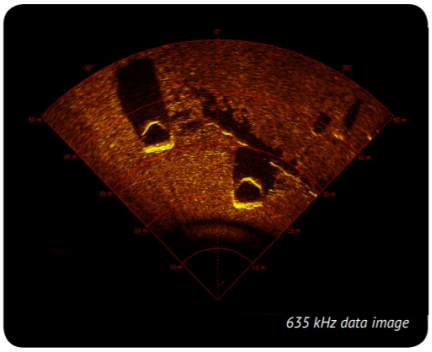

Figure 2.16. Seabat 7130 data image, colors indicate topography (Teledyne Marine, 2019a)

Table 2.15. Benefits, limitations, and options for SeaBat 7130

Apparent Benefits	Apparent Limitations	Options
• **Portable** • **High resolution and long range** • **Flexible in attachment**	• Cannot have high resolution and long range at the same time (operating at different frequencies)	• Teledyne PDS • SVP-70 sound velocity probe • System integration and training • Pressure housing • Range of frequencies • AUV/ROV

Teledyne SeaBat IDH T20/50-R: This product is like the SeaBat 7130 except it has an Integrated Dual Head (IDH) that is connected to the compact Rack mounted Sonar Processor (RSP). The RSP allows for a single point for all the cable connections and has accurate sensor time tagging and motion stabilization. The SeaBat has a range of frequency that allows for improved swath performances, less interference from other sensors, and reduced time for surveying. This product also works well in challenging acoustic conditions and develops quality data. Teledyne offers an all-in-one fully integrated survey system with a single sonar processor for two sonar heads. Since the SeaBat IDH is so compact, it allows for faster mobilization, minimal interfacing and low space requirements compared to the other SeaBat versions. The dual head sonar can be seen in **Figure 2.17** and an example of a data image from the SeaBat can be seen in **Figure 2.18** (TeledyneMarine, 2019b).

Figure 2.17. SeaBat IDH sonar head (Teledyne Marine, 2019b)

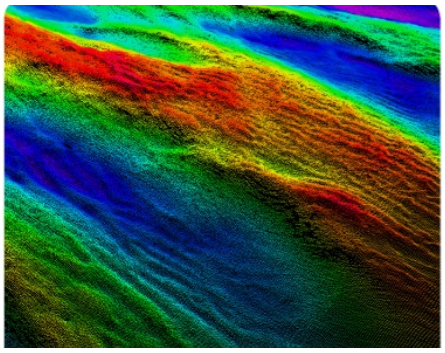

Figure 2.18. SeaBat IDH data image, color indicates topography (Teledyne Marine, 2019b)

Table 2.16. Benefits, limitations, and options for SeaBat IDH

Apparent Benefits	Apparent Limitations	Options
• **Reduced processing time** • **Faster surveys** • **Fully integrated survey system** • **Compact system**	• Cannot have high resolution and long range at the same time (operating at different frequencies)	• Optional built in inertial navigation system (INS)

Teledyne MotionScan: This product involves a 3D scanning sonar system that collects motion corrected 3D point clouds from a moving platform. The different types of platforms that are compatible with the MotionScan are surface vessels, remote operated underwater vehicles, and customized deployments. This product uses a GPS, sensors, a control console, and Teledyne data acquisition software. MotionScan is useful for bridge inspections with scour and undercut monitoring and many other applications. An example of the data imagery can be seen in **Figure 2.19** (Teledyne Marine, 2019c).

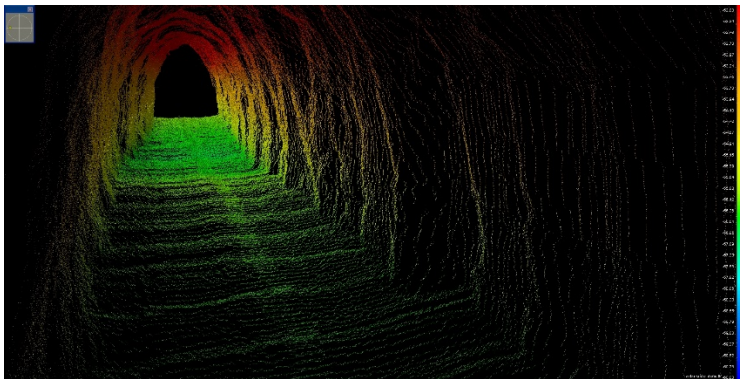

Figure 2.19. SeaBat IDH data image, color indicates topography (Teledyne Marine, 2019b)

Table 2.17. Benefits, limitations, and options for Teledyne MotionScan

Apparent Benefits	Apparent Limitations	Options
• **3D point cloud generation while scanning** • **3D scanning while in motion** • **Geo-referenced 3D point clouds**	• Software requirements	• Different cable lengths • Different platform options

Teledyne 3D Multibeam Scanning Sonar: This sonar creates high resolution imagery of underwater areas and structures even when visibility is poor. The system creates 3D point clouds with an easy to operate set up and little training. The sonar can be set up on a tripod, Remote Operated Underwater Vehicle, or surface vessel. The system collects the point clouds without positioning information from a stationary stance and combines with software referred to as Quick Stitch to create the 3D profiles of the environment surveyed. The 3D scanning sonar is useful for scour monitoring and bridge inspections. The equipment can be seen in Figure **2.20** and an example of data collected and processed can be seen in **Figure 2.21** (Teledyne Marine, 2019d).

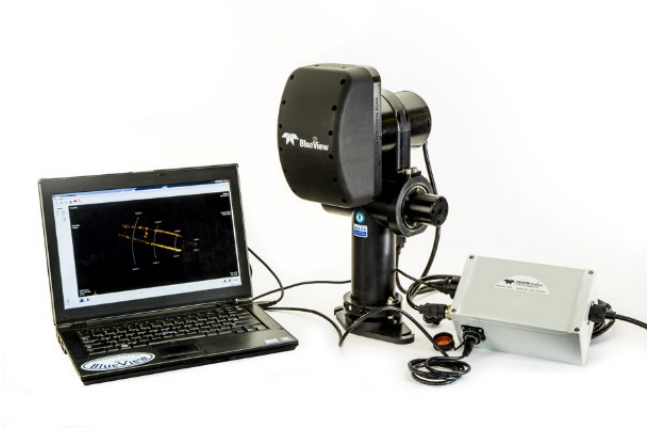

Figure 2.20. 3D multibeam scanning sonar (Teledyne Marine, 2019d)

Figure 2.21. 3D multibeam scanning sonar data image, color indicates topography (TeledyneMarine, 2019d)

Table 2.18. Benefits, limitations, and options for 3D multibeam scanning sonar

Apparent Benefits	Apparent Limitations	Options
• **3D mosaic imaging** • **Compact size** • **Operates in low and zero visibility** • **Little training needed**	• Requires third party software	• Quick Stitch • MotionScan • Different pan and tilt cameras

Kongsberg M3 Sonar Multibeam Echo sounder: This device is portable and lightweight and is cost effective. It features imaging and underwater datasets from one sonar head. The sonar also has single beam image quality that collects data efficiently. Real time data is collected and the images are put together into one continuous image using a specific software. The pulses used for this sonar are more complex but allows for listening modes on the sonar along with multiple window zooms. The sonar is well-

suited for shallow water surveys. The best options for installation are on a pole mount on a surface vessel; vehicles such as small class remotely operated vehicles (ROVs); or mounted on a tripod. The M3 device is shown in **Figure 2.22** and a data image is shown in **Figure 2.23** (Kongsberg, 2019a).

Figure 2.22. M3 sonar multibeam echo sounder (Kongsberg, 2019a)

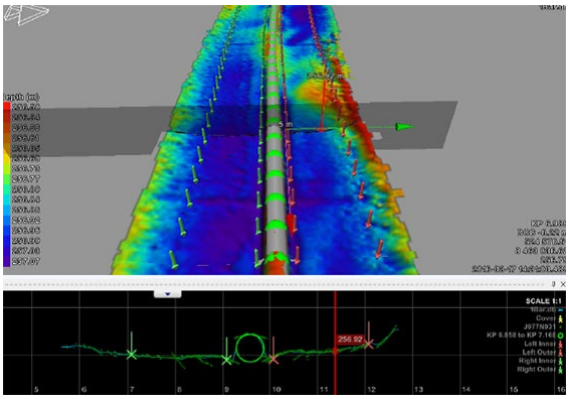

Figure 2.23. M3 data image (from manufacturer website), color indicates topography (Kongsberg, 2019a)

Table 2.19. Benefits, limitations, and options for Kongsberg M3

Apparent Benefits	Apparent Limitations	Options
• **Portable** • **Cost effective** • **Real time mosaic images**	• Requires third party software	• Different cable lengths

Kongsberg GeoSwath 4R: The GeoSwath 4R can utilize ultra-high-resolution underwater scanning and side scan seabed mapping simultaneously. It is intended to be set up on small vessels like jet skis, and the data collected has been shown to exceed the standards for hydrographic surveys. The sonar has a wide range of frequency and the ability to cover an area of twelve times the water depth in diameter. The device is

operated from a laptop PC and the data software includes data acquisition, processing, and presentation. The device is shown in **Figure 2.24** and a data image is shown in **Figure 2.25** (Kongsberg, 2019b).

Figure 2.24. GeoSwath 4R (Kongsberg, 2019b)

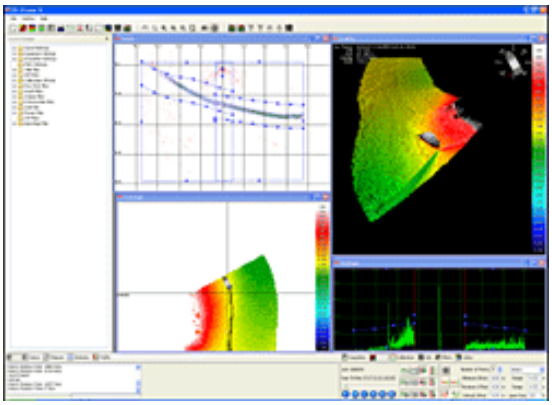

Figure 2.25. Geoswath data image (Kongsberg, 2019b)

Table 2.20. Benefits, limitations, and options for GeoSwath 4R

Apparent Benefits	Apparent Limitations	Options
• **Simultaneous bathymetry and side scan seabed mapping** • **Exceeds International Hydrographic Organization (IHO) standards**	• Third party software needed for some features	• AUV and ROV versions • Different cable options • Transducer mounts

Kongsberg EM 2040C, Compact: The EM 2040C is a compact multibeam echo sounder intended for shallow water applications. The sonar head is made up of the receiver and transmitter integrated together

and the system reaches hydrographic standards. The EM 2040C offers high resolution and a wide range of frequency. The sonar head can operate in single and dual head modes which allows data to be collected more efficiently. The maximum depth is 500 meters (1,640 ft), but Kongsberg also produces similar products that can reach to depths of 11,000 meters (36,000 ft). In **Figure 2.26**, the dual head sonar can be seen and **Figure 2.27** is an example of data imaging (Kongsberg, 2019c).

Figure 2.26. EM 2040C Dual Head Sonar (Kongsberg, 2019c)

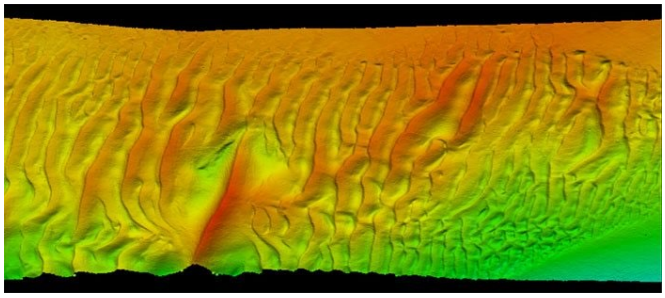

Figure 2.27. EM 2040C Data Image (Kongsberg, 2019c)

Table 2.21. Benefits, limitations, and options for Kongsberg EM 2040C

Apparent Benefits	Apparent Limitations	Options
• **High resolution** • **Wide range of frequencies** • **Exceeds IHO standards**	• Third party software	• Range of third party software

EdgeTech 2000: For this application, the sonar and sub-bottom profiler features are combined into a single product. There are three different types of tow fish and a wide range of frequencies. This product is designed for water depths up to 300 meters (980 ft). All types of tow fish are equipped with dual simultaneous frequency CHIRP side scan sonar. CHIRP sonar is a compressed high intensity radiated pulse that has been in use since 2009. This type of sonar transmits a sweeping range of frequencies that have pulses at least ten times the duration of a single transducer. The EdgeTech 2000 features a fully integrated

system that has all the hardware and software necessary for the data acquired. The user can choose between the side scan sonar or the sub-bottom profiler frequencies along with the built-in heading, pitch, and roll sensors. The scanner and profiler can be seen in **Figure 2.28** and a data image of concrete blocks is shown in **Figure 2.29** (Edgetech, 2017a).

Figure 2.28. EdgeTech 2000 scanner and profiler (Edgetech, 2019a)

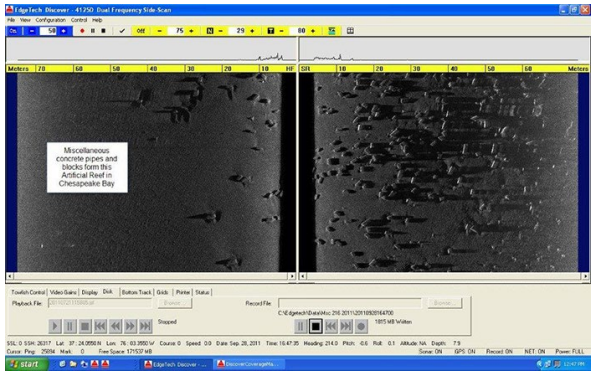

Figure 2.29. Image of concrete blocks from EdgeTech 2000 (Edgetech, 2019a)

Table 2.22. Benefits, limitations, and options for EdgeTech 2000

Apparent Benefits	Apparent Limitations	Options
• **Fully integrated turnkey system** • **Side scan and sub-bottom frequencies**		• Three different tow fish

EdgeTech 2205: This is a flexible and compact system that operates on underwater vehicles, including Unmanned Underwater Vehicles and Remotely Operated Vehicles. Side scan sonar data imagery and sub-bottom profiler data can be collected by the sonar system. The sonar system can independently store the data, or the information can be automatically exchanged between the system and the vehicle during the

time the vehicle is out. EdgeTech provides its own software called “Discover” to load the data but the data is also compatible with other software. It is dual frequency and includes transducer arrays, sensors, and a pressure vessel. The sonar head can be seen in **Figure 2.30** and an example of the data image is shown in **Figure 2.31** (Seatronics, 2019a).

Figure 2.30. EdgeTech 2205 sonar head (Seatronics, 2019a)

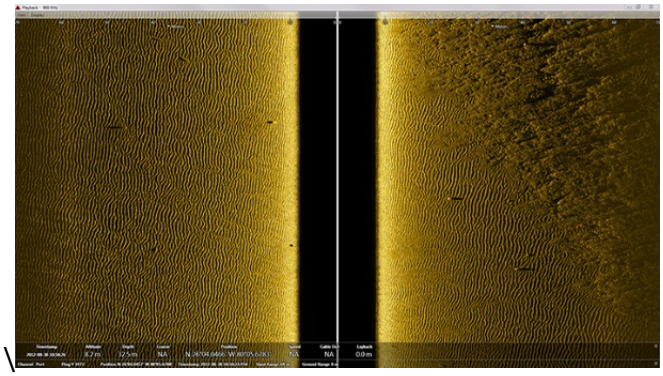

Figure 2.31. Side scan image (Seatronics, 2019a)

Table 2.23. Benefits, limitations, and options for EdgeTech 2205

Apparent Benefits	Apparent Limitations	Options
• **Smaller** • **Low power and noise** • **On-line self-tests** • **Combination of side scan sonar and sub bottom profiler**		• Range of platforms • Range of frequencies

EdgeTech 2400 - Deep Towed: Like the EdgeTech 2205, side scan and sub-bottom profile features are combined in this product. It is designed for deep water operations and can go up to depths of 6,000 meters (19600 ft). The EdgeTech 2400 has a fully integrated turnkey system and digital telemetry over single coaxial or fiber optic tow cable. The user supplied sensors are either analog or digital channels and the system includes built-in sensors. The standard system has a choice of the combined deep tow fish, digital telemetry that runs with the coaxial cable, or a processor with EdgeTech software. The equipment can be seen in **Figure 2.32** and a data image of a pipeline from this product is shown in **Figure 2.33** (Edgetech, 2017b).

Figure 2.32. EdgeTech 2400 scanner and profiler (Edgetech, 2017b)

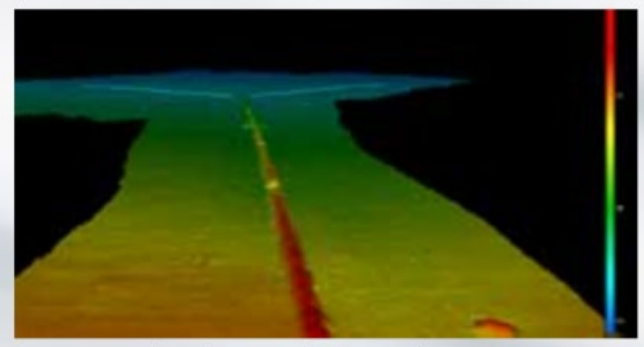

Figure 2.33. EdgeTech pipeline image (EdgeTech, 2017b)

Table 2.24. Benefits, limitations, and options for EdgeTech 2400

Apparent Benefits	Apparent Limitations	Options
• **Fully integrated turnkey system** • **Dual frequency side scan sonar and sub-bottom profiler**		• Range of frequencies • Optional sensors • Deep tow fish

EdgeTech 3100: Portable Sub-Bottom Profiler: This product is like the ones described above but is a portable version. The system produces high-resolution imagery of the sub-bottom structure at depths up to 100 meters (328 ft). The EdgeTech 3100 is intended for rivers, lakes, ponds, and shallow ocean environments. The user can choose between two different tow fish having different frequency ranges. One tow fish can produce a higher resolution at lesser depths, while the other has a resolution that is slightly lower but can scan at greater depths. The system also comes with a portable splash proof topside processor, with a laptop running the EdgeTech software for the sonar data display. The tow cable length is 115 feet (35 m) but user specified lengths are available. The EdgeTech 3100 offers a portable version of the sub-bottom profiler with high resolution imagery and requires low amounts of power (AC or DC). A pole mount version is available for shallow water surveys. In **Figure 2.34**, the profiler is shown and a data image of a lake is shown in **Figure 2.35** (Seatronics, 2019b).

Figure 2.34. EdgeTech 3100 profiler (Seatronics, 2019b)

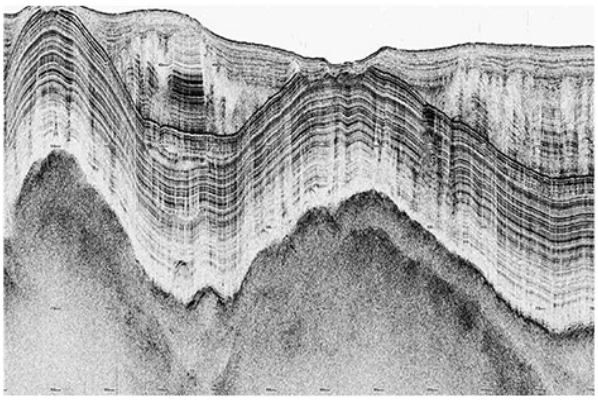

Figure 2.35. Tow vehicle lake image (Seatronics, 2019b)

Table 2.25. Benefits, limitations, and options for EdgeTech 3100

Apparent Benefits	Apparent Limitations	Options
• **Portable** • **High resolution imagery** • **Low power**		• Pole mount option for shallow water surveys • Two different tow fish

EdgeTech 3200: High Penetration Sub-Bottom Profiler: This product is a wideband frequency modulated (FM) sub-bottom profiler that produces high resolution imagery. It is useful for lakes, rivers, and oceans with depths to 200 meters (656 ft). This profiler is compatible with three different low drag tow fish that have different frequencies and operate at depths up to 300 meters. The user can select the type of tow fish based on the sub-bottom profile and the resolution and depth required. The EdgeTech "DISCOVER" Software comes with this product operating on a topside processor along with the user specified cable length and optional sensors. In **Figure 2.37**, the profiler is shown and **Figure 2.37** shows a data image of a channel infill (Seatronics, 2019c).

Figure 2.36. EdgeTech 3200 Profiler (Seatronics, 2019c)

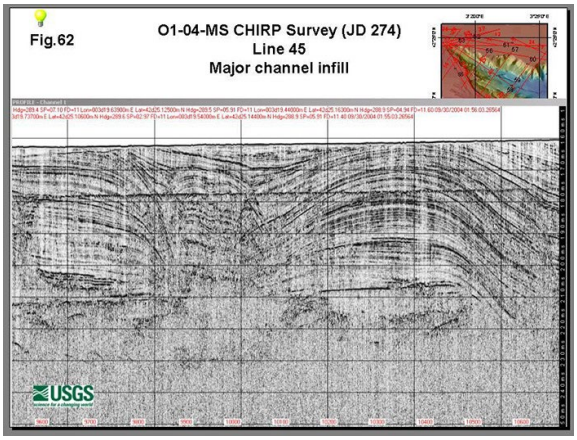

Figure 2.37. Major channel infill (Seatronics, 2019e)

Table 2.26. Benefits, limitations, and options for EdgeTech 3200

Apparent Benefits	Apparent Limitations	Options
• **Low frequency for greater depth** • **High resolution imagery**		• Three different tow fish • Pole mount option for shallow water surveys • Optional sensors

EdgeTech 3300: Hull Mount Sub-Bottom Profiler: This product is based on EdgeTech's Full Spectrum Technology. Advantages over other sub-bottom systems include an increase in depth along with higher resolution. EdgeTech also changed the shape of the profiler to increase accuracy of the beam patterns. This is useful for deeper water surveys and improves resolution while giving more accurate data, resulting in superior sub-bottom imagery even in full ocean depths. There is an option for dual frequency and multiple configuration options for transmitting and receiving data. The EdgeTech 3300 is versatile and creates cross sectional images of the channel bottom. The profiler can be seen in **Figure 2.38** an example of the data imagery is shown in **Figure 2.39** (Edgetech, 2016).

Figure 2.38. EdgeTech 3300 profiler (Edgetech, 2016)

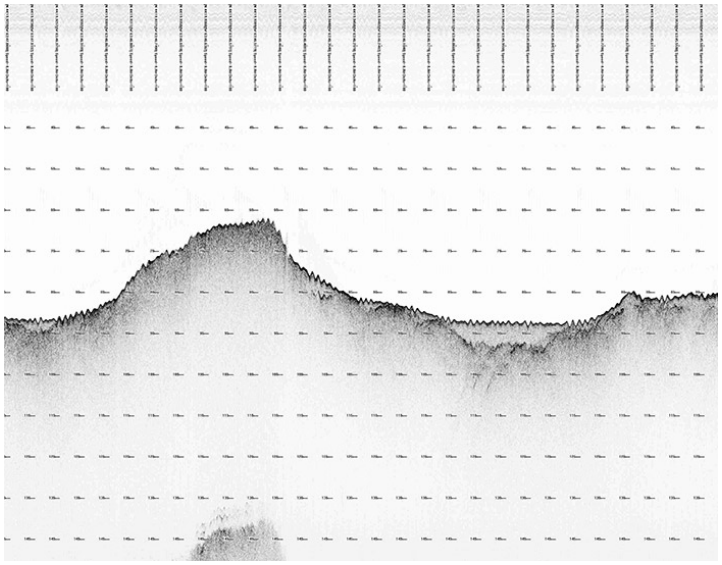

Figure 2.39. Hull mount data image (Edgetech, 2019d)

Table 2.27. Benefits, limitations, and options for EdgeTech 3300

Apparent Benefits	Apparent Limitations	Options
• **Superior sub-bottom images** • **Increased depth** • **High resolution** • **Dual frequency**		• Range of frequencies • Optional polyvinylidene difluoride (PVDF) receiver

Kongsberg MS 1171: This product is compact and is claimed to have the highest quality and highest resolution on the market. The transducer is protected within an oil filled, pressure compensating dome. The power output is increased compared to other products and the image quality is relatively high. The scanning sonar has a 360-degree field view and a lateral range of 40 meters (131 ft). The data can be viewed in real time and shows more detail than a multi-beam sonar but software is required to process the data acquired in the field. The domed sonar head is shown in **Figure 2.40** for the Kongsberg MS117 (Kongsberg, 2019d).

Figure 2.40. MS 1171 domed sonar head (Kongsberg, 2019d)

Table 2.28. Benefits, limitations, and options for Kongsberg MS1171

Apparent Benefits	Apparent Limitations	Options
• **Compact and lightweight** • **Superior image quality** • **High resolution**	• Requires MS1000 processing software to operate equipment and process data	• Range of transducer types

Kongsberg Dual Axis Sonar (DAS): This product is based on position and can show more detail than the multi-beam sonar mentioned previously. DAS systems provide information on the dynamics of sediment scour and produce 3D point profiles. It is designed for long term monitoring in harsh conditions and can cover large areas. It works with the Kongsberg software program or in “standalone mode” which is when

the data is logged in the DAS and transmitted wirelessly. This is a continuous 3D surveying system which is useful for obtaining information about scour. The equipment can be seen in **Figure 2.41** and a data image is shown in **Figure 2.42** (Kongsberg, 2019e).

Figure 2.41. Dual-axis scanning sonar head (Kongsberg, 2019e)

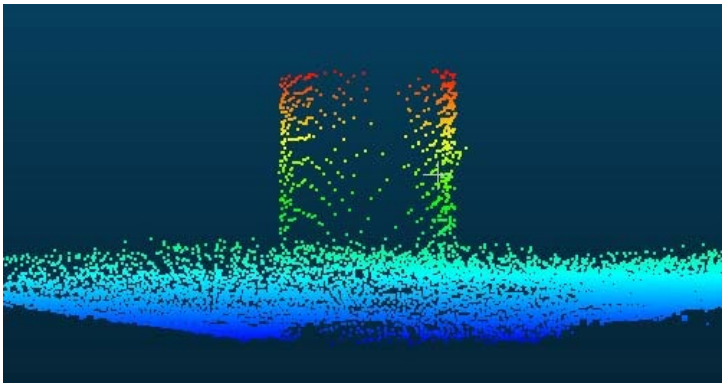

Figure 2.42. Data image of a north piling view (Kongsberg, 2019e)

Table 2.29. Benefits, limitations, and options for Kongsberg dual axis sonar

Apparent Benefits	Apparent Limitations	Options
• **Can operate in harsh conditions** • **Long term deployment** • **Covers large areas**		• MS1000 or standalone mode • Single or multiple distributed antenna system (DAS) heads

Micro Electro-Mechanical Systems (MEMS) Sensor Scour Monitoring: MEMS sensors are integrated with wireless sensor networks that are used for monitoring real-time bridge scour depths. This type of

monitoring can process the scouring and deposition for structures and offer high accuracy for a relatively low cost. An interface is provided between the mechanical and electrical system. MEMS are integrated with the wireless Zigbee network on a sensor board which works for real-time bridge scour monitoring. This is a newly researched topic but has been shown to measure scouring/deposition processes and various water levels at a bridge pier (Lin et al., 2010).

Table 2.30. Benefits, limitations, and options for MEMS

Apparent Benefits	Apparent Limitations	Options
• **Accurate measurements of scour and depositions**	• New research	

Commercial sonar "fish finders": Many companies produce sonar-based "fish finder" products for recreational fishing. In addition to helping anglers to locate fish, these products also report water depth and other underwater conditions. While this technology is not intended for scour monitoring, it could conceivably be used for basic monitoring and for identifying bridges for more detailed evaluations. Automated mapping software is available as an add-on feature for some fish finder products. An example product is the Hummingbird Solix (**Figure 2.43**) which can be combined with proprietary AutoChart mapping software. One limitation of AutoChart is that the data are not compatible with CAD software used by bridge engineers (Ross, 2019).

Figure 2.43. Display unit for Hummingbird Solix (Hummingbird, 2020)

Table 2.31. Benefits, limitations, and options for commercial sonar products

Apparent Benefits	Apparent Limitations	Options
• **Lower cost than other technologies** • **Readily available**	• Not specifically intended for scour monitoring • Data from proprietary mapping software is not compatible with CAD programs	• Integrated mapping software

Summary

None of these products have been used by the state DOTs that we interviewed. Washington DOT has used a multibeam sonar for scour inspections, but it was from a different company than those listed. It is recommended that the Kongsberg MS 1171 and the multibeam sonars designed by Teledyne and Kongsberg be investigated for use. These products have multiple features as well as supporting software.

2.3. Approaches for Culvert Inspections

Culverts function primarily as hydraulic conduits, conveying water from one side of a roadway or similar traffic embankment to the other. Inspections for culverts are often limited, only assessing the ends. Using robotic technology for these inspections will allow the user to examine the inside of the culvert as well. The devices listed below consist of waterproof crawlers, tunnel profilers, and other types of technology that can travel into the culvert with video and camera footage to allow inspectors to better understand the condition. Previous evaluations of culvert inspection technologies have been conducted by the Minnesota Department of Transportation (Youngblood and Smith, 2017) and Ohio University (Masada et al., 2017)

In this report, the following robotic technologies were chosen to study the possibility for culvert inspection. The technologies are Super Droid SST2, Super Droid PTW-42-L 4WD, Super Droid SCT-32-W, Super Droid MLT-42, HIVE Product, and JPEG Mosaic Inspection. They were chosen because they have wireless control or have a long-tethered cable, and camera. They are maneuverable.

Teledyne BlueView T2250-360 Tunnel Profiler: This profiler has 360 degree profiling with data logging and real-time collection through Teledyne PDS software (an optional feature). This system is meant to be mounted on a Remotely Operated Underwater Vehicles (ROV) or Autonomous Underwater Vehicles (AUV) and is used for tunnel, pipe, or cave inspections. The tunnel profiler is a modular sensor and requires a vehicle of some sort to be attached for navigation through the pipe or culvert of interest. The product can be seen in **Figure 2.44** and a data image is shown in **Figure 2.45** (Teledyne Marine, 2019e).

Figure 2.44. Teledyne profiler (Teledyne Marine, 2019e)

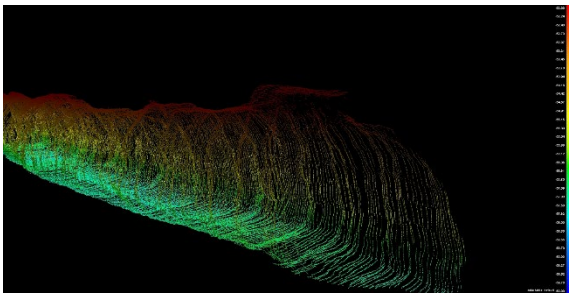

Figure 2.45. Teledyne profiler data image (Teledyne Marine, 2019e)

Table 2.32. Benefits, limitations, and options for Teledyne BlueView T2250-360 tunnel profiler

Apparent Benefits	Apparent Limitations	Options
• **Full 360 degrees of coverage** • **Real time display of data** • **High resolution**	• Requires a vehicle to provide movement through the culvert	• Optional Teledyne PDS software

SuperDroid SST2 Tracked Inspection Robot (with Pan and Tilt Camera): This is an all-terrain inspection robot designed for tight spaces like culverts. It features a wide view color camera that allows the operator to see in both dark and light settings. The camera has full coverage with pan and tilt. The robot is controlled using a standard one hundred-foot Ethernet cable connected to the robot and the operator using a controller. The vehicle can maneuver along most terrain and can change direction easily. An image of this product is shown in **Figure 2.46** (SuperDroid Robots, 2019a).

Figure 2.46. SuperDroid SST2 Robot (SuperDroid Robots, 2019a)

Table 2.33. Benefits, limitations, and options for SuperDroid SST2

Apparent Benefits	Apparent Limitations	Options
• **All-terrain vehicle** • **Designed for tight spaces** • **Full camera coverage**		• Different cable sizes available

SuperDroid PTW-42-L 4WD: This vehicle is made for all terrain and includes a scissor lift with a pan-tilt-zoom (PTZ) camera. The robot is controlled wirelessly but can also be tethered and has a colored video display. The PTW-42-L is useful for inspecting larger objects than culverts but can still be used if the culvert is large enough (**Figure 2.47**) (SuperDroid Robots, 2019b).

Figure 2.47. SuperDroid PTW-42-L 4WD (SuperDroid Robots, 2019b)

Table 2.34. Benefits, limitations, and options for SuperDroid PTW-42-L 4WD

Apparent Benefits	Apparent Limitations	Options
• **All-terrain vehicle** • **Full camera coverage**	• Useful for inspections with minimum obstructions	• Wireless or tethered

SuperDroid SCT-32-W Inspection Robot: This robot is specifically made for inspecting pipes and culverts. The camera has full pan and 90-degree tilt ability and has a camera installed on the back for reverse mode. The SCT-32-W is controlled with a tablet using wireless or tethered connections. The vehicle also includes LED lights that can be turned on and off to illuminate the view of the camera. The recommended tablet is a Microsoft Surface and with this the user can record the video display or take still pictures of the culvert. The SCT-32-W is designed to fit into culverts ten inches in diameter or larger. This product can be seen in **Figure 2.48** (SuperDroid Robots, 2019c).

Figure 2.48. SuperDroid SCT-32-W (SuperDroid Robots, 2019c)

Table 2.35. Benefits, limitations, and options for SuperDroid SCT-32-W

Apparent Benefits	Apparent Limitations	Options
• **Waterproof** • **Full camera coverage**	• Can only fit into pipes 10 inches in diameter or larger	• Wireless or tethered • Track configurations for narrow or larger pipes

SuperDroid MLT-42 Compact Inspection Robot: This robot is useful for tight spaces with low clearance height and has a camera with full pan and tilt. The MLT-42 can be controlled wirelessly or tethered with a maximum length of 500 feet. The tablet recommended for use is the Microsoft Surface and the operator can record the video display or take pictures of what is seen in color. This vehicle offers an encoder option which allows the user to track specific distances when something important is seen and it comes with LED lights to help improve sight in the culverts (**Figure 2.49**) (SuperDroid Robots, 2019d).

Figure 2.49. SuperDroid MLT-42 (SuperDroid Robots, 2019d)

Table 2.36. Benefits, limitations, and options for SuperDroid MLT-42

Apparent Benefits	Apparent Limitations	Options
• **Full camera coverage** • **Ease of use for tight spaces**	• Heavier than other Super Droid products mentioned	• Wireless or tethered

SuperDroid MLT-42 W Watertight Compact Inspection Robot: This vehicle is specifically designed for inspection of pipes and culverts with low clearance heights and is watertight. The camera has pan and tilt and the vehicle has LED lights for illumination. The MLT-42-W can be controlled wirelessly or with a tethered cable having a maximum length of 500 feet using a provided tablet that controls the vehicle and shows the video display (**Figure 2.50**) (SuperDroid Robots, 2019e).

Figure 2.50. SuperDroid MLT-42-W (SuperDroid Robots, 2019e)

Table 2.37. Benefits, limitations, and options for SuperDroid MLT-42 W

Apparent Benefits	Apparent Limitations	Options
• **Watertight** • **Full camera coverage**	• Heavier than other Super Droid products mentioned	• Wireless or tethered

Hydraulic Inspection Vehicle Explorer (HIVE) Camera Inspection: This is a lightweight alternative to the CCTV crawler that has onboard lighting and a video camera that can pan and tilt. It is remote controlled and has video imagery transmitted by Wi-Fi to a tablet. The crawler can travel over debris and is waterproof. This crawler does not have a counter to measure distances. An image of this product is shown in **Figure 2.51** (Minnesota DOT, 2016).

Figure 2.51. HIVE product (Minnesota DOT, 2016)

Table 2.38. Benefits, limitations, and options for HIVE

Apparent Benefits	Apparent Limitations	Options
• **Operated via radio control**	• Specialist required	

JPEG Mosaic Inspection/Sidewall Scanning: This crawler has camera rigs attached with a series of digital imaging cameras that can capture a continuous 360 degree image of the interior walls. These images are then post-processed and combined into a photographic model that the user can pan and zoom in the model to view the culvert. This is an accurate way to gain detailed documentation of the inside of the culvert. It is costly and not commonly used. A data image from this product is shown in **Figure 2.52** (Youngblood et al., 2017).

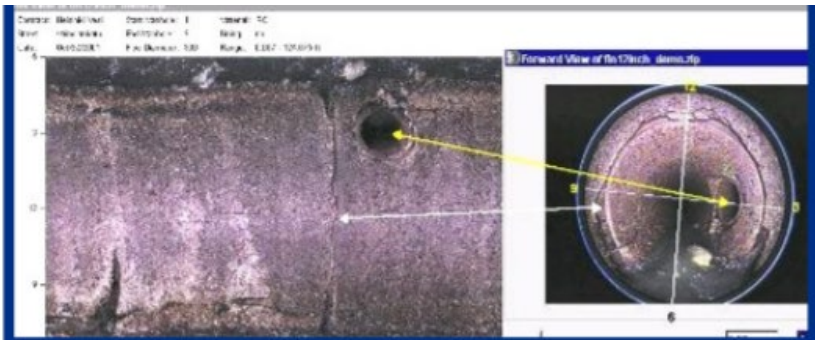

Figure 2.52. JPEG mosaic data image (Youngblood et al., 2017)

Table 2.39. Benefits, limitations, and options for JPEG Mosaic

Apparent Benefits	Apparent Limitations	Options
• **Detailed documentation**	• Emerging technology – not commonly used at this time	

Summary

None of the products described above have been used by the state DOTs that we interviewed. Washington DOT has used a tunnel profiler for culvert inspections but it is from a different company than those listed. It is recommended that the Super Droid SCT-32-W Inspection Robot and the Super Droid MLT-42 W Watertight Compact Inspection Robot be further investigated. These products have many desirable features like a 360-degree camera and a watertight vehicle as well as supporting software. All the listed technology appears to be applicable to culvert inspections.

2.4. State DOT Survey Results

The survey was conducted by interviewing employees from four different state departments of transportation with a set of survey questions (Table 2.39). The questions were not comprehensive but aimed to collect a snapshot of the DOTs work. The survey template can be seen below as well as the tabulated results. The purpose of this survey was to gather information from other state DOTs about inspections using drones, sonar, and technology for culverts. This information helped guide our research and recommendations for the product reviews.

Table 2.40. State DOT survey

DOT	Drones		Sonar		Culvert		Other
	Use	Research	Use	Research	Use	Research	
Washington		x	x		x		Ultrasound, Dye Penetration, Phased Array, Pachymeter, Ground Penetrating Radar, Infrared Camera
Florida		x		x			Infrared Camera, Brim Data Collector Software
Minnesota	x		x		x		Phased Array, Laser Ring Scanning, Hammer Sound Testing
Virginia		x				x	Gamma Ray Radiographic, Ground Penetrating Radar, Ultrasonic Pulse Echo

3. Laboratory Investigations

The aim of the demonstrations is to investigate technologies that may have potential for rapid evaluation of bridge components in the field. A realistic demonstration setup, composed of structural components, was assembled as a testbed.

3.1 Demonstration Setup and Components

The demonstration site was selected based on available space, consideration of surrounding buildings and trees, and proximity to the University of South Carolina Structures and Materials Laboratory. The University of South Carolina Biomass facility adjacent lot met the selection criteria. Bridge components were sourced from the SCDOT, Clemson University, and the University of South Carolina to be used during the demonstrations. Most components used in the demonstration were at one point used in bridges with various service lives. Each component had different defects including corrosion, cracking, and impact deformation. The setup was composed of two concrete double-T girders (**Figure 3.1**), two large steel beams (**Figure 3.2**), one small steel beam (**Figure 3.3**), and a prestressed concrete pile (**Figure 3.4**). All components were supported by concrete blocks or K-rails. The layout is represented in **Figure 3.5**.

Figure 3.1. Concrete double-tee girders

Figure 3.2. Large steel beams

Figure 3.3. Small steel beam

Figure 3.4. Concrete pile

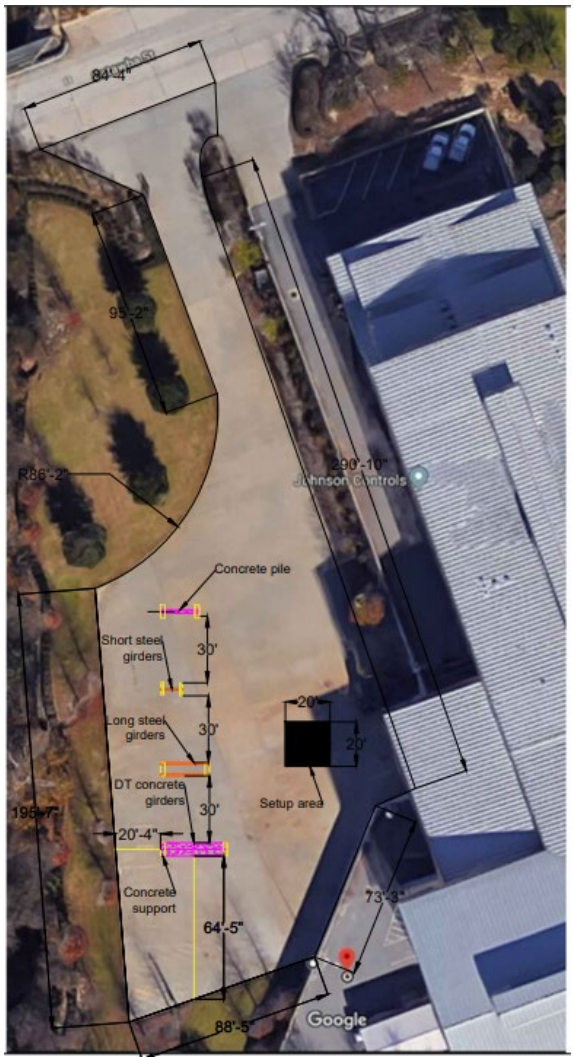

Figure 3.5. Demonstration layout

3.2 Technology Demonstration

Several manufacturers and vendors were contacted to assess interest in showcasing their drone systems and robotic technologies. Participants in the demonstration included Gresco UAS in partnership with DJI; Robotic Technologies of Tennessee; Bridge Diagnostics Inc. (BDI); Digital Aerolus; UAV Exploration; and FLIR. During the demonstration, each operator was given the opportunity to use their technology on components of their choosing to highlight the benefits of their system.

3.2.1. Drone Demonstration

Of the aerial drone systems discussed in the literature review, five were evaluated during the demonstrations and were piloted by vendors as well as by University of South Carolina researchers. Unmanned systems included Parrot Anafi; DJI Mavic Pro; TIG Hitco/McNair Drone; Digital Aerolus Aertos 120; and the DJI Matrice 210. Other drone systems mentioned in the literature review would have been

useful to assess, however, they were either unavailable for demonstration or cost prohibitive to purchase or rent.

Parrot Anafi: During the demonstration, the drone pilot flew the Anafi under every bridge component (**Figure 3.6**), getting within inches of the structural members and allowing for high quality photographs (**Figure 3.7**) and videos. The controls are easy to use, and the pilot commented on how intuitive the system was. The drone was stable with and without GPS enabled.

Some drawbacks noted during testing are the lack of collision avoidance sensors and no payload capacity for additional cameras and sensors. However, the system has since been outfitted with a set of propeller guards which greatly improve its ability to withstand contact during flight. Additionally, during testing an attempt was made to fly between the large steel beams with the GPS on. The beams created enough interference for the drone to begin veering to the side, strike a beam, and fall to the ground. It was not immediately clear how to disengage the GPS system to allow the system to fly between the beams and further investigation/testing is needed to verify the capabilities of tight proximity flight. Propeller guards and a tablet mount for the controller have been used successfully to further improve the Anafi's effectiveness for inspection.

Figure 3.6. Parrot Anafi flying under steel beams

Figure 3.7. View from below double-tee girders

DJI Mavic Pro: The system appeared to have an issue with the navigation system during the early stages of the demonstration and needed to be calibrated several times to allow it to fly properly (**Figure 3.8**). The pilot was unable to take pictures of the bottom side of the bridge components due to the lack of an upward facing camera, which limited the effectiveness of an otherwise promising system.

Figure 3.8. Mavic Pro observing steel beams

McNair Center/TIG Hitco Drone: Wout DeBacker and Arturs Burgs of the McNAIR Center for Aerospace Innovation and Research and TIG Hitco respectively, brought a custom drone system to demonstrate (**Figure 3.9**). There were some technical problems with the onboard navigation system that would eventually impact most of the drones and prevented a proper demonstration of this system.

Figure 3.9. McNair/TIG HItco Drone

Aertos 120: Representatives from Digital Aerolus demonstrated the capabilities of the Aertos 120, which represented the most robust aerial option for visual inspection at the demo (**Figure 3.10**). To showcase this, the pilot intentionally struck the bridge components repeatedly (**Figure 3.11**). The system endured many collisions and hard landings without sustaining damage.

Since it does not use GPS for navigation, it was able to navigate down a narrow section between the two steel beams, contacting the sides as it went along and returning unscathed (**Figure 3.12**). This function would be useful when navigating the tight spaces between structural members under a bridge as well as the confined space of a culvert. Notable drawbacks are low flight time, high noise level, high cost, and the apparent difficulty to pilot as it appears to be far less stable than commercial drone systems.

Figure 3.10. Aertos 120

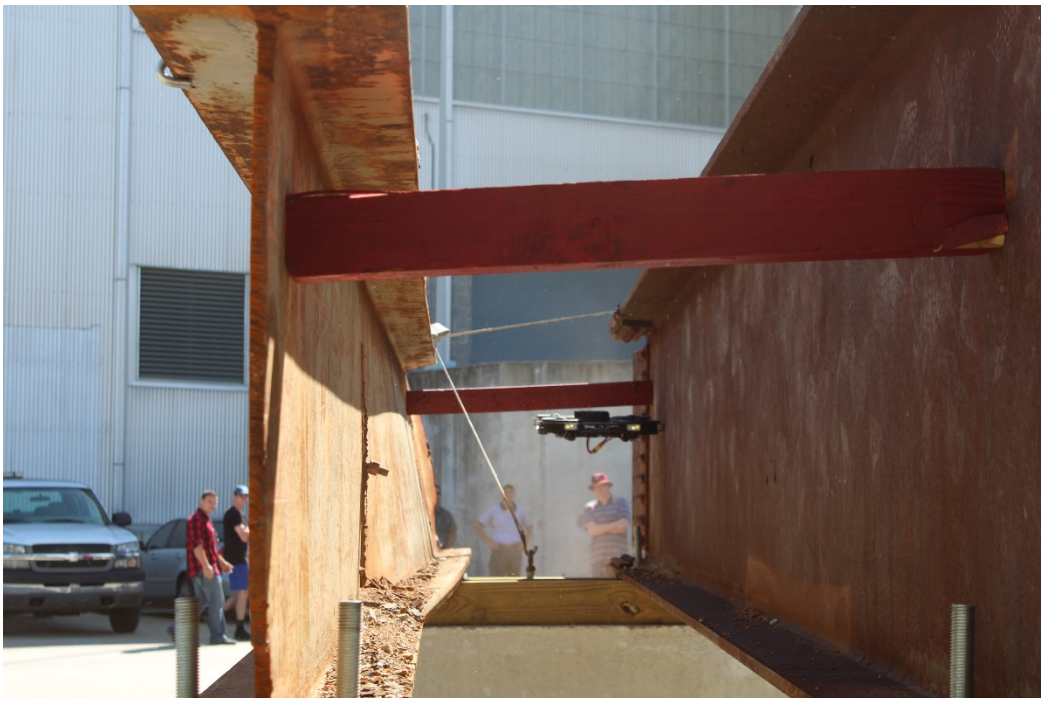

Figure 3.11. Aertos 120 navigating the tight space between two steel beams

Figure 3.12. Aertos 120 striking beam supports

DJI Matrice 210: Gresco and US Aerial Video demonstrated the DJI Matrice 210. The drone offers payload options of a single camera on the bottom, two cameras on the bottom, and a single camera on top. The double lower mount was demonstrated by Gresco and the single upper mount was demonstrated by US Aerial Video. In both cases the cameras demonstrated were the DJI Flir XT which is a 640 x 512 resolution thermal imaging camera, and the DJI Zenmuse Z30 which is a visible light camera with 30x optical zoom capability. The impressive capability of the camera is showcased in **Figure 3.13** and **Figure 3.14** where the former is an image of the position of the drone when the latter image was taken.

Despite the lower mount for the cameras, the system showed promise in capturing excellent footage of the bridge components from below. The Z30 camera was particularly impressive due to the offset which it allowed the user to have from the area of interest (**Figure 3.14**). An XT2 Camera system was also present, which is a combination of visual and infrared cameras, allowing for simultaneous capture of footage (**Figure 3.15**).

The top mount camera allowed for an impressive view of objects overhead, but the view of objects below was obstructed by the frame and propellers. Ideally, an operator would have the ability to view above and below the drone when needed without changing payload frames.

For comparison purposes, some images were taken from a 1x and then a 30x zoomed perspective (**Figure 3.16** and **Figure 3.17**).

The M210 system also allows for a pilot and an inspector to simultaneously operate the drone. The pilot can control the drone using the FPV camera, and the inspector can control the payload cameras to take

pictures of areas of interest (**Figure 3.18**). Potential drawbacks of the system are cost, size, and a lack of a collision avoidance system, which makes the two former issues more of a concern.

Figure 3.13. Matrice 210 line of sight view

Figure 3.14. View from Matrice 210, Zenmuse Z30 (30x zoom)

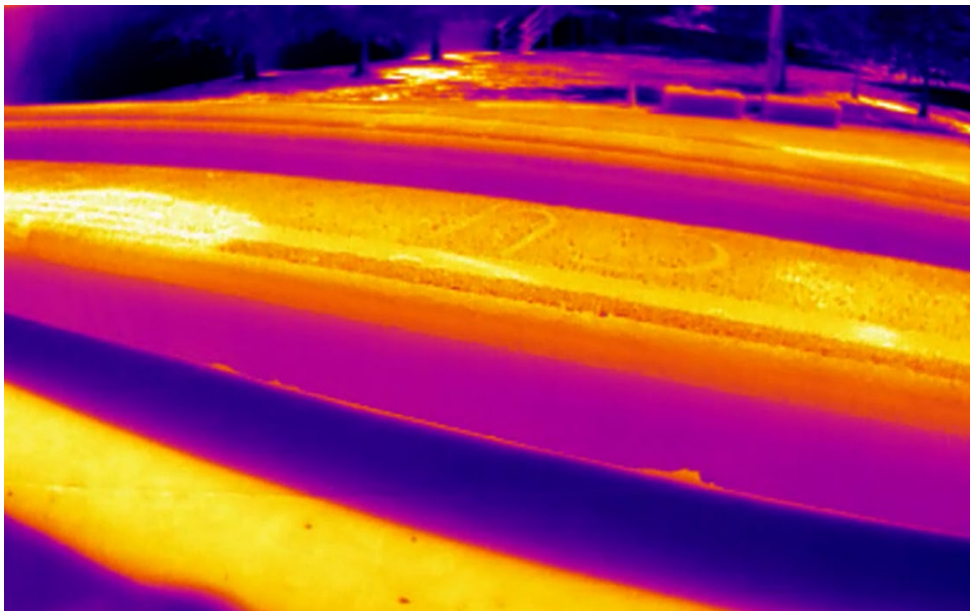

Figure 3.15. Matrice 210 with XT2 camera system (screenshot of recording)

Figure 3.16. Zenmuse Z30 1.0x magnification

Figure 3.17. Zenmuse Z30 30x magnification

Figure 3.18. A representative from US Aerial Video pilots the drone while a researcher acts as the inspector with control of the camera payload

3.2.2. Crawler Robot Demonstration

The Robotics portion of the demonstration was performed by Robotic Technologies of Tennessee. The representatives brought two robotic platforms a) a magnetic crawler robot dubbed the MRIS-MN1 for steel components, and b) a crawler robot which uses vacuum to remain attached to all components (steel and concrete surfaces).

RTT MRIS-MN1: This crawler system is tethered, which allows it to run nearly indefinitely, as well as providing direct contact with onboard sensory equipment and cameras (**Figure 3.19**). The tether does present some inherent drawbacks for bridge inspection, and it did snag on some exposed fasteners. Additionally, the tether limits the distance that the robot can be from the operator. Wireless operating capability would significantly enhance the effectiveness of this crawler for bridge inspection.

Figure 3.19. RTT MRIS-MN1 on steel beam

RTT Vacuum Robotic Prototype: Unlike the MRIS-MN1 system, the vacuum prototype robotic system can bond to any surface which allows a seal to be formed, and the robot is then held up by air pressure (**Figure 3.20** and **Figure 3.21**). Concrete and steel surfaces were both effectively demonstrated. It is mentioned that a gap in the material, such as during a transition, may be enough to cause the robot to lose its bond. There are no sensory provisions yet adapted to the system as it is in the development and demonstration phase. As with the MRIS-MN1, the system is tethered both by control wires and a vacuum hose. A similar system with an onboard pump and wireless operation may be well-suited for inspection of many structures.

Figure 3.20. RTT vacuum prototype on double-tee concrete girder

Figure 3.21. RTT vacuum prototype operating under double-tee concrete girder

3.2.3. NDE Sensory Equipment Demonstration

Bridge Diagnostics Inc. (BDI) brought several nondestructive examination options to the demonstration including terrestrial infrared thermography, ground penetrating radar (GPR), and ultrasonic thickness testing. Unfortunately, there were no images shared or recommendations given from the terrestrial infrared thermography portion of the demonstration and it is excluded from this section.

Ground Penetrating Radar: The GPR hardware (GSSR SIR 3000) (**Figure 3.22**) was able to identify reinforcement locations in the double-tee and pile specimens. The output of the scanner is a graphical representation of wave reflections in real time. From this, the relative location in distance traversed from starting point and the depth at which the reinforcement lies are shown. With a known starting point, a map of the reinforcement may be developed for existing structures where this information is not known.

Figure 3.22. Shane Boone demonstrating GPR hardware on concrete double-tee girder

Ultrasonic Thickness Testing: The ultrasonic thickness testing was conducted with an MG2-XT Gauge (**Figure 3.23**). The large steel beams were used for this test (see **Figure 3.24**) as well as a calibration block to demonstrate the accuracy of the system. During the calibration process, the system output value was within 0.001” of the expected output. (actual value: 0.200”, tested value: 0.200”). Defects within the steel would have shown as an additional reflection point in the output waveform. No defects were identified in the specimens with the gauge as it requires a clean surface for accurate measurement, and the surface of the beams were quite corroded. This limitation indicates the gauge may not be effective in the field without surface preparation.

Figure 3.23. Olympus MG2-XT ultrasonic thickness gauge, photo credit: Shane Boone, BDI

Figure 3.24. Demonstration of ultrasonic thickness gauge on steel beam.

4. Field Investigations

Four in-service bridges were selected to investigate technologies that may have potential for rapid evaluation of bridges. The sites were chosen based on potential for technology application; low traffic to avoid impacting traffic flow; and differing superstructure types. The four bridges are referred to as Highway 378 Bridge Construction site, SC Highway 105 Pacolet River Bridge, Parr Shoals Reservoir Bush River Road Bridge, and HWY 601 Congaree Bridge.

Highway 378 Bridge Construction Site: This bridge is in Lexington SC, between the intersections of State Rd S-32-46/HWY 378 and Front Street/HWY 378 (**Figure 4.1**). The construction of a new bridge parallel to the current bridge made access convenient and presented a good opportunity to investigate capabilities of the Parrot Anafi. A boat dock located 20 yards (18.3 m) south of the bridge was used for the launch location. The drone approached the bridge from the south and took photographs and video of areas where damage was noted.

Because the bridge was low the operator was able to remain relatively close to the drone and maintain good line of sight. As the inspection began it was clear that the ability to move such a small drone around the equipment was necessary, as larger drones would be a distraction to work and a potential danger to the crew (**Figure 4.3**). Images of cracks were taken from several angles on plane with the bridge (**Figure 4.4**).

Figure 4.1. Map of Highway 378 Bridge over Lake Murray, photo credit: google maps

Figure 4.2. View of bridge from take-off location

Figure 4.3. Inspection area of interest (to the right of machinery)

Figure 4.4. Exterior girder (outer surface)

After inspection of the exterior girder the operator moved the drone under the bridge to inspect the interior girders, beams, and deck. Cracks and delamination were observed on many of the structural members located near the eastern support. While these defects are visible from the ground on the bank, similar defects on a taller bridge (or defects above supports further away from the bank) would not be visible or easily accessible (**Figure 4.5** and **Figure 4.6**).

Figure 4.5. Exterior girder (inner surface)

Figure 4.6. Cracking and corrosion (interior girder)

The drone performed well when the system was approximately 18 in (7.1 inches). or more away from the deck. When moving the drone closer, the system experienced GPS interference which negatively impacted stability. The stability issues led to the decision to purchase propeller guards for subsequent site visits. Despite the proximity restrictions, the drone accessed areas under the bridge and obtained high fidelity images of damaged areas. It was clear that battery life, although comparable to other off-the-shelf options, was still a limiting factor for extensive inspections.

SC Highway 105 Pacolet River Bridge*:* This bridge is located near York, SC, where Mt. Taber Church Road becomes Skull Shoals Road (**Figure 4.7)**. The bridge was selected based on the combination of steel and concrete sections, low traffic, and ease of access. A view of the bridge from the access road is shown in **Figure 4.8**.

The corrosion seen in **Figure 4.9** was not visible from the ground as it was obscured by the concrete supports. Visual investigation of such a defect would require a boom or snooper truck for access in the absence of a drone. Delamination as shown in **Figure 4.10** was visible from the ground station, but the areas of development were less noticeable and the Parrot Anafi drone allowed for close investigation.

The inspection of the Pacolet River bridge highlighted the benefits of the system. The previous site inspection was a low bridge and the system had not yet been equipped with the propeller guards and an additional battery pack. With the equipment now upgraded, proximity to the bridge was no longer an issue. The drone was able to get close enough to the deck to observe cracks which could not be seen from the ground (**Figure 4.11**) and obtain closeup footage of defects. One limitation of the technology is the inability to determine the location of a defect without distinguishing features in the image. Potential

solutions to remedy this are: a) intentionally frame a photograph to include distinguishing features, or b) use video instead of photographs to search for defects, so that the position can be tracked.

Figure 4.7. SC HWY 105 Pacolet River Bridge

Figure 4.8. SC HWY 105 Pacolet River Bridge (launch location)

Figure 4.9. Drone image of corrosion on steel superstructure

Figure 4.10. Delamination and crack development in SC HWY 105 Pacolet River Bridge

Figure 4.11. Image taken from drone recording (overhead view) of cracks in bridge deck

Parr Shoals Reservoir Bush River Road Bridge: The primary benefit of this location is the presence of a boat ramp near the bridge (**Figure 4.12**), which was necessary to accommodate autonomous kayaks outfitted with sonar and GPS guidance. The site may experience large changes in water level throughout the day. Testing of the kayaks went well and the group was able to perform manned and unmanned missions. Drone footage was taken of the kayak testing and of the nearby bridge (**Figure 4.13**, **Figure 4.14**, **Figure 4.15**, **Figure 4.16**).

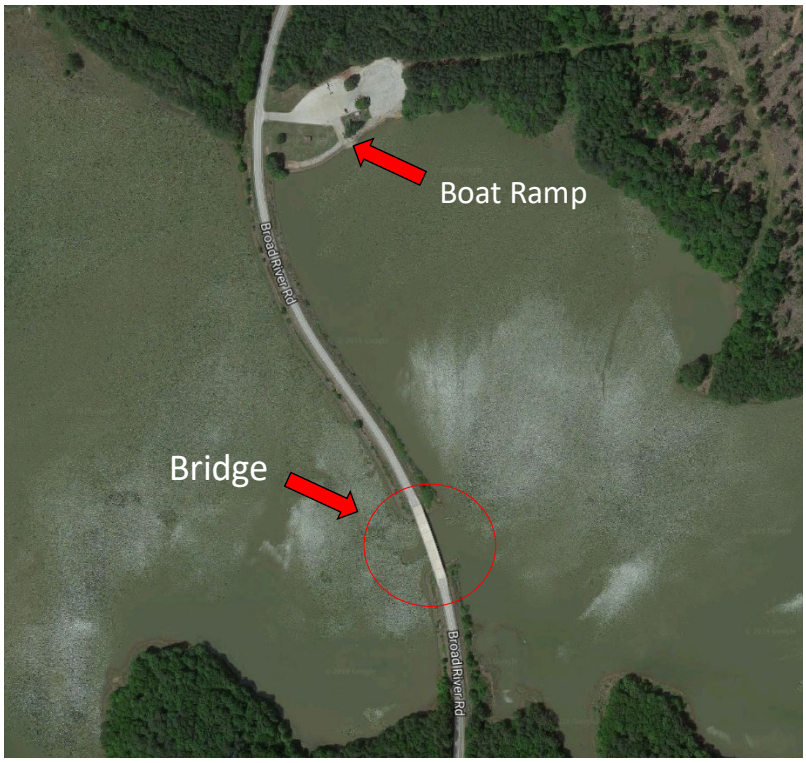

Figure 4.12. Parr Shoals Reservoir showing bridge and boat ramp

Figure 4.13. Under bridge view from Parrot Anafi drone

Figure 4.14. Aerial view of the bridge intended for investigation (note the water line)

Figure 4.15. View of Parr Shoals Reservoir and autonomous kayak (yellow)

Figure 4.16. Autonomous kayak navigating the reservoir

HWY 601 Congaree Bridge: This site, shown in **Figure 4.17**, served as the primary demonstration location for the autonomous kayak system equipped with sonar equipment to capture information from the riverbed and linking to the GPS location. Post-processing of the data can generate a topological map of the riverbed, which is useful for monitoring the development of scour as well as accrual of debris. Supplementing the autonomous kayaks is a HEX H2O drone (Figure 4.18) which is water-proof and capable of taking off from, and landing in, water. The eventual goal of the system is to allow the kayaks to act as a carrier of the drone while conducting their own data acquisition.

The team demonstrated the autonomous and manned capabilities of the kayaks, as well as the capability of the drone to take off and land in water. No demonstration was shown of the drone landing on the kayaks, which is a process still under development by the research group. The demo started with discussions of the capabilities of the kayak and expected applications (**Figure 4.19**). **Figure 4.20** shows the kayak embarking in autonomous mode.

In regard to observations of the superstructure, a gap was noticed between a build-up and a prestressed rod baseplate as shown in **Figure 4.21**. The observation was made with the parrot Anafi drone, and this was used as an opportunity to test the proximity tolerance when deprived of GPS. The pilot was able to navigate the drone safely within two feet of the defect and take additional photographs. During the drone inspections the birds began to swarm the drones. While this did not negatively impact the drones or the field test, a mid-air collision with a bird may be inevitable in the future. Precautions should be taken to avoid loss of equipment and harm to wildlife such as the use of a small drone with floatation capabilities.

Figure 4.17. HWY 601 Congaree River Bridge

Figure 4.18. HEX H2O drone (capable of landing on and taking off from water)

Figure 4.19. Explanation of autonomous kayak capabilities and expected applications

Figure 4.20. Kayak embarking in autonomous mode

Figure 4.21. Image of superstructure with loose baseplate (taken by Parrot Anafi drone)

5. Live Load Testing

Monitoring the current condition and deterioration of bridges is critical to the service life evaluation process. To establish the condition and deterioration, nondestructive evaluation (NDE) methods and Live Load testing can be utilized. Both can be conducted on in-service bridges. When implemented, these techniques allow for the accurate determination of bridge condition and thereby provide guidance for determining further courses of action.

For the selection of NDE techniques several factors must be considered such as the type of structure, existing condition, cost of implementation, availability of hardware, ease of installation, accuracy, and ability to analyze the data (specialized software and training). Although visual inspection is primarily used in the United States, it is not well suited for identification of hidden defects and damage, as well as those which are in areas not easily accessed (Hadzor et al. 2011). NDE techniques have been implemented in many industries to evaluate the properties of a materials, components, and systems without decreasing service life impacting its usefulness and have proven to be a viable alternative to more traditional visual inspection methods (Cartz 1995). When evaluating shear strength many different NDE sensors and techniques have been used including Digital Image Correlation (DIC) (Küntz et al. 2006; Yoneyama et al. 2007); Demec Points (De Silva et al. 2008; Zakaria et al. 2009); Linear Variable Differential Transformers (LVDTs) oriented at 90° to each other (Jain, and Singh 2016); and Acoustic Emission (AE) (Tinkey et al. 2002; Ohno and Ohtsu 2010; ElBatanouny et al 2014a; Anay et al. 2015). AE monitoring when used in conjunction with other methods can offer a more complete evaluation, and in some cases is well suited for the evaluation of older bridges and other structures (Golaski et al. 2002; Anay et al. 2015; Hadzor et al. 2011; and Swit, 2018).

Load tests of reinforced and prestressed concrete bridges in different states of deterioration have been performed and documented with loading conditions such as regular traffic, loaded trucks, and overloads. Live Load testing is performed to determine certain response characteristics of bridges such as load distribution, verify and adjust predictions from an analytical model, and determine the influence of damage. Unknown reserves of capacity and previously ignored composite action can also be identified. Live Load tests serve to adjust the results from analytical models by imposing the bridge to loads outside of normal traffic but similar to service levels (ARCHES-D16 2009). Some of the main benefits of diagnostic load testing according to the MBE are as follows:

1. Analytical load rating can be verified. Many AASHTO equations are conservative in nature so the capacity of a bridge may be over (or under) estimated.
2. Load distribution for specific bridges can be found, these values are used in the load rating equations.
3. The influence of damaged and deteriorated members can be understood.

5.1. Description of Sites

A meeting was held with the SCDOT to select bridges for diagnostic load testing (Task 9) and load testing of two bridges has been completed (Task 10). Results are summarized in chapter 6. The purpose of the diagnostic test was to demonstrate the benefits of this type of testing for bridge evaluation and load rating.

The first bridge is US 221 over Hard Labor Creek near Greenwood, SC, and tested on July 31, 2019. The bridge was built in 1948 and was designed as four 30-foot-long simple spans for an H15 loading. Each span consists of four reinforced concrete T-beam, and the southern exterior span (exterior span 4) was selected for load test (see **Figure 5.1**). The bridge is two lanes wide without shoulders or emergency lanes and is cast-in-place T-Beam construction. The overall bridge width is 33.5 ft (10.21 m) while the roadway width is 26 ft (7.92 m). The beams are spaced 8 ft (2.43 m) apart and 21.5 in (0.54 m) tall concrete barriers are present on the roadway edges, each with a width of 10 in (0.25 m) (see **Figure 5.1**).

The second bridge is S-97 over Johnson Creek near Abbeville SC and was tested on November 5, 2019. The bridge was built in 1959 and designed as 8 – 15-foot-long simple spans for an H10 loading and the western interior span (interior span 2) was selected for load test (see **Figure 5.2**). Each span consists of four interior and two exterior panels (flat slabs with 9.25 in (0.23 m) thickness) supported by reinforced concrete pier cap and timber piles. The bridge is two lanes wide without shoulders or emergency lanes and the overall bridge width is 27.5 ft (8.38 m) while the roadway width is 26 ft (7.92 m). The panels are spaced 5.5 ft (1.67 m) apart while the piles are set apart 5'-10.5" (1.8 m). Concrete barriers of 12 in (0.3 m) tall are present on the roadway edges, each with a width of 8 in (0.2 m) at top and 9 in (0.22 m) at bottom (see **Figure 5.2**).

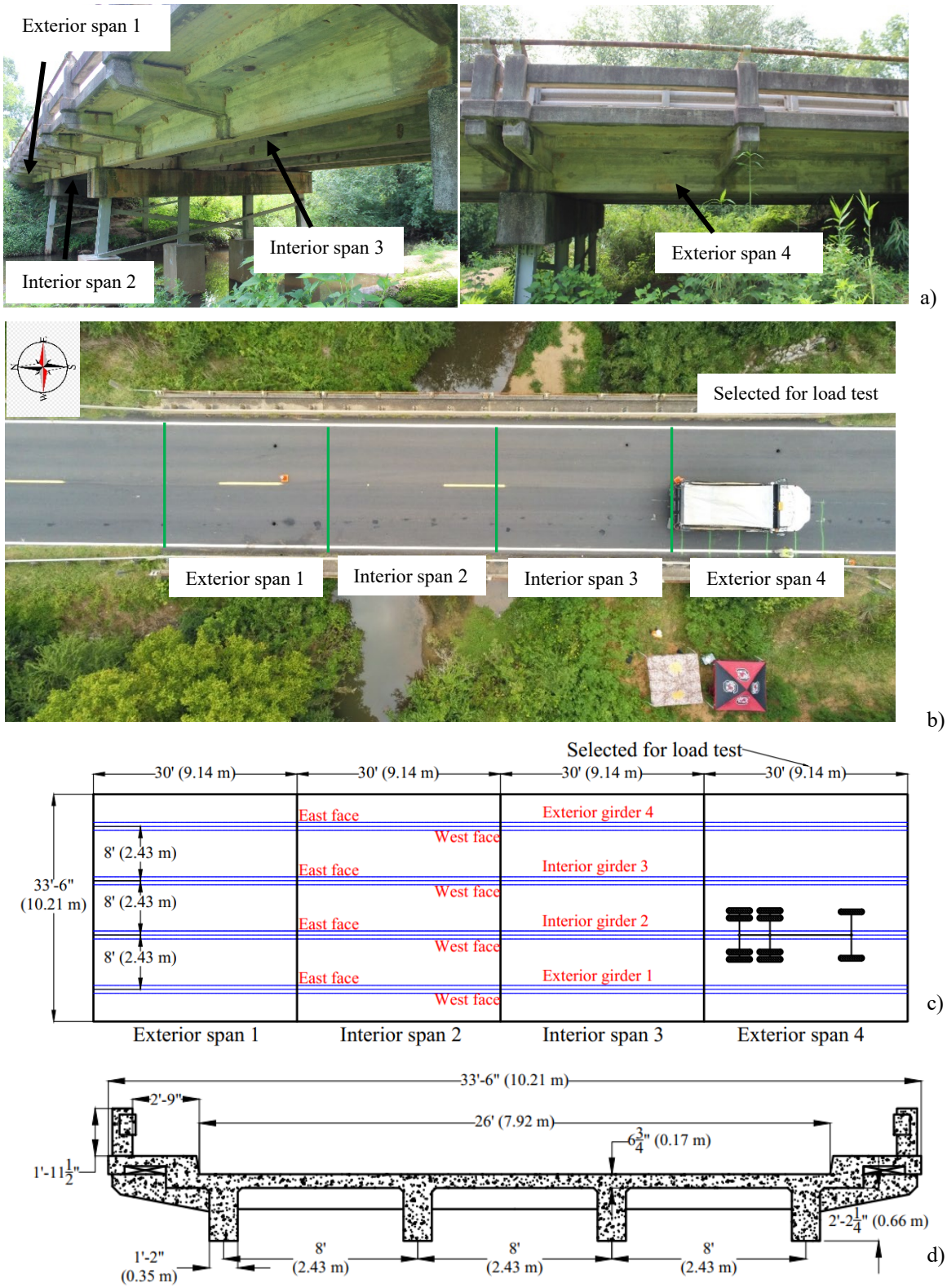

Figure 5.1. US 221 bridge details, a) photograph of the bridge, b) photograph taken by Parrot Anafi drone, c) plan view, d) cross section

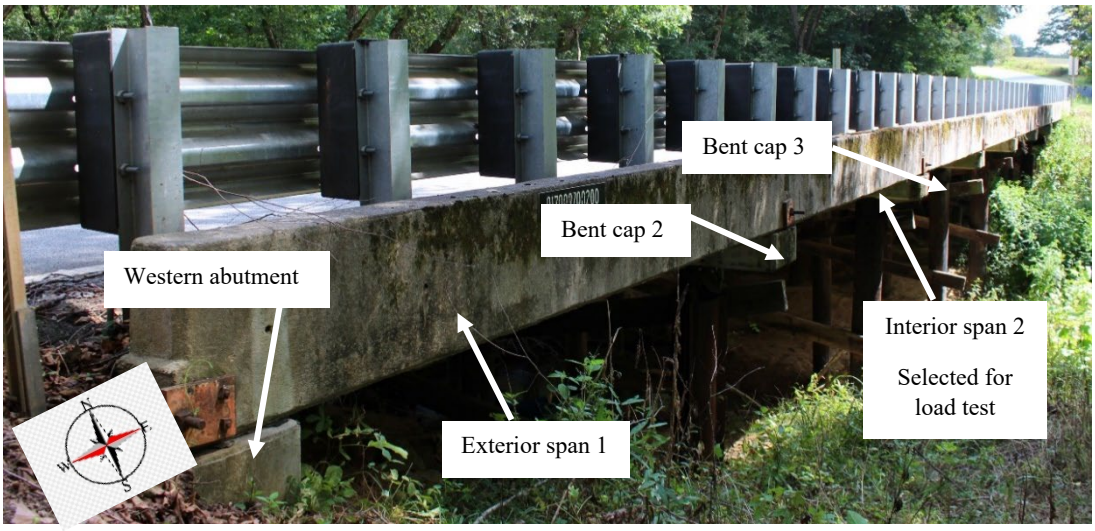

a)

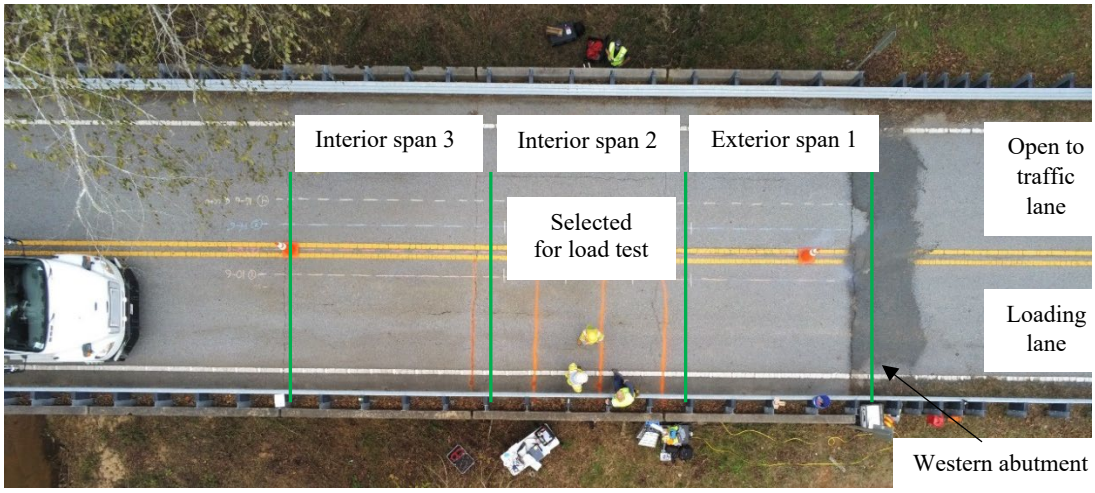

b)

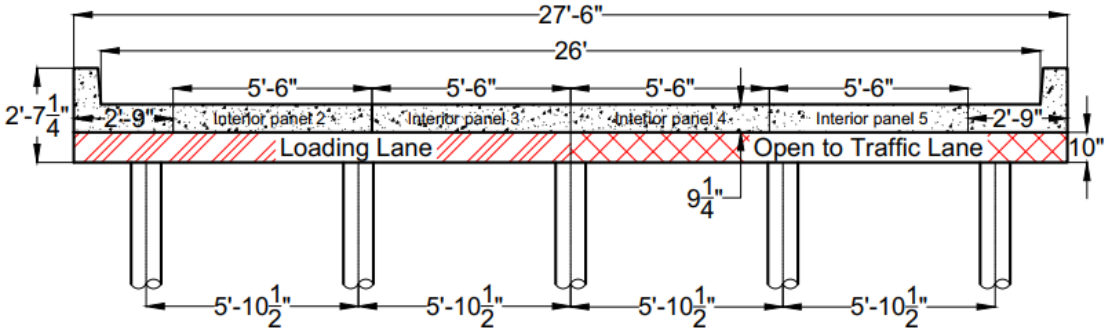

c)

Figure 5.2. S-97 Bridge details, a) photograph of the bridge, b) photograph taken by Parrot Anafi drone, c) cross section

5.2. Visual Inspection

5.2.1. US-221 over Hard Labor Creek Bridge

At the time of the load test (July 31, 2019), the most recent inspection had been performed on March 8, 2018 and the National Bridge Inventory (NBI) condition ratings were 6 for the deck and for the superstructure (satisfactory condition), and 4 for the substructure (poor condition) (on the NBI rating scale, the best condition possible is a 9). Flexural cracks have been seen throughout. The exterior span 4 was selected for the load test since the girders showed more extensive cracking than other spans, and the girders are more easily accessible. **Figure 5.3** shows examples of the visible flexural cracks near the midspan of interior girders. In general, the interior girders showed more cracking than the exterior girders. This data analysis is focused on AE and strain data collected from the sensors attached to interior girders 2 and 3, and crack opening displacement data collected form girders 1, 2 and 3.

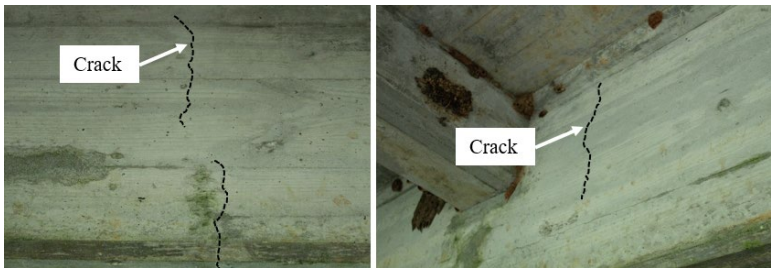

Figure 5.3. Visible cracks near to the midspan of interior girders

5.2.2. S-97 over Johnson Creek Bridge

At the time of the load test (November 5, 2019), the most recent inspection had been performed on November 14, 2018 and the National Bridge Inventory (NBI) condition ratings were 5 for the deck and for the superstructure (satisfactory condition), and 4 for the substructure (poor condition) (on the NBI rating scale, the best condition possible is a 9). Flexural cracks have been seen throughout. The interior span 2 (from the western side of the bridge) was selected for the load test since the panels showed extensive cracking and they are more easily accessible that other spans. **Figure 5.4** shows examples of the visible flexural cracks near the midspan of interior panels. In general, the interior panels showed more cracking than the exterior panels. This report focuses on: a) the AE data collected from the sensors attached to interior panels 2 and 3 and the AE sensors attached on the bent cap 2 (between exterior span 1 and interior span 2) ; b) strain, deflection and acceleration data collected form all panels in interior span 2 and bent cap 2; and c) crack opening displacement data collected form interior panels 2 and 3.

Figure 5.4. Visible cracks near to the midspan of interior panels (interior span 2)

5.3. Experimental Program and Instrumentation

5.3.1. Instrumentation

US-221 over Hard Labor Creek bridge: Truck loading was applied to the southern exterior span 4, and both interior girders in this span were instrumented with AE sensors (manufactured by MISTRAS Group, Inc., Princeton Junction, New Jersey). Two types of AE sensors were used; eight were WDI (broadband) and eight were R6i (resonant), with an operating frequency range between 100 – 900 kHz and 40 – 100 kHz, respectively. Double bubble epoxy was used as a coupling agent to affix sensors to the girders. Eight sensors were placed near the abutment of exterior span 4 in the shear region/support areas where no cracks have been developed (four on each interior girder), while the other eight sensors were placed near the midspan in the moment regions surrounding the existing cracks in a general layout to cover the cracked areas. AE sensors were divided into groups named as shown in **Table 5.1**. **Figure 5.5** shows the AE sensor layout; the red circles refer to resonant sensors (e.g., 1R where the 'R' stands for resonant) and the black squares refer to broadband sensors (e.g., 2B where the 'B' stands for broadband). Photographs of AE sensors groups attached on interior girders are shown in **Figure 5.6.** Sensor Highway II AE system (16-channel system manufactured by MISTRAS Group, Inc., Princeton Junction, New Jersey) was used to collect the data.

Six PI Displacement Transducer with the gauge length of 2 in. (50 mm) from Texas Measurements, Inc. were attached on girders 1, 2 and 3 (two on each girder) near to the midspan area surrounding visible flexural cracks (see **Figure 5.7**). The crack opening displacement data was recorded by the Model P3 Strain Indicator and Recorder from Vishay Precision Group.

For the live load test deflections and strains were continuously recorded using a wireless data acquisition system. Wire potentiometers and surface mounted strain transducers were used to measure the vertical displacement of individual slabs and bottom surface strains on the T-beams. Potentiometers and strain transducers were wirelessly connected to a data acquisition system, which logged data at 100 readings/second. In order to maximize the measured response all gages were placed at mid-span on each girder in the tested span. **Figure 5.8** shows a strain transducer attached on girder 3.

Table 5.1. AE sensor groups

Group number	Sensors numbers	Girder number/region	Girder face/Fig. 5.3
1	1R, 2R, 3B, 4B	Interior girder 2/moment	East face/Fig. 5.3a
2	9R, 10B, 11B, 12R	Interior girder 2/shear	East face/Fig. 5.3b
3	5R, 6B, 7B, 8R	Interior girder 3/moment	West face/Fig. 5.3c
4	13R, 14B, 15B, 16R	Interior girder 3/shear	West face/Fig. 5.3d

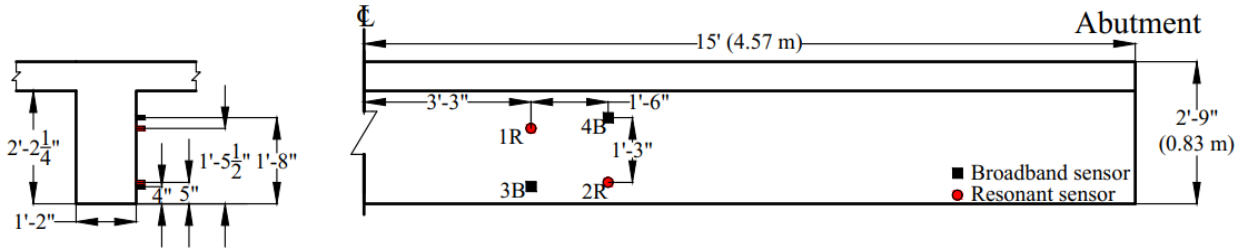

a) Interior girder 2 - moment region sensors - Group 1

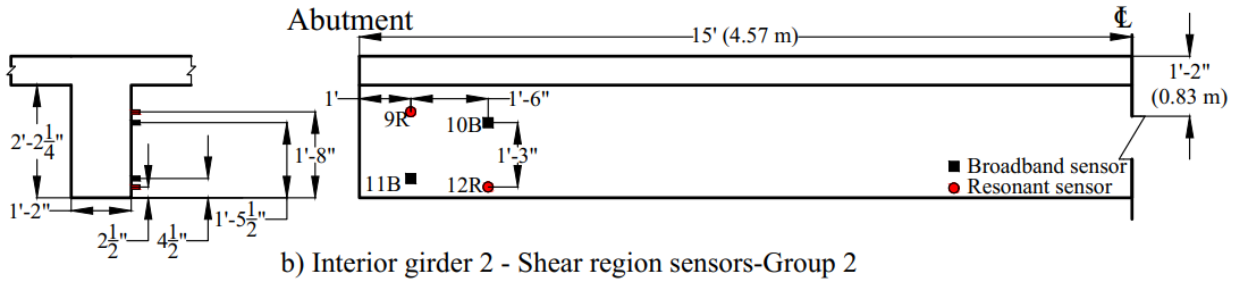

b) Interior girder 2 - Shear region sensors-Group 2

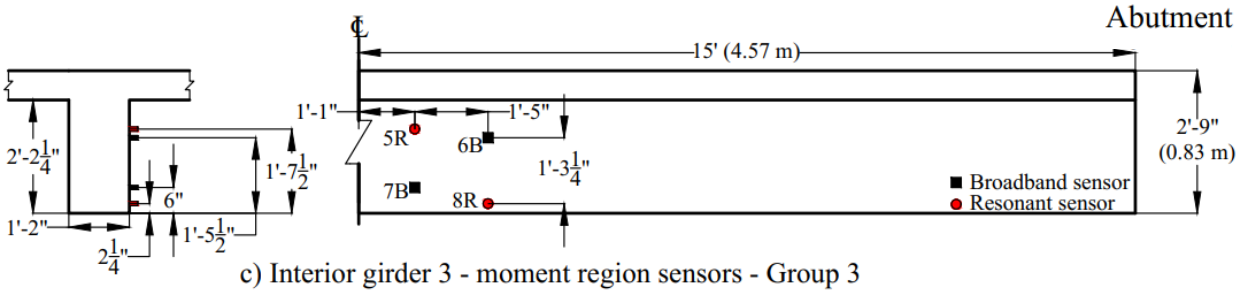

c) Interior girder 3 - moment region sensors - Group 3

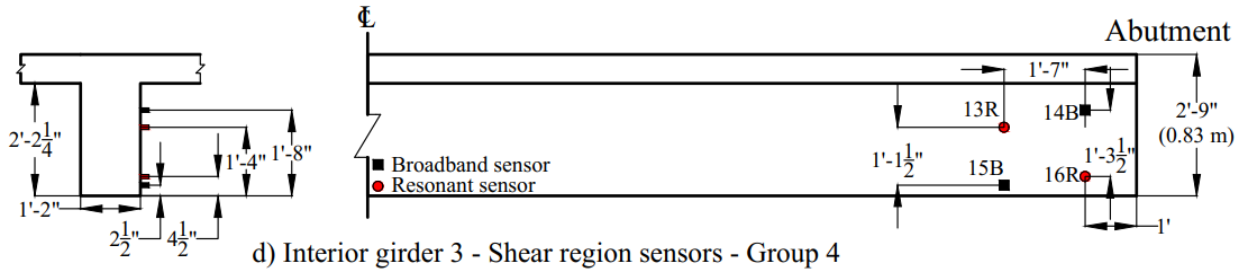

d) Interior girder 3 - Shear region sensors - Group 4

Figure 5.5. AE sensor layout

a) Interior girder 2

a) Interior girder 3

Figure 5.6. Photographs of AE sensor groups

Figure 5.7. PI gauge attached on interior girder 3 to measure crack opening displacement

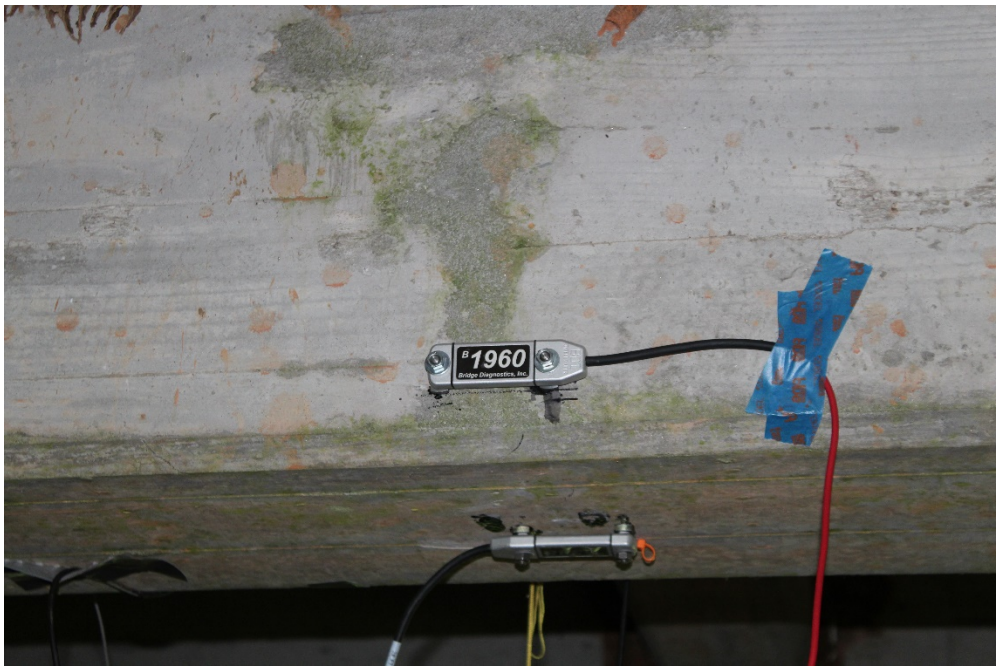

Figure 5.8. BDI strain gages attached on interior girder 3

S-97 over Johnson Creek bridge: Truck loading was applied to the northern interior span 2, and both interior panels in this span were instrumented with AE sensors (manufactured by MISTRAS Group, Inc., Princeton Junction, New Jersey). Two types of AE sensors were used; five were WDI (broadband) and nine were R6i (resonant), with an operating frequency range between 100 – 900 kHz and 40 – 100 kHz, respectively. Double bubble epoxy was used as a coupling agent to affix sensors to the panels and bent cap. Four and three sensors were placed near midspan of interior panels 2 and 3 (loaded lane panels) respectively. Additional two sensors were placed on interior panels 4 and 5 (open to traffic lane panels) where no cracks have been developed to work as guard sensors (one sensor per panel) (**a**). The other five sensors were placed near the midspan of bent cap 2 (**Figure 5.9. b**). AE sensors were divided into groups named as shown in **Table 5.2**. **Figure 5.9** shows the AE sensor layout; the circles refer to resonant sensors (e.g., 1R where the 'R' stands for resonant) and the squares refer to broadband sensors (e.g., 2B where the 'B' stands for broadband). Photographs of AE sensors groups attached on interior panels and bent cap 2 are shown in **Figure 5.10.** Sensor Highway II AE system (16-channel system manufactured by MISTRAS Group, Inc., Princeton Junction, New Jersey) was used to collect the data.

Four PI Displacement Transducer with the gauge length of 2 in. (50 mm) from Texas Measurements, Inc. were attached on interior panels 2 and 3 (two on each panel) near to the midspan area surrounding visible flexural cracks (see **Figure 5.11**). The crack opening displacement data was recorded by the Model P3 Strain Indicator and Recorder from Vishay Precision Group.

The deflections and strains were continuously recorded using a wireless data acquisition system. Strain gages from Bridge Diagnostic Inc. (BDI) were attached on all panels at midspan and bent caps 2 and 3. **Figure 5.12** shows some of the BDI strain sensors layout attached on the interior panels 2, 3 and bent cap 2, and **Figure 5.10** shows photograph of a strain gauge attached on bent cap 2.

For the Live Load tests deflections were continuously recorded using a wireless data acquisition system. Wire potentiometers were used to measure the vertical displacement of individual slabs. Potentiometers were wirelessly connected to a data acquisition system, which logged data at 100 readings/second. In order to maximize the measured response all gages were placed at mid-span on each girder in the tested span. **Figure 5.9** shows wire potentiometer locations for the Live Load test.

Table 5.2. AE sensor groups

Group number	Sensors numbers	Location description, Interior span 2	Figure No.
1	1R, 2B, 3R, 4B	Interior panel 2/moment region	5.10-a
2	5B, 6R, 7R	Interior panel 3/moment region	5.10-b
3	8R	Interior panel 4/moment region	5.10-c
4	9R	Interior panel 5/moment region	5.10-c
5	10R, 11R, 12B	Bent cap 2/moment region /exterior span	5.10-d
6	13R, 14B	Bent cap 2/moment region /interior span	5.10-e

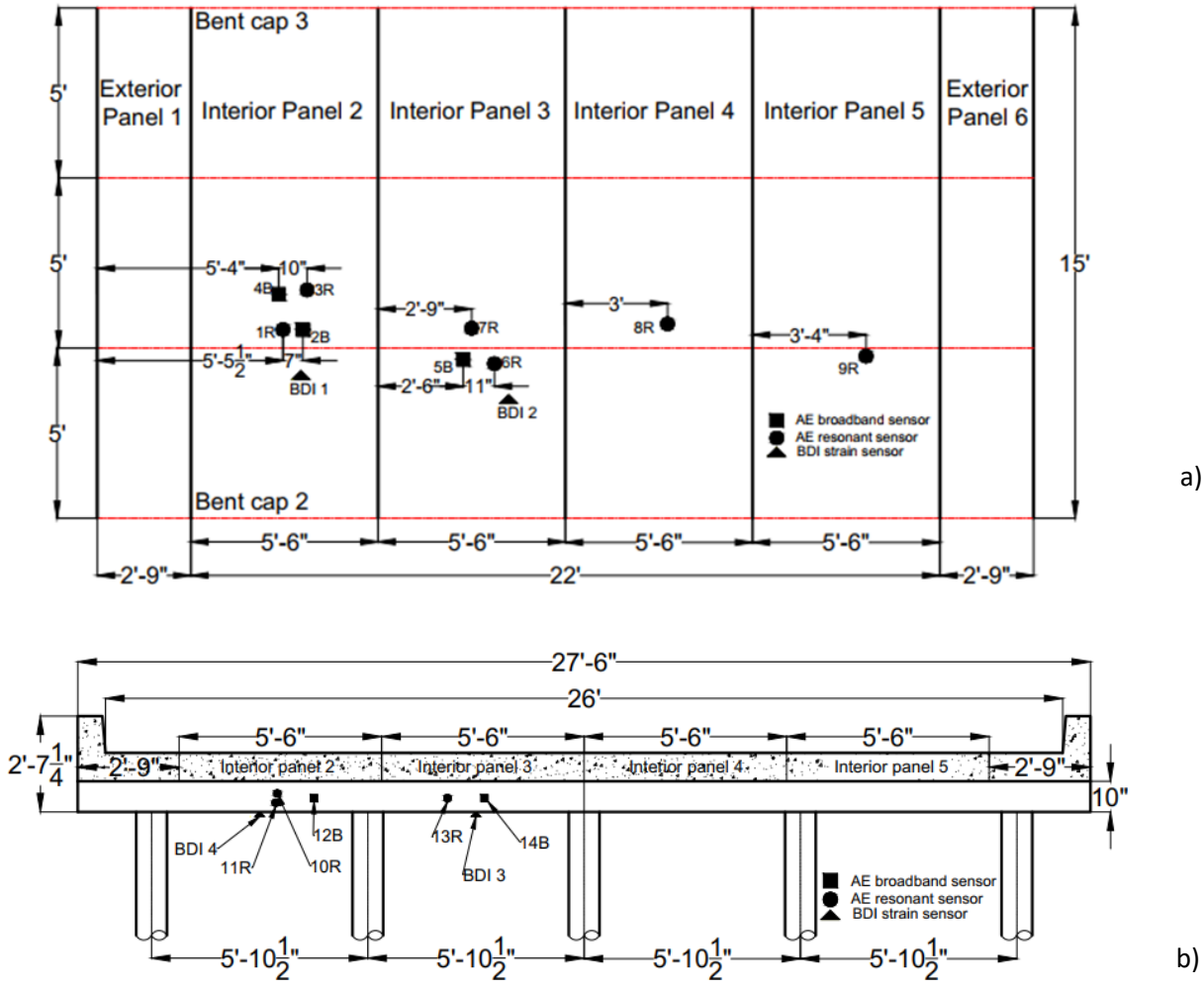

Figure 5.9. AE and BDI strain sensor layout, a) panels of interior span 2, b) bent cap 2

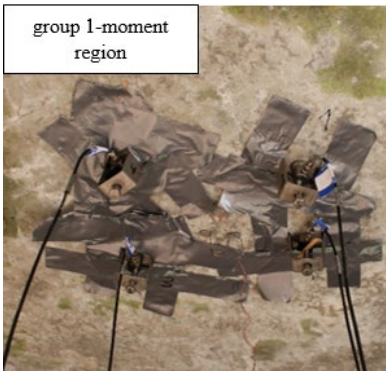

a) Interior panel 2

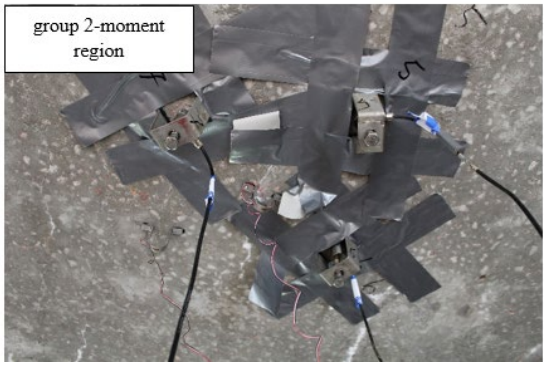

b) Interior panel 3

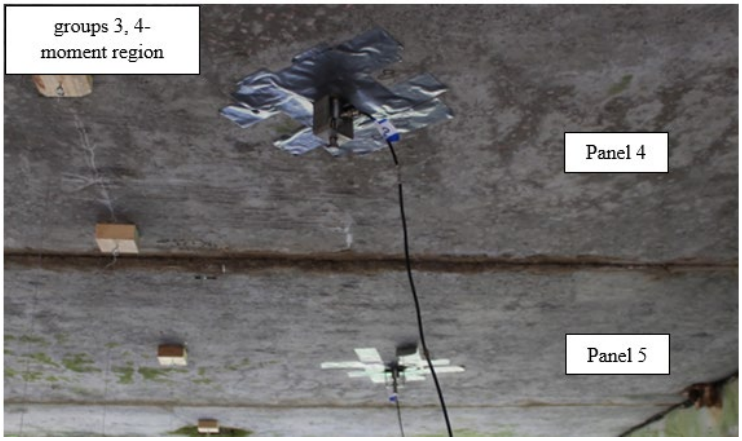

c) Interior panels 4 and 5

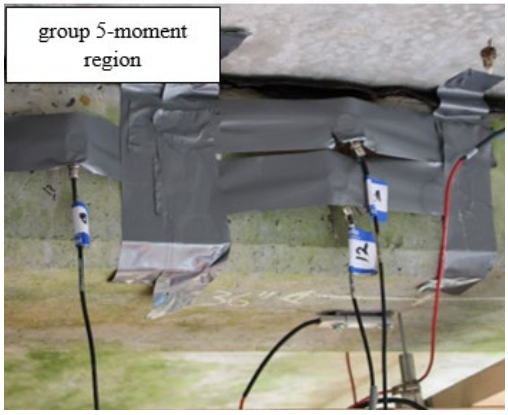

d) Bent cap 2, east face

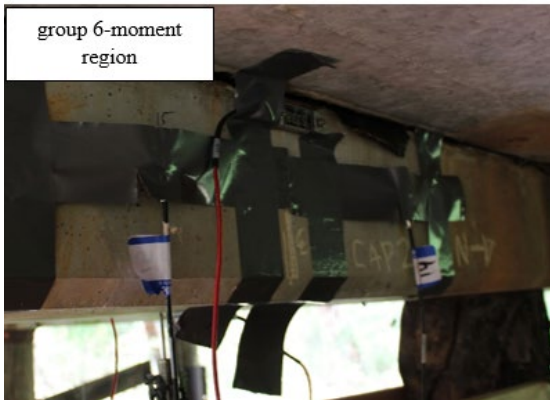

e) Bent cap 2, west face

Figure 5.10. Photographs of AE sensor groups

Figure 5.11. PI gauge attached on interior panel 2 to measure crack opening displacement

Figure 5.12. BDI strain gages attached on bent cap 2

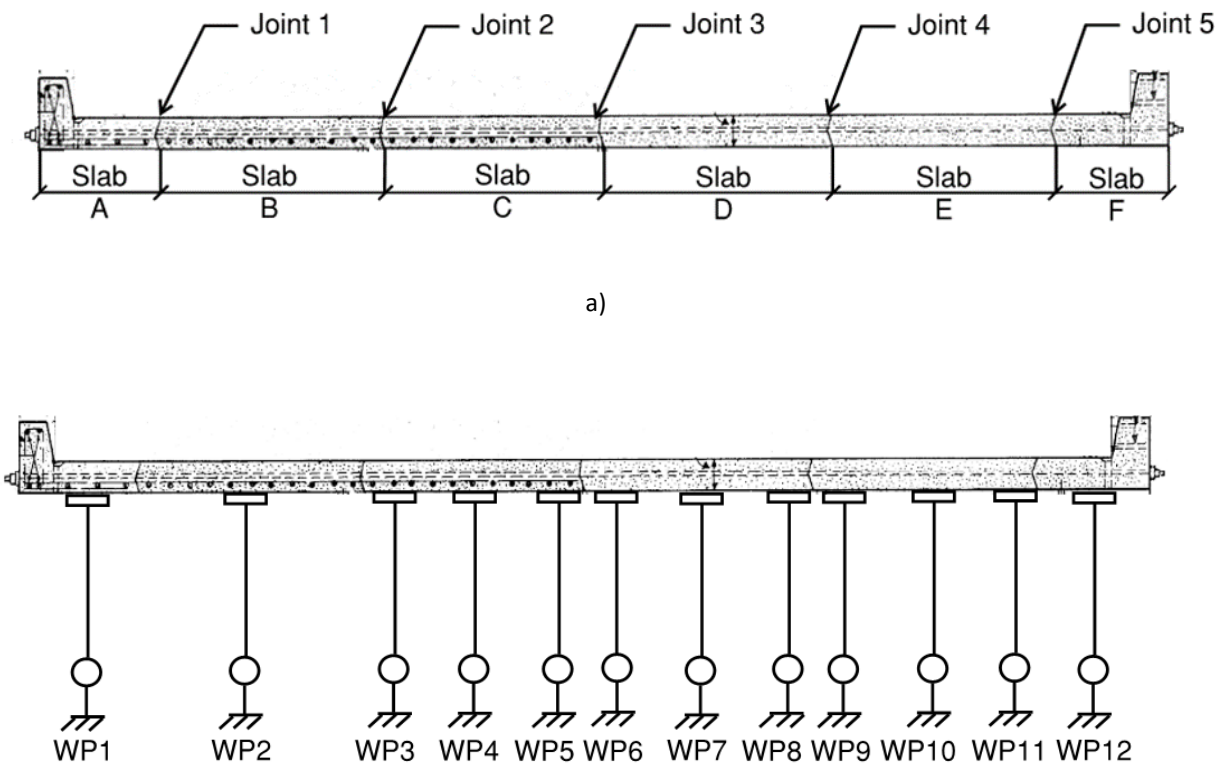

Figure 5.13. Bridge slab labeling (a) and wire potentiometer locations at mid-span (b)

5.3.2. Load Testing Protocol

US-221 over Hard Labor Creek bridge: Three different load trucks of varying size (supplied by SCDOT) were used during the test: light, medium, and heavy. The specific truck weights and dimensions are shown in **Figure 5.14**. Note that two heavy trucks were used for side-by-side loadings. The largest test trucks exceed the size of the H15 design truck.

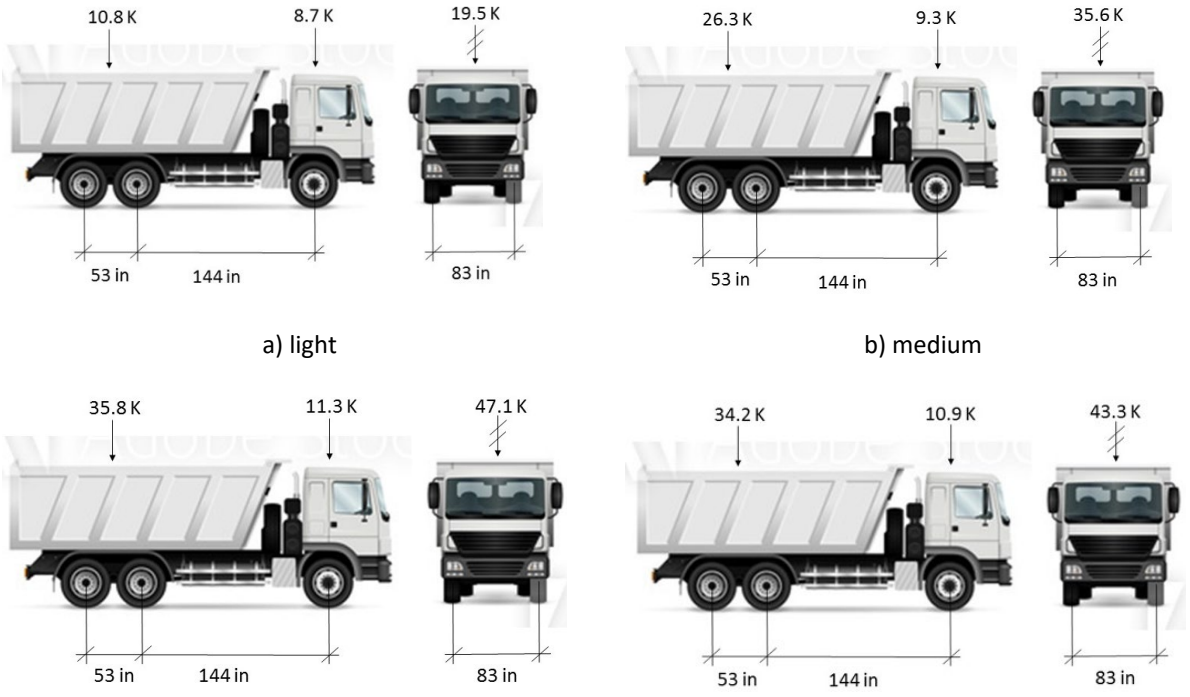

Figure 5.14. Load trucks

Two scenarios were used to drive the test truck longitudinally across the bridge while midspan vertical deflection, surface strain, crack opining displacement and AE signals were recorded on the interior span 2. First, the truck was driven at slow speeds along the bridge, and second, the truck(s) was moved (loading) and stopped (holding) in 5 ft (1.52 m) increments. **Figure 5.15** shows example of holding stations along the bridge. These two scenarios were repeated since the crossings of the truck were oriented to cause maximum effects in specific panels as shown in **Figure 5.16** to **Figure 5.18**.

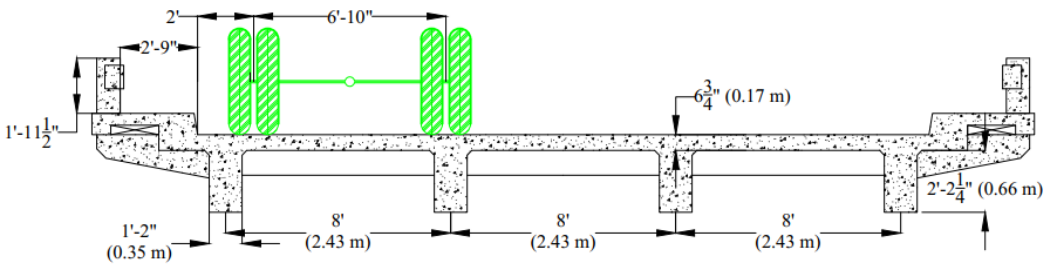

a)

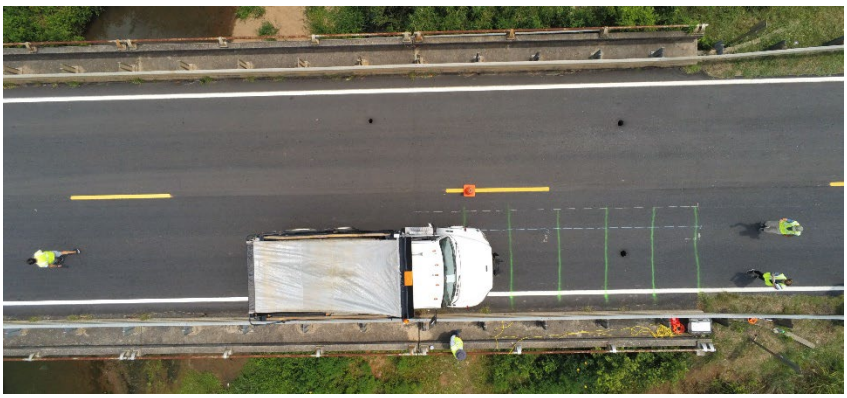

b)

Figure 5.15. Single truck on exterior girder 1, a) sketch, b) photograph taken by Parrot Anafi drone

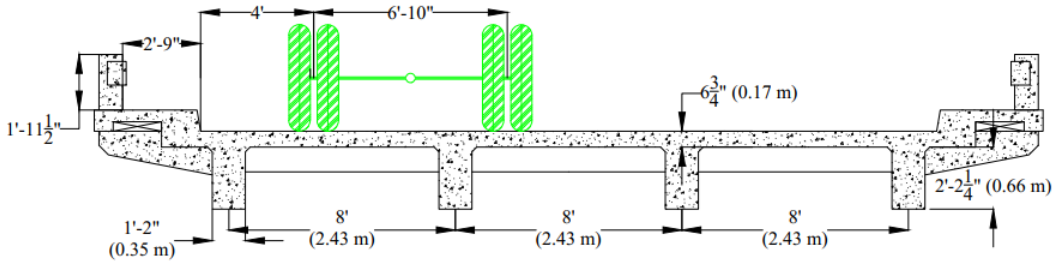

a)

b)

Figure 5.16. Single truck on interior girder 2-case 1, a) sketch, b) photograph

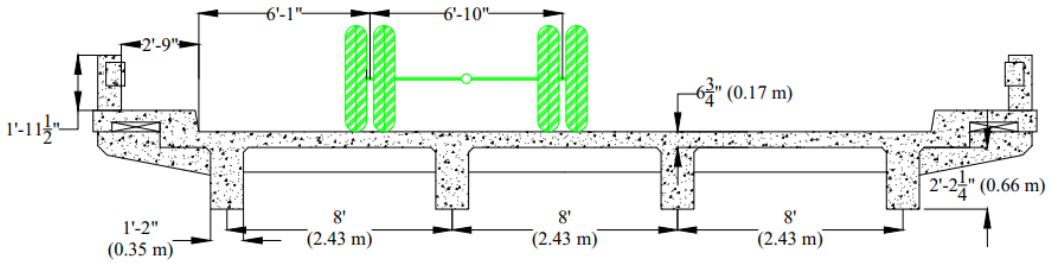

a)

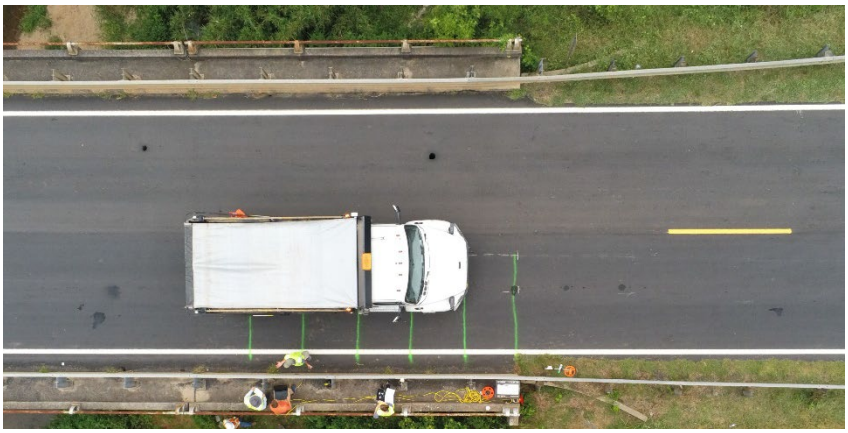

b)

Figure 5.17. Single truck on interior girder 2-case 2, a) sketch, b) photograph taken by Parrot Anafi drone

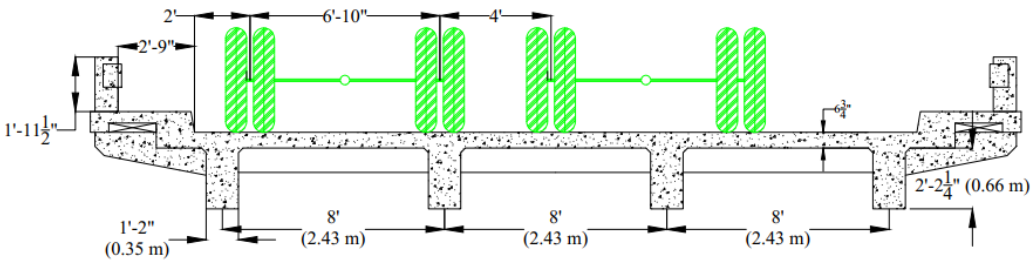

a)

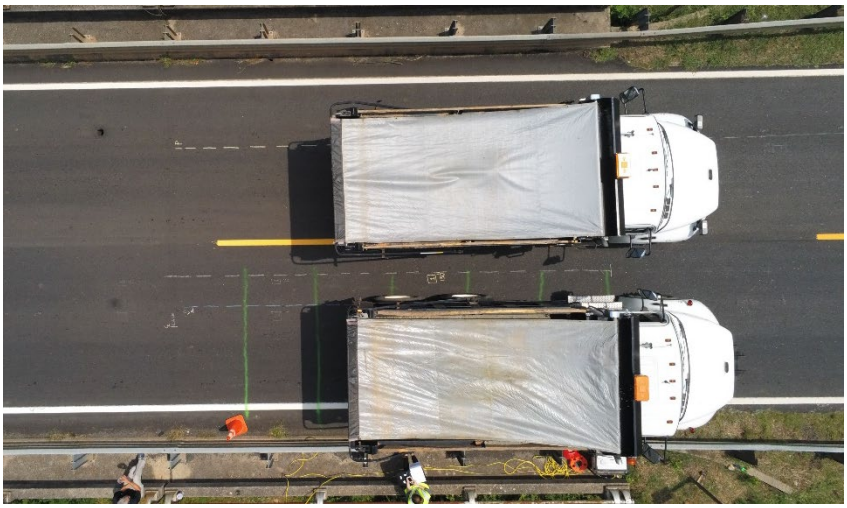

b)

Figure 5.18. Two trucks side-by-side, a: sketch, b: photograph taken by Parrot Anafi drone

S-97 over Johnson Creek Bridge: Truck loading (supplied by SCDOT) was used to load the bridge in four load paths applied to interior span 2. The specific truck weight and dimensions are shown in **Figure 5.19**.

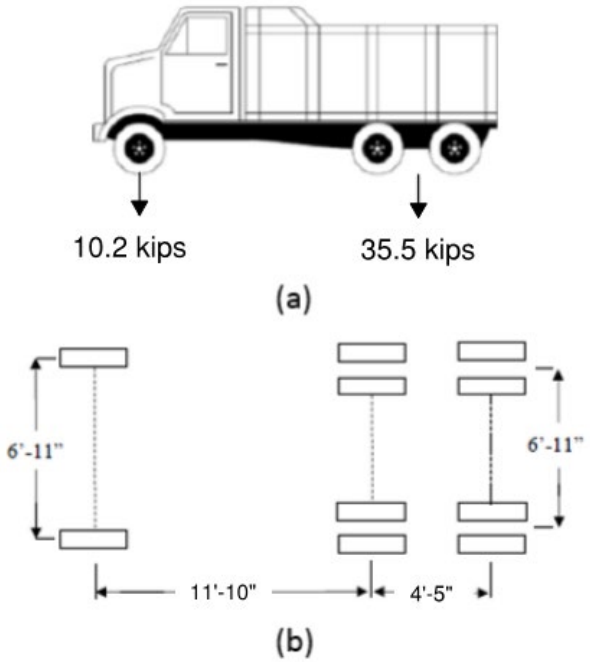

Figure 5.19. Load truck

Truck orientations for acoustic emission: Two scenarios were used to drive the test truck longitudinally across the bridge while midspan vertical deflection, surface strain, crack opining displacement and AE signals were recorded on the interior span 2. First, the truck was driven at slow speeds along the bridge, and second, the truck was moved (loading) and stopped (holding) in 5 ft (1.52 m) increments. **Figure 5.20** and **Figure 5.21** shows example of holding stations along the bridge. These two scenarios were repeated since the crossings of the truck were oriented to cause maximum effects in specific panels as shown in **Figure 5.22**.

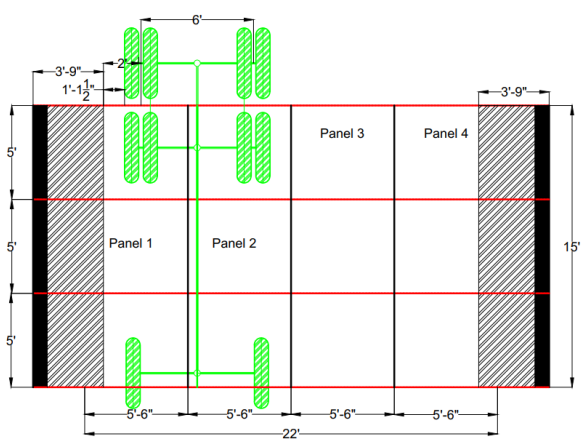

a) holding position 1

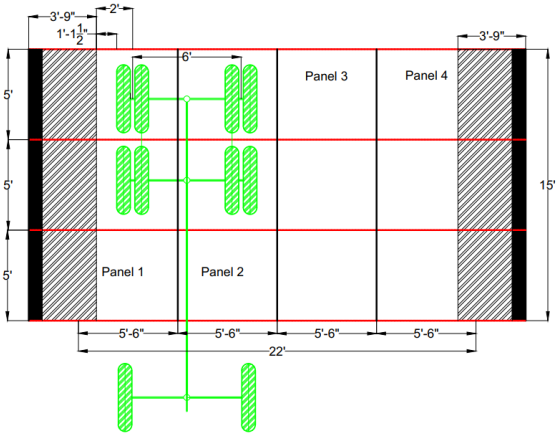

b) holding position 2

Figure 5.20. Longitudinal locations of the test truck: position 1 and 2

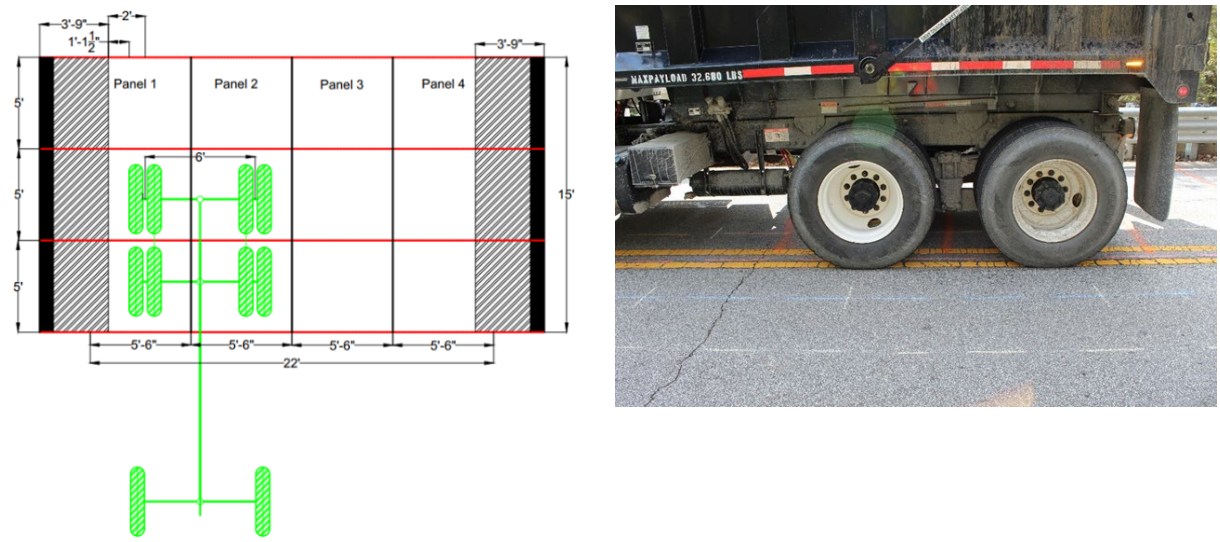

a) holding position 3

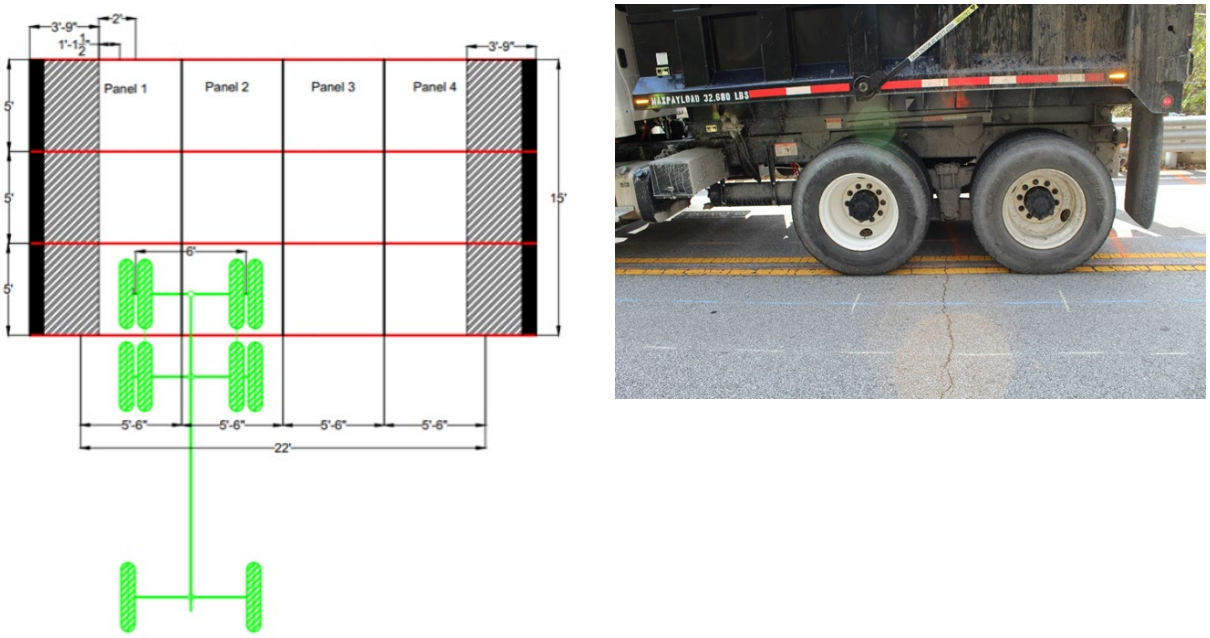

b) holding position 4

Figure 5.21. Longitudinal locations of the test truck: position 3 and 4

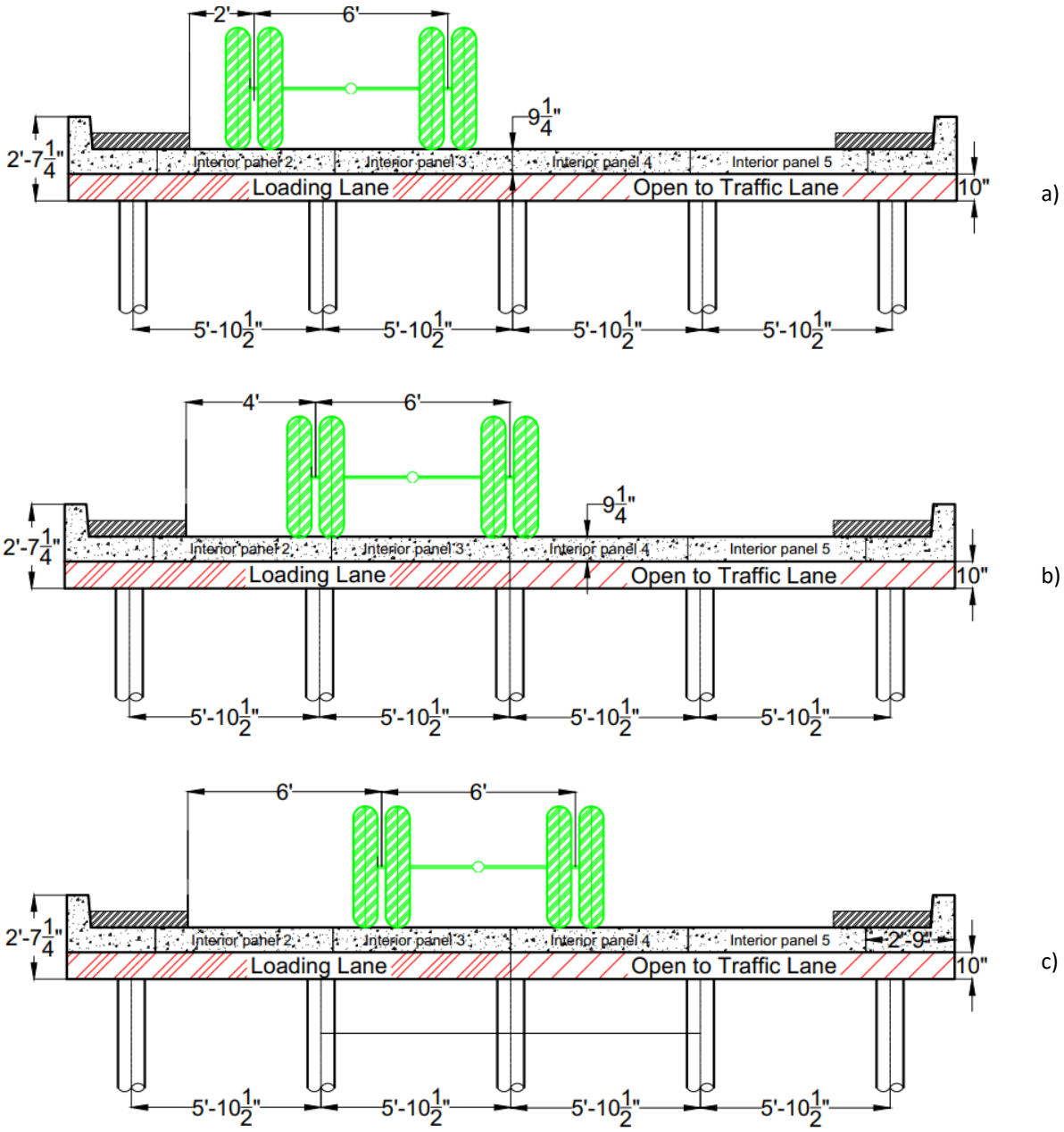

Figure 5.22. Transverse locations of the test truck, a) load case 1, b) load case 2, c) load case 3

Truck orientations for live load testing: Five different truck positions were used during the load test (**Figure 5.23**) and each truck position was repeated three times. For each repeat the truck drove slowly along the bridge while maintaining its transverse position. The first truck position was closest to the guardrail and the wheel lines evenly straddled an interior slab-to-slab joint (joint #4). Position two had the wheel lines placed directly adjacent to the interior joints to observe how the load distribution was affected when the loads were placed at the edge of the slabs. The third truck position placed wheel lines on the opposite side of the joints from position two. In position four, the truck was centered on the bridge in order to

evaluate how the center joint distributed the truck's load. Position five was the mirror loading of position one and was used to evaluate if the bridge response was symmetric.

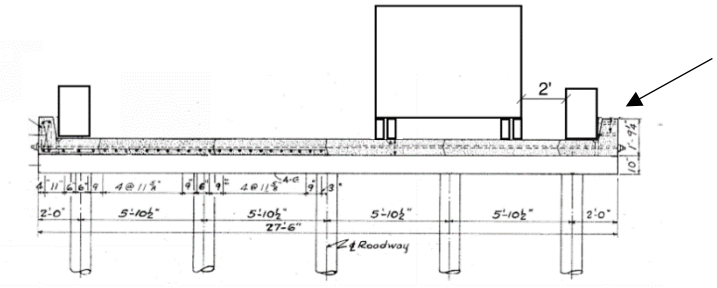

a)

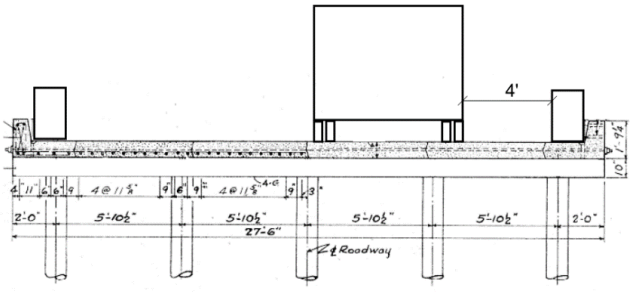

b)

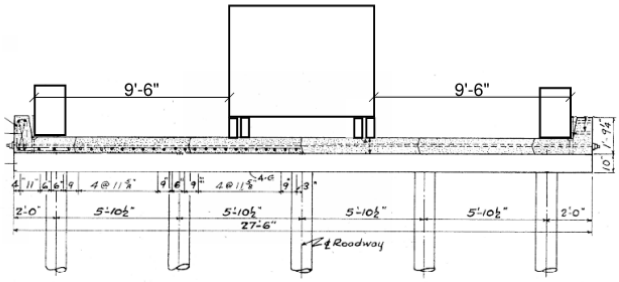

c)

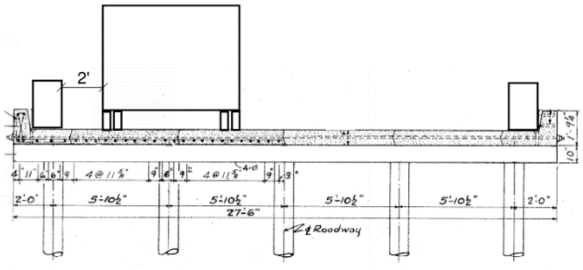

d)

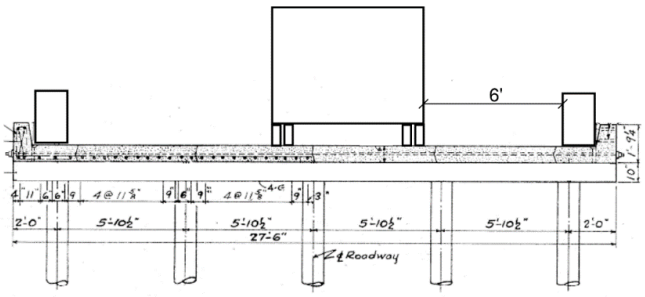

e)

Figure 5.23. Truck positions a) 1, b) 2, c) 3, d) 4, e) 5

6. Results and Discussion (Live Load Testing)

The results of live load testing are discussed in this Chapter. Response measurements include strain, deflection, crack mouth opening, and acoustic emission. The diagnostic load tests were conducted on two selected bridges to better understand and demonstrate the benefits of this type of testing for bridge evaluation and load rating. The first bridge was **US 221 over Hard Labor Creek** near Greenwood SC and the second bridge was **S-97 over Johnson Creek** near Abbeville SC. Photos of the two bridges are shown in **Figure 6.1**.

Figure 6.1. US 221 Bridge over Hard Labor Creek (top); S-97 Bridge over Johnson Creek (bottom)

6.1. US-221 over Hard Labor Creek Bridge

The test trucks were driven across the bridge at slow speeds while mid-span vertical deflection and surface (bottom) strain was measured on the southern-most span. The deflections and strains were continuously recorded using a wireless data acquisition system. The crossings of the truck were oriented to cause maximum effects in specific girders. Based on a review of the data, the following was observed about the structural behavior of this bridge:

1. Surface strain measurements indicate that for each level of load applied to the bridge, the cracking moment of the girders was exceeded.

2. Vertical deflection of the girders was significantly less than that found through a beam line analysis.

There are several contributing factors for the second conclusion, all of which yield more bridge stiffness then assumed in a beam line analysis: 1) resistance to horizontal movements at the bearings (i.e., the bearings are not acting as simple supports); 2) added stiffness due to large, integral barrier rails and sidewalks on a relatively narrow bridge; and 3) a recently added 3-inch thick asphalt overlay. A typical load rating for a bridge of this type would assume simple supports, however, for this bridge review of the data reveals that this assumption would produce very conservative analysis results.

Selected results are discussed with respect to the maximum loading paths on interior girders 2 and 3. When the trucks were moved into position ('loading') acoustic emission signals with high signal strength were generally detected, and when the trucks were parked ('holding') the AE signal strength diminished with time. This is as expected because crack extension results in acoustic emission activity. Holding of the trucks in position is done to assess whether crack extension continues unabated during the holding period, which (if it occurs) is a sign of unstable crack propagation and warrants further consideration, and this effect can be used to better understand the state of damage in reinforced and prestressed concrete structures (ElBatanouny et al. 2012; Anay et al. 2018). Examples of one loading step and one holding step (highlighted regions) are shown in **Figure 6.2** -**6.4** (units for signal amplitude and cumulative signal strength are Decibel (dB) and pico-Volt-sec (pVs)). Girder 2 exhibited more acoustic emission activity than girder 3 due to differences in load distribution (wheel loads were concentrated over this girder) and also due to the fact that this girder had more visible cracks than girder 3 prior to live load testing. **Figures 6.5** and **6.6** demonstrate that a large number of AE hits with high amplitude (95 to 100 dB) occurred as two trucks crossed the bridge side by side, with more activity related to crack extension occurring in the moment region. This is an indication that shear cracking may not be as significant a concern as the moment region for this bridge.

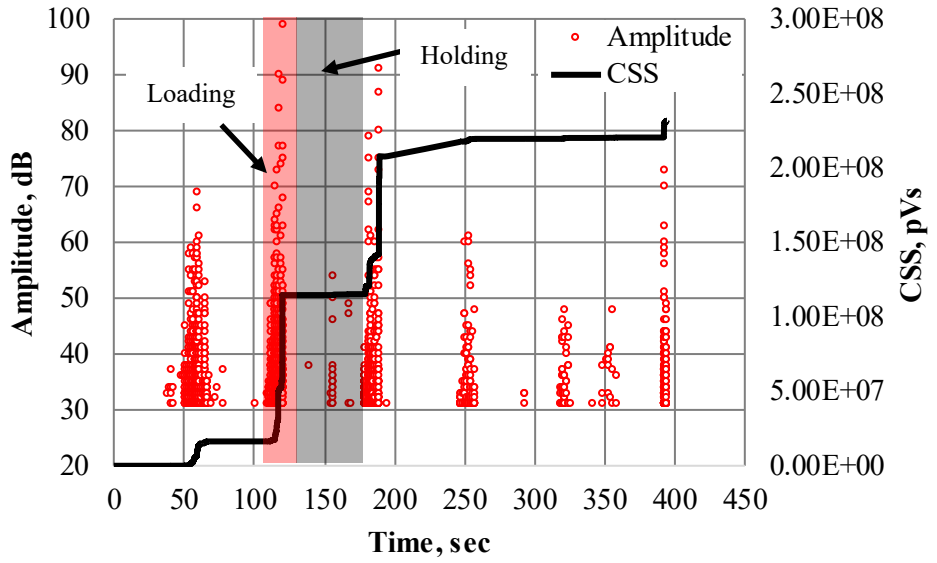

a) Sensors in moment region

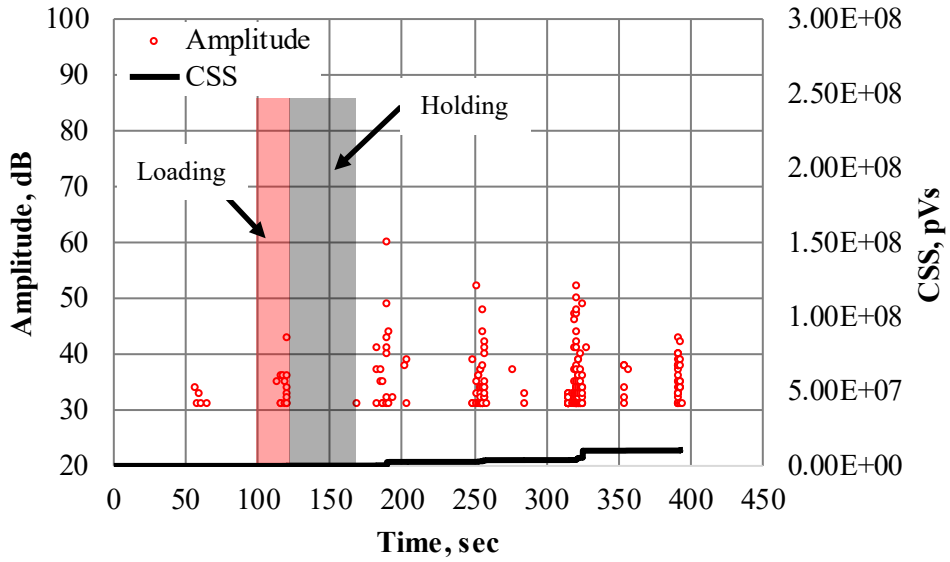

b) Sensors in shear region

Figure 6.2. AE data for interior girder 2 (single truck six ft from bridge rail)

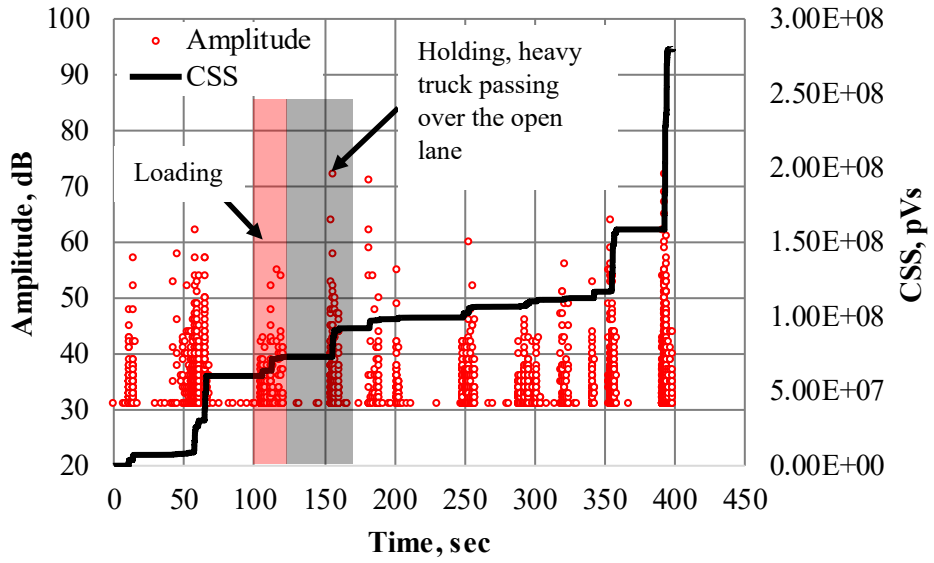

a) Sensors in moment region

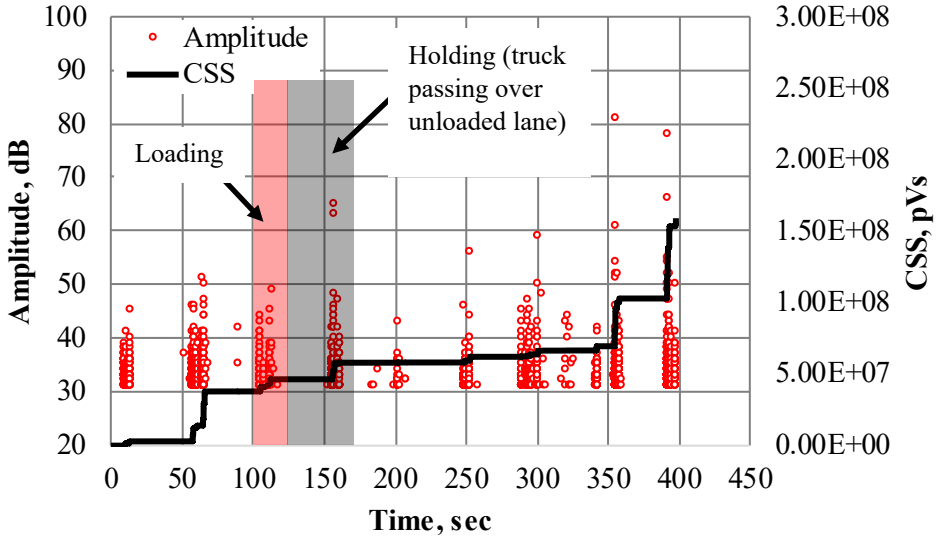

b) Sensors in shear region

Figure 6.3. AE data for interior girder 3 (single truck six ft from bridge rail)

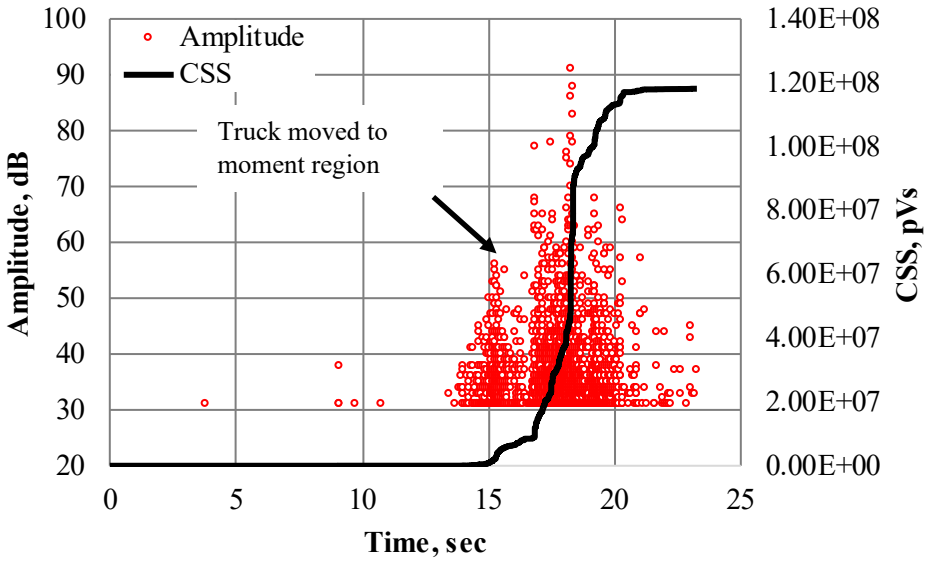

a) Sensors in moment region

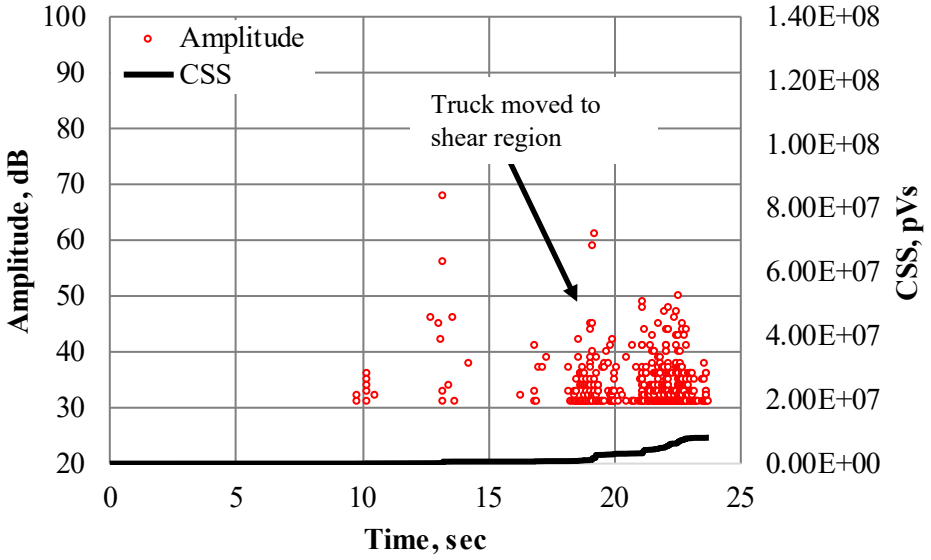

b) Sensors in shear region

Figure 6.4. AE data for interior girder 2 (single truck moving at constant speed two ft from bridge rail)

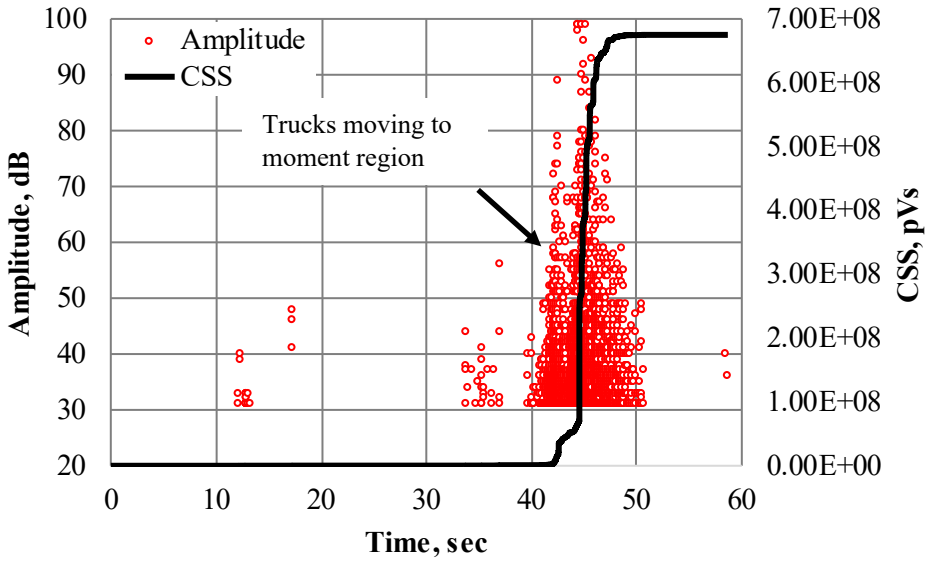

a) Sensors in moment region

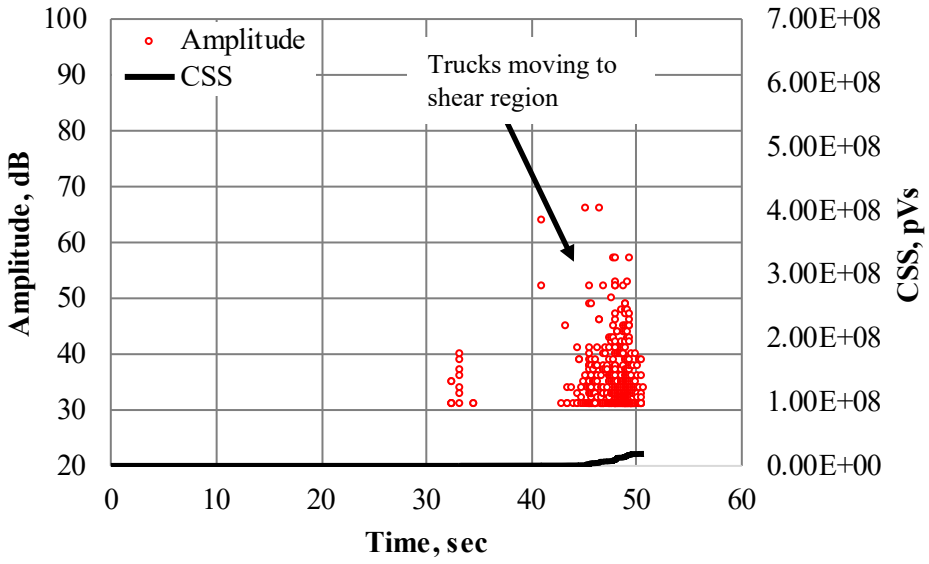

b) Sensors in shear region

Figure 6.5. AE data for interior girder 2 (two trucks side-by-side moving at constant speed two ft from bridge rail)

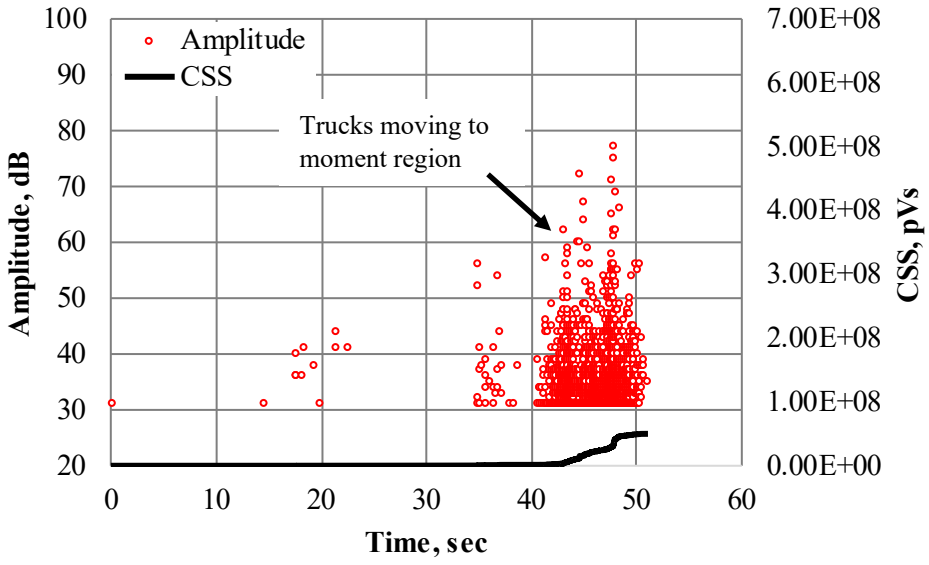

a) Sensors in moment region

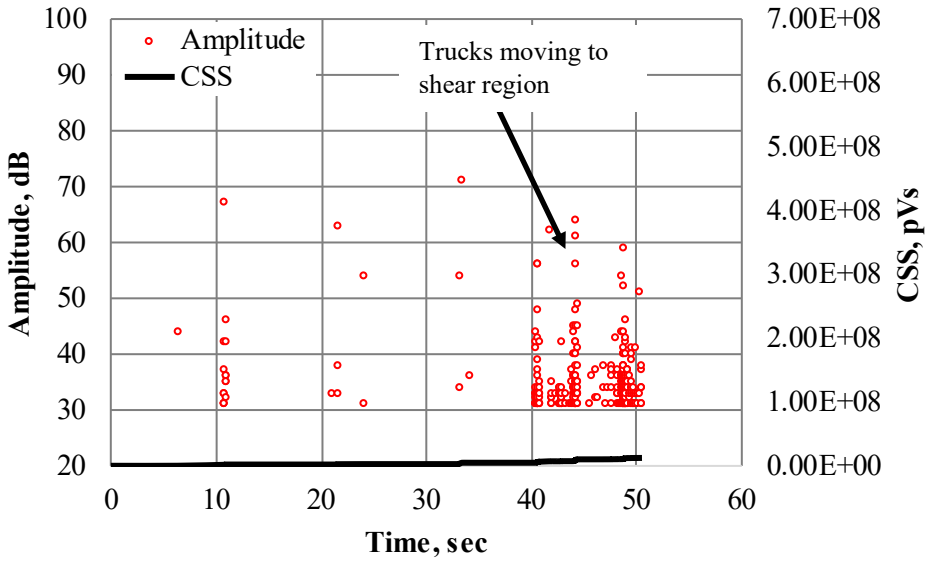

b) Sensors in shear region

Figure 6.6. AE data for interior girder 3 (two trucks side-by-side moving at constant speed, two ft from bridge rail)

Correlation between acoustic emission and strain data recorded at midspan of interior girder 3 is shown in **Figures 6.7** (single truck) and **Figure 6.8** (two trucks side by side). In **Figure 6.7** the effect of heavy vehicles (photograph from above) passing in the unloaded lane can be seen in the acoustic emission data. With the exception of passing vehicles in the unloaded lane, the acoustic emission data remains relatively quiet during the hold periods which is an indication of desirable structural performance. This observation is supported by the fact that the strain readings returned to zero at the conclusion of the testing. In **Figure**

6.8 relatively large amounts of acoustic emission data were recorded, as expected for this loading case. Strain readings again returned to original values at the conclusion of this live load test. It is difficult to draw conclusions from the acoustic emission data for this loading case in the absence of additional field data from similar bridge types.

To better understand the effect of regular traffic loading on this bridge, both strain and AE data were continuously recorded for approximately 25 minutes (**Figure 6.9)**. Maximum values recorded during this time period were amplitude of 80 dB and strain of 160 με. These values are in the range of, but lower than, those observed for the most severe live loading case of two trucks side-by-side (for that case, 99 dB and 189 με). This indicates the bridge is subjected to relatively significant loading due to heavy trucks, and when combined with the acoustic emission data as presented in **Figures 6.7** and **Figure 6.8**, is an indication that damage (crack extension) is continuing for this bridge under normal traffic loading. However, based on the stable nature of the acoustic emission data during load holds the nature of this damage is not of significant concern at this time, meaning that the bridge is performing within intended parameters.

As mentioned in prior chapters, microscopic images with 200x magnification were taken for selected cracks at midspan of interior girders during loading. The maximum crack widths recorded for interior girders 2 and 3 were 0.19 mm and 0.16 mm.

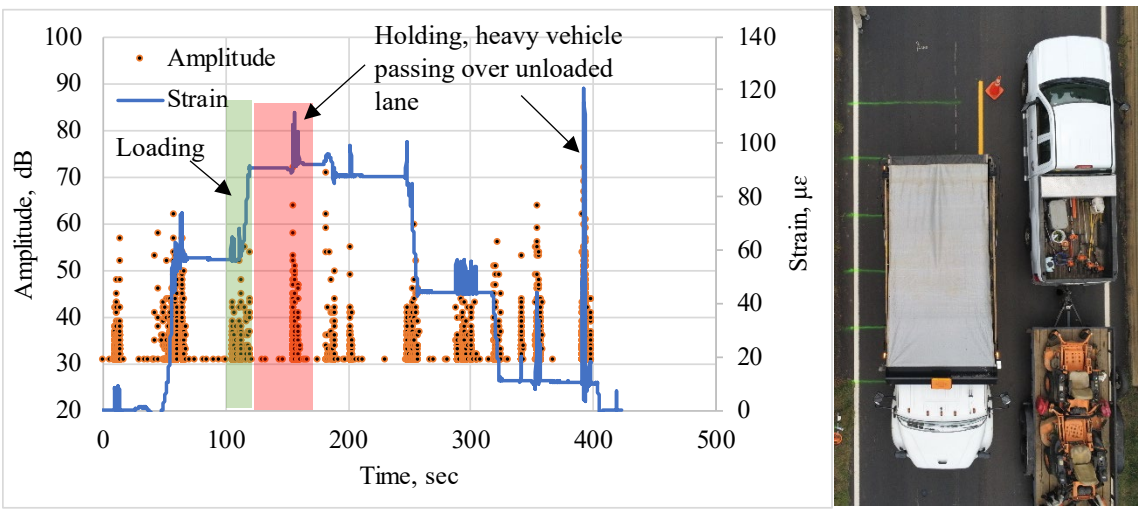

Figure 6.7. Midspan strain and AE data for interior girder 3 (single truck at 6 ft from bridge rail)

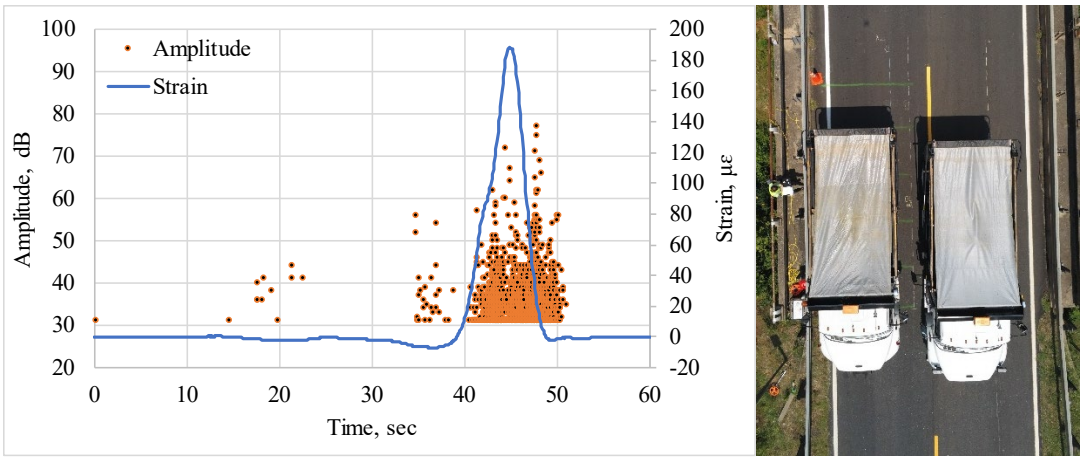

Figure 6.8. Midspan strain and AE data for interior girder 3 (two trucks side-by-side moving at 2 ft from bridge rail)

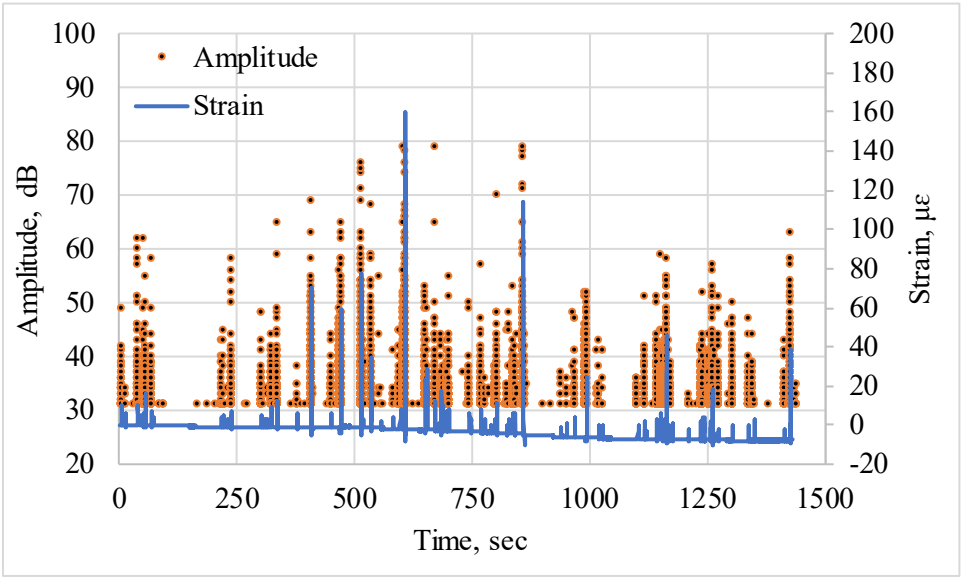

Figure 6.9. Midspan strain and AE data for interior girder 3 (regular traffic)

6.2. S-97 over Johnson Creek Bridge

General Behavior: Displacement data was collected utilizing Bridge Diagnostics Incorporated wire potentiometers at a sampling rate of 100 readings/second. Typical displacement data collected from one wire potentiometer during a truck passing is shown in **Figure 6.10**.

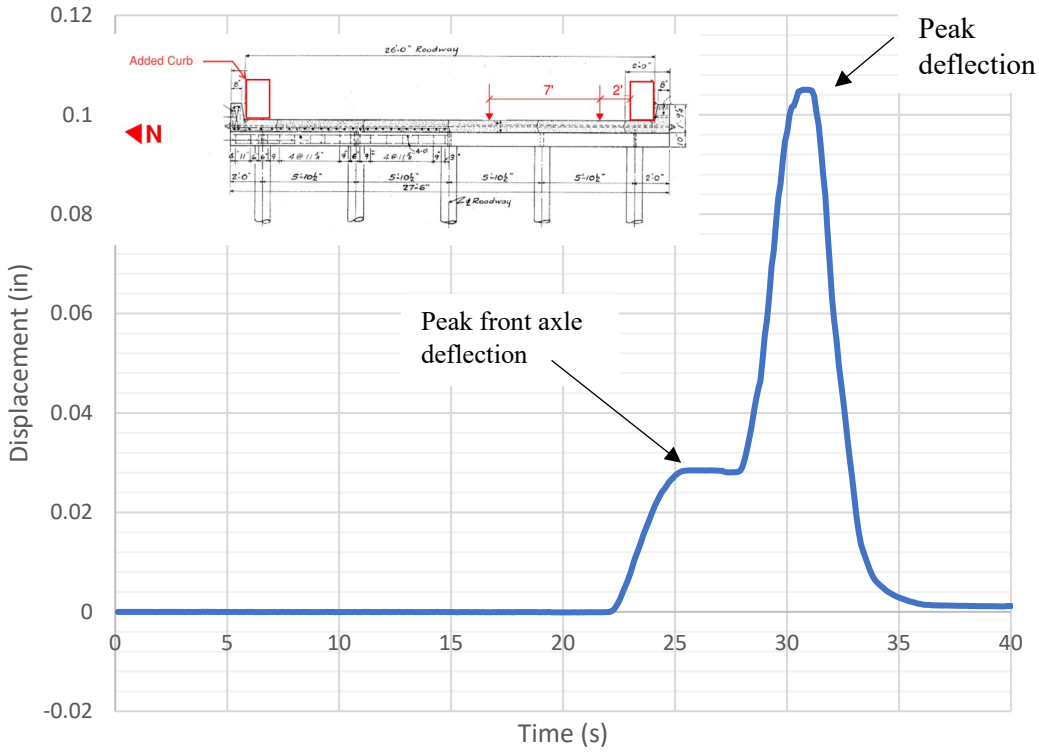

Figure 6.10. Displacement data collected from wire potentiometer 11 during test case 1, trial 1

The data in **Figure 6.10** corresponds to the first truck position, wherein the truck crossed the span at a location two ft from the bridge rail. Data in this figure is from instrument #WP11, where maximum displacement occurred. **Figure 6.10** shows when the front axle and the back axles of the truck crossed over this potentiometer. The first leveling of this curve, at approximately 26.5 seconds, corresponds to the front axle crossing mid-span and then peak displacement occurs at approximately 31 seconds consistent with the back axles crossing mid-span. **Figure 6.11** shows the displacements from each wire potentiometer located at the center of the slab during the same truck crossing. Data from WP7 and WP10 have a similar shape to that shown in **Figure 6.11**. Note that the displacements decrease, and the shape of the graph no longer has two distinct plateaus the further each wire potentiometer is from the truck load. There was effectively no displacement measured by WP1 and WP2 which were placed on the opposite side of the bridge as the truck.

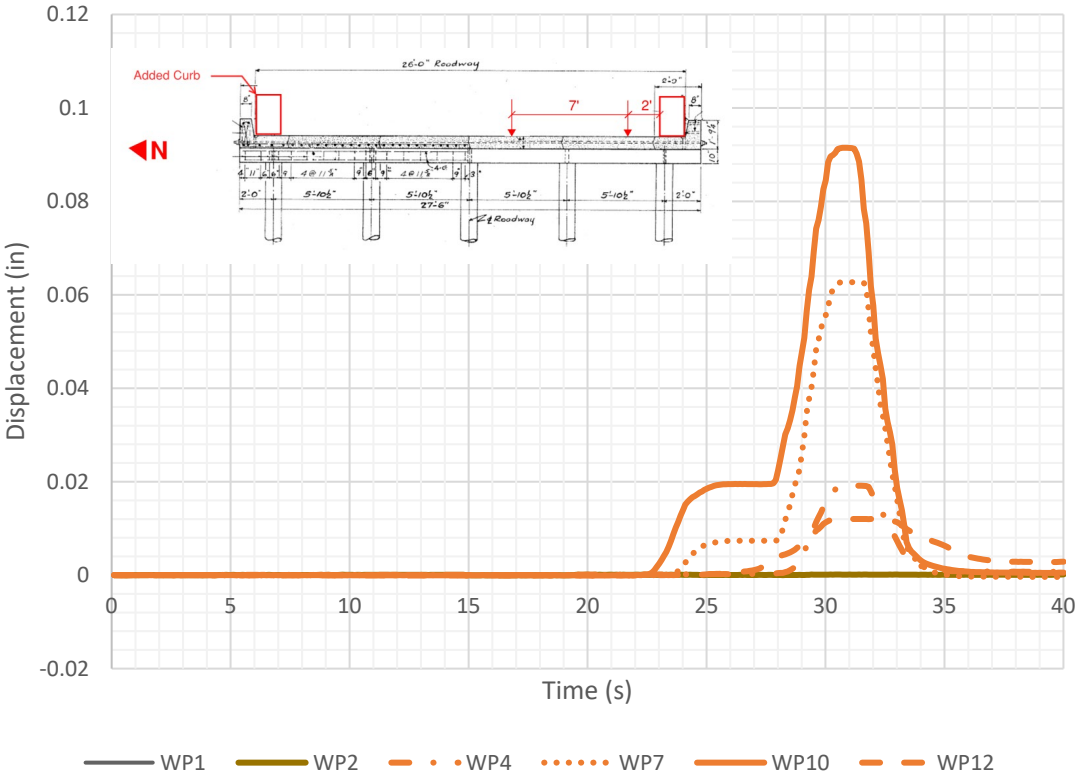

Figure 6.11. Displacement data collected from wire potentiometers at mid-panel width during test, case 1, trial 1

Table 6.1 presents the maximum displacements from each potentiometer and crossing for load position number one. The average, standard deviation, and coefficient of variation of the maximum displacements for truck position number 1 are also shown in this table. Based on these statistical measures, the data are considered to be low variance as the displacements are similar to the mean. Therefore, for calculating joint efficiency (how effectively the joints transmit loads to between adjacent slabs) and Distribution Factors for Moment (DFMs) the average of the three trial runs was used.

Table 6.1. Wire potentiometer results, load position 1

Wire Potentiometer	Max Disp. Trial 1	Max Disp. Trial 2	Max Disp. Trial 3	Average	Std. Dev.	Coefficient of Variation
WP1	0.0001	0.0001	0.0001	0.0001	0.0000	0.0000
WP2	0.0002	0.0001	0.0001	0.0001	0.0000	0.0000
WP3	0.0085	0.0076	0.0087	0.0083	0.0005	0.0602
WP4	0.0192	0.0187	0.0194	0.0191	0.0003	0.0157
WP5	0.0261	0.0260	0.0275	0.0265	0.0008	0.0302
WP6	0.0725	0.0724	0.0733	0.0727	0.0005	0.0007
WP7	0.0755	0.0748	0.0753	0.0752	0.0003	0.0040
WP8	0.0785	0.0772	0.0773	0.0776	0.0007	0.0009
WP9	0.0792	0.0784	0.0792	0.0789	0.0005	0.0006
WP10	0.0915	0.0914	0.0921	0.0917	0.0004	0.0004
WP11	0.1050	0.1047	0.1048	0.1048	0.0002	0.0002
WP12	0.0120	0.0110	0.0094	0.0108	0.0013	0.1204

Figure 6.12 displays the average maximum displacement recorded in each wire potentiometer for truck position number 1. On slab D the center wire potentiometer had a smaller displacement compared to the two edge wire potentiometers during each trial. This same result was observed throughout the test program and is assumed to be from faulty readings at this location. It is considered unlikely that the middle of slab D would consistently deflect less than its edges. To correct for this apparent error, linear interpolation between the two wire potentiometers on the edges of slab D were used to approximate the displacement at the center point. The dashed line segment in the figure across slab D is the approximated displacement behavior with the errant point removed. All calculations and analyses presented in this paper are based on linear interpolation to remove the errant point and approximate displacement of slab D.

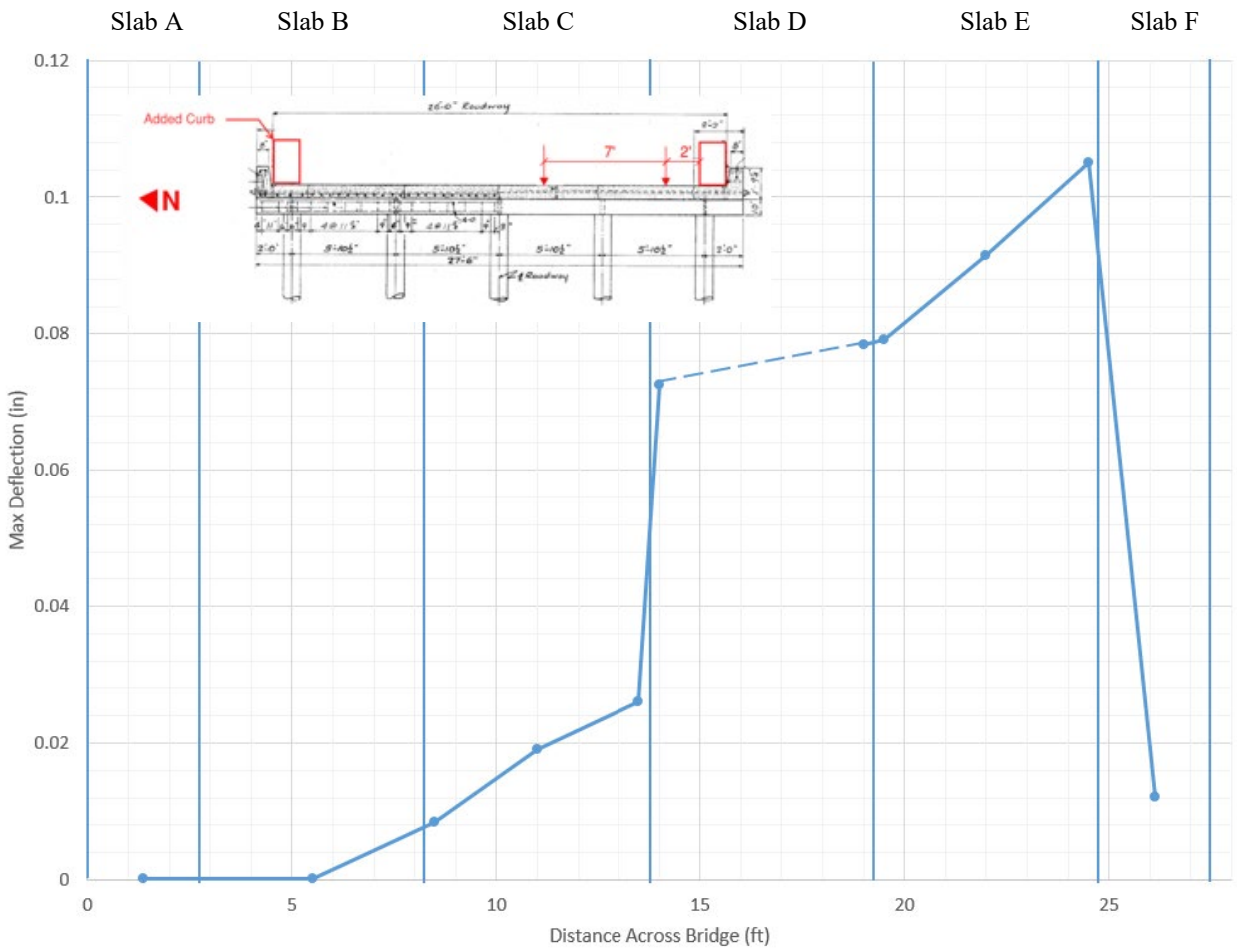

Figure 6.12. Maximum average displacement collected from each wire potentiometer

As previously shown in **Figure 6.11** and **Figure 6.12** shows that the wire potentiometers located directly beneath the truck measured the largest vertical deflections and that displacements were lower at locations farther away from the truck. **Figure 6.12** shows data from when the truck was positioned over slab D and slab E. These slabs experienced the greatest vertical displacements while slab A and B, furthest away from the truck position, saw almost zero displacement. Slab C displaced approximately 75% less compared to loaded slab D, and slab F displaced approximately 85% less than loaded slab E. The drastic difference in displacements between the unloaded and loaded slabs is due to the panel-to-panel joints not adequately transferring load from loaded to unloaded panels. This observation will be discussed in more detail in the section on Joint Efficiency.

Symmetry: Considering the data from the symmetric loadings (truck positions 1 and 5), it is evident that measured vertical deflections of the slabs are effectively symmetrical about the centerline of the bridge. This can be observed in the data shown in **Figure 6.13** as the displacement responses from the truck positions approximately mirror each other about the bridge centerline. Based on this result, it is assumed that the bridge behavior is effectively symmetrical. Hence DFM values calculated from loading one side of the bridge can be reasonably applied to loads on the other side of the bridge.

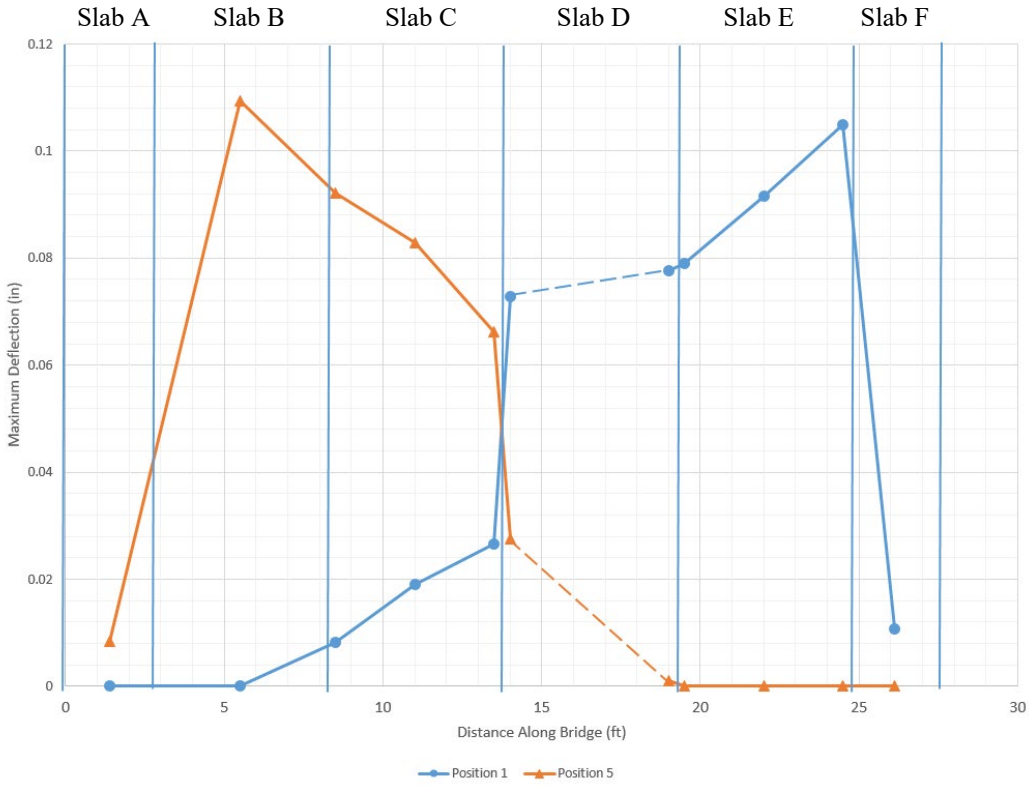

a)

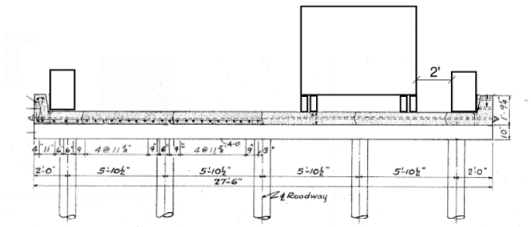

Truck Position 1

b)

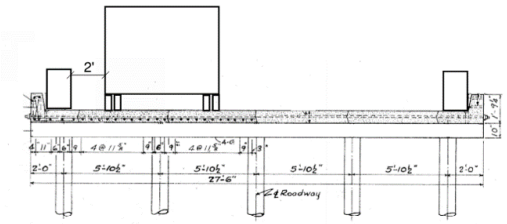

Truck Position 5

c)

Figure 6.13. Live load test: a) symmetry data, b) truck position 1, c) truck position 5

Experimental DFM: Using the test data the experimental DFMs (g_i) were calculated using **Equation 1** (Fu et al. 1996).

$$g_i = \frac{\Delta_i}{\sum_{j=1}^{n} \Delta_j} \qquad (1)$$

In the above equation, Δ_i is the displacement experienced in slab i under a particular load and Δ_j is the displacement experienced in all slabs, including slab i, in the same span under the same particular load.

Experimental joint efficiencies (η_i) were calculated from the test data using Equation 2.

$$\eta_i = \frac{\Delta_u}{\Delta_l} \qquad (2)$$

In the above equation, Δ_u is the displacement on the unloaded side of joint i under a particular load and Δ_l is the displacement on the loaded side of joint i under the same particular load.

Experimental DFMs were calculated using **Equation 1**. With the exception of slab D, displacements from wire potentiometers located in the center of each panel were used for the calculations. For slab D the displacement was determined by averaging the data from two edge potentiometers. Displacements used in the calculations were an average displacement of all three crossings at a given truck position. A DFM was calculated for each slab during each truck location. Table 6.2 lists the maximum calculated DFMs for each.

Table 6.2. Maximum experimental DFMs for each slab

Slab	Exp. DFM
A (exterior slab)	0.04
B	0.51
C	0.43
D	0.44
E	0.47
F (exterior slab)	0.06

The maximum distribution factor in interior panels ranged between 0.43 and 0.51. The two exterior panels, slab A and slab F, never had the truck's wheels applied directly, which resulted in small DFM values of 0.04 and 0.06, respectively. To provide context for these results, it is helpful to the experimental DFM to a hypothetical bridge with equal distribution to each slab. In the hypothetical case of even distribution, the DFM would be around 0.17 for all slabs and it would not matter where the truck was positioned. Because the experimental DFMs for the interior slabs are much greater than 0.17, it is evident that the truck loads were not evenly distributed.

Figure 6.14 shows the experimental DFM for each slab and truck position. Horizontal lines are also placed on the figure to show factors associated with equal distribution, distribution of one half of a truck axle per slab, and the recommended DFM value. The highest experimental DFM value is 0.51, which indicates that the worst case scenario a given interior slab will carry 51% of a truck load. Therefore, a recommended DFM for this bridge typology is no less than 0.55 for calculating the moment demand. This value is similar, but slightly greater, than the larger experimental DFM from the load tests.

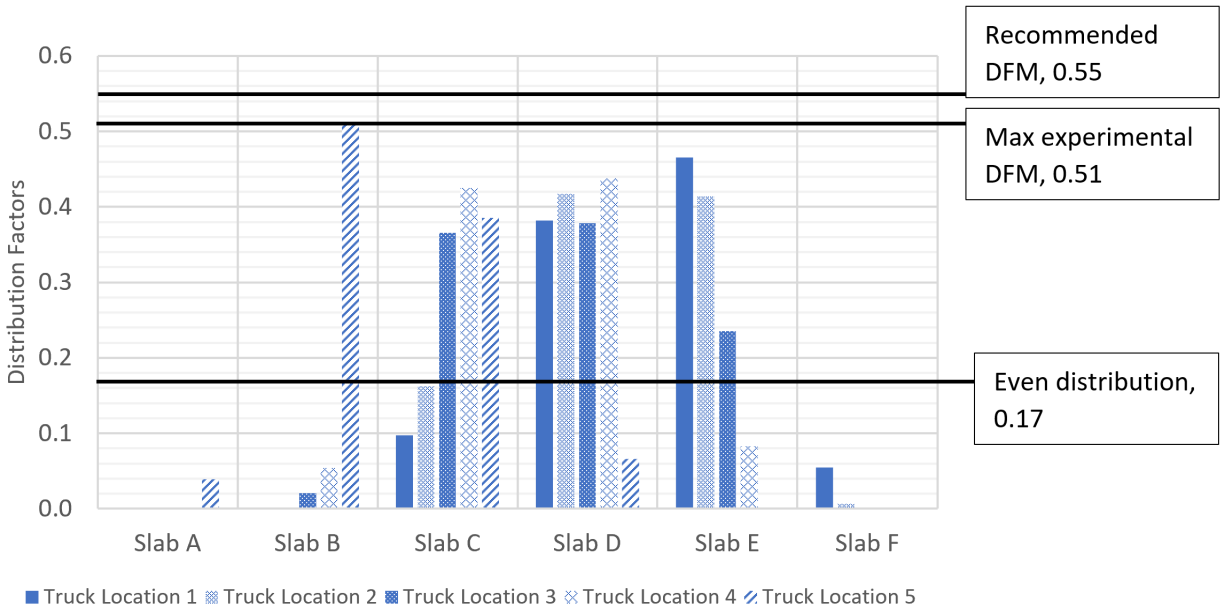

Figure 6.14. Average experimental DFMs for each slab and each truck location

DFM values were lower in situations where a given slab was not directly loaded by the truck. The variation in the DFMs between slabs for a given truck location can be attributed to poor load transfer across the panel-to-panel joints. Poor joint performance is a function of the age of the bridge and deficiency of the shear key detailing. The stiffness of the outside slab due to the integrated curb was greater than the stiffness of the interior slabs but did not result in increased load because truck loads did not effectively transfer to the outer slabs through joints 1 and 5.

Joint Efficiency: Joint efficiency is defined as the ability of a joint to transit loads between adjacent panels. It is quantified using **Equation 2**. Joint efficiencies were calculated for joints 3, 4, and 5. For a given truck position and joint, the efficiency was calculated using the average displacements from the three crossings. Calculated efficiencies are presented in **Figure 6.15** according to joint number and truck location.

The calculated joint efficiencies demonstrate that the bridge lacks transverse distribution between slabs. When the loaded truck is spaced evenly across a joint (e.g., truck position 1 and joint 4) joint efficiency is almost 1.0. This means that the slabs on either side of the joint displace a similar amount. However, the more critical condition to consider is joint efficiency between loaded and non-loaded panels. In these cases, the calculated joint efficiency is as low as 0.02 (truck position 2 joint 5). For cases where neither of the adjacent panels were loaded, the calculated efficiency ranged from 0.00 to 0.55. **Figure 6.15** is a visual representation of how joint efficiency changes based on the truck position. Joint 4 distinctly shows how the change from evenly distributed load (truck position 1) to load not being on the slabs directly next to it (truck position 5) affects its efficiency.

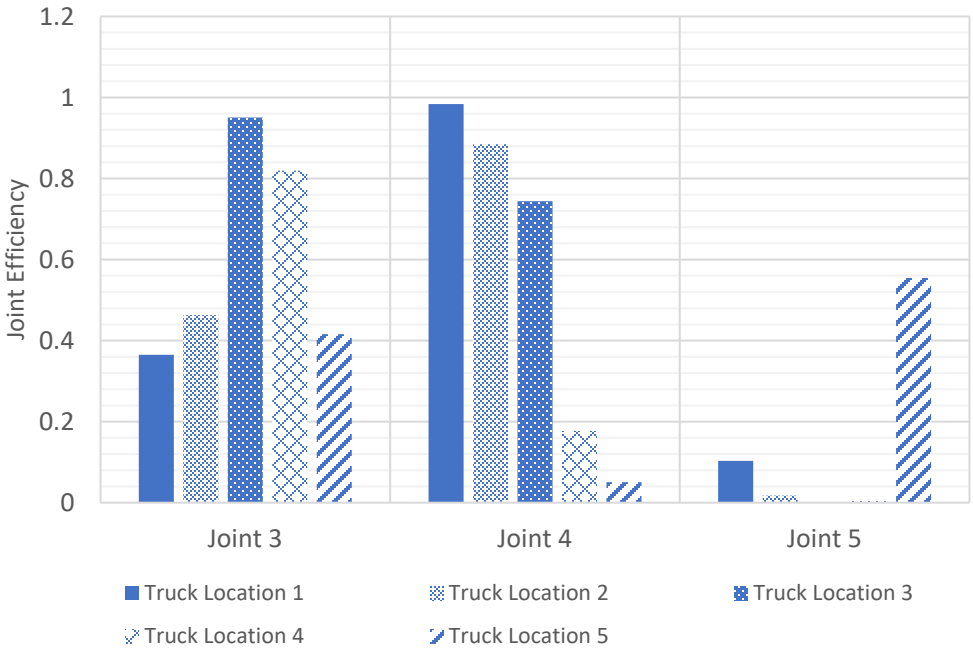

Figure 6.15. Average joint efficiency for each calculated joint and each truck location

Joint 5 has an increase in efficiency when the load is applied the furthest away. This could be due to an increase in stiffness on the exterior slab as well as the last truck position having minimal displacement on that side of the bridge as the two wire potentiometers had nearer displacements compared to other positions. The range of joint efficiencies can be attributed to deficient shear keys hence each slab is acting more like an individual entity than a multi-slab cohesive unit.

Acoustic Emission: Results are discussed with respect to the maximum loading paths on interior panels B and C. Two loading scenarios were applied including: a) the truck was driven at slow speeds along the bridge, and b) the truck was moved (loading) and stopped (holding) in 5 ft (1.52 m) increments. Examples of one loading step and one holding step (highlighted regions) are shown in **Figure 6.16** and **Figure 6.17**.

Data was recorded when the rear axles passed over interior span 2 toward bent cap 2. In contrast to the data obtained from the bridge previously discussed (US-221 over Hard Labor Creek), a relatively large number of high amplitude hits (i.e., amplitude exceeding 80 dB) and sharp changes in the slope of the CSS curve were observed for essentially all sensor groups. For load case number 1 (note that the load cases from the AE tests to not correspond to the truck positions from the DFM tests), slab B showed relatively high levels of activity when compared to slab C, and of interest is the continuation of acoustic emission activity during the load hold periods. As described above, this is an indication of continuing crack extension under a constant load and in one indication that the bridge is experiencing ongoing damage under this relatively minor load case (single truck). This is consistent with the behavior described above in relation to DFM and joint efficiency for this bridge. Of the two slabs instrumented, slab B shows consistently poorer behavior than slab C. This behavior (acoustic emission activity continuing throughout the load hold period)

is observed for both the slabs and the reinforced concrete bent caps, indicating that the bent caps are also undergoing damage during this minor loading case (single truck).

Figure 6.18 presents acoustic emission data as the truck is moved at constant speed across the bridge. This figure resembles the wire potentiometer results discussed above, in that the effect of the front wheels is clearly present in the data. As with the prior bridge, it is difficult to draw conclusions from this data in the absence of similar data taken from similar bridge types. It can be said that significant accoustic data were observed throughout the movement of the loading truck which is an indication that crack extension occurred throughout the process.

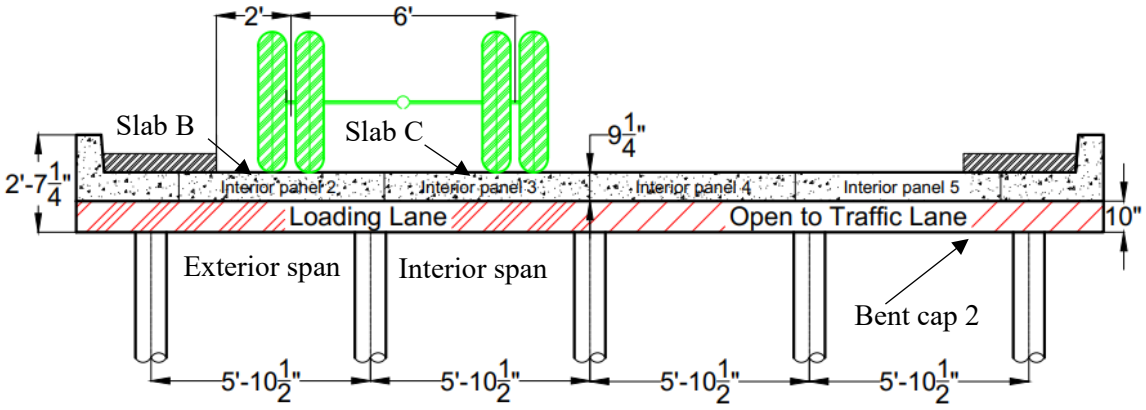

a) Wheel location

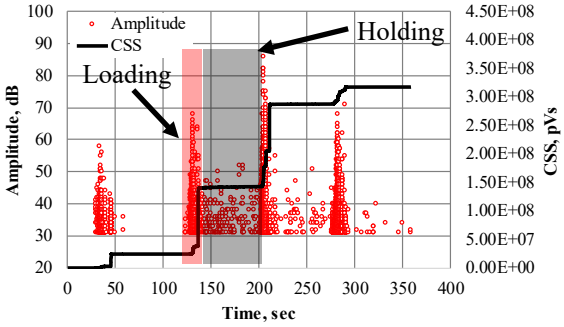

b) Sensors on slab B

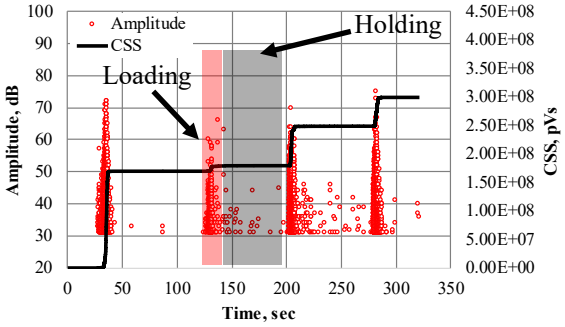

c) Sensors on slab C

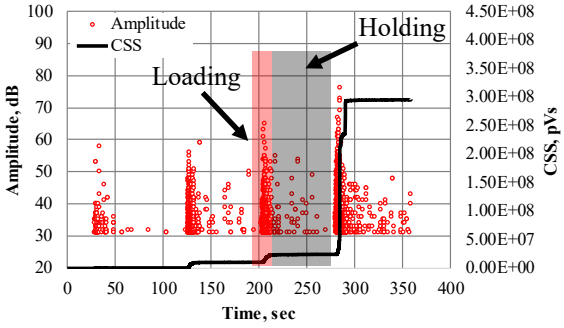

d) Sensors on bent cap 2 (exterior span)

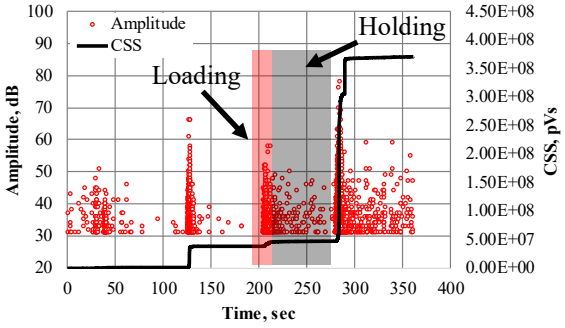

e) Sensors on bent cap 2 (interior span)

Figure 6.16. AE data, load case 1 (single truck)

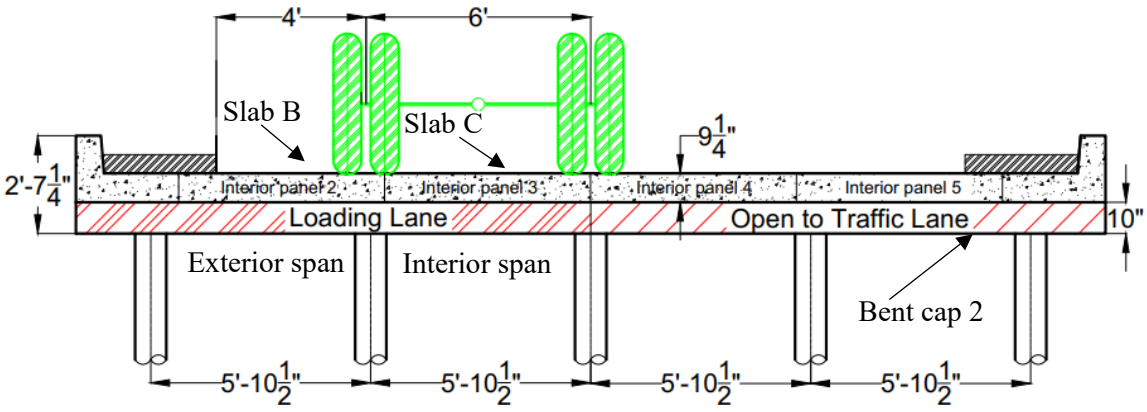

a) Wheel location

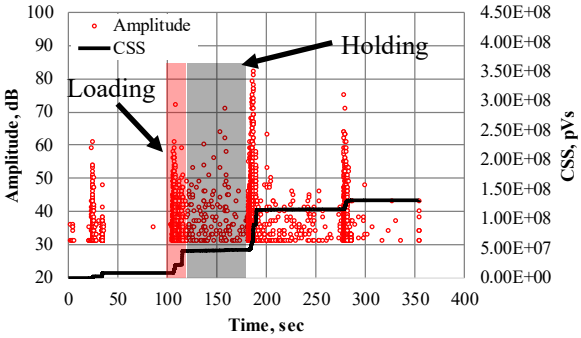

b) Sensors on slab B

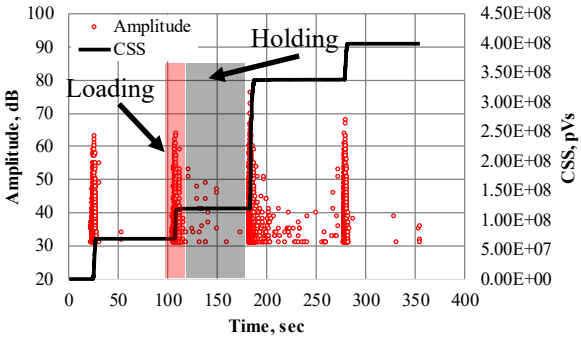

c) Sensors on slab C

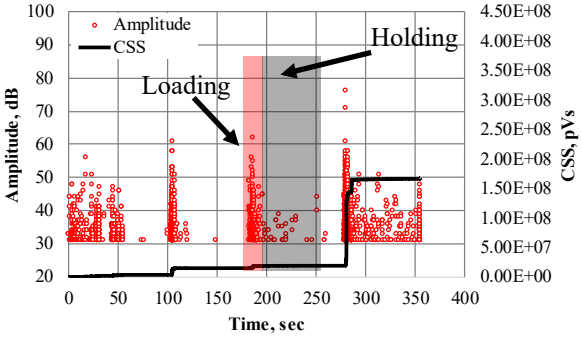

d) Sensors on bent cap 2 (exterior span)

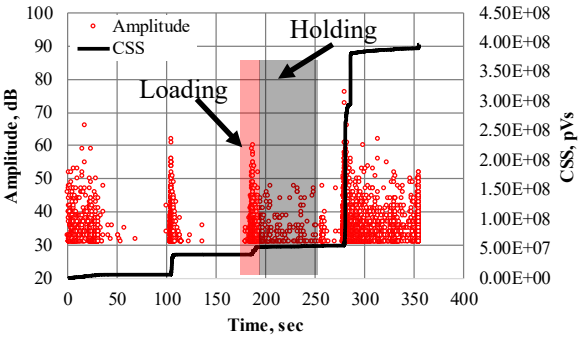

e) Sensors on bent cap 2 (interior span)

Figure 6.17. AE data, load case 2 (single truck)

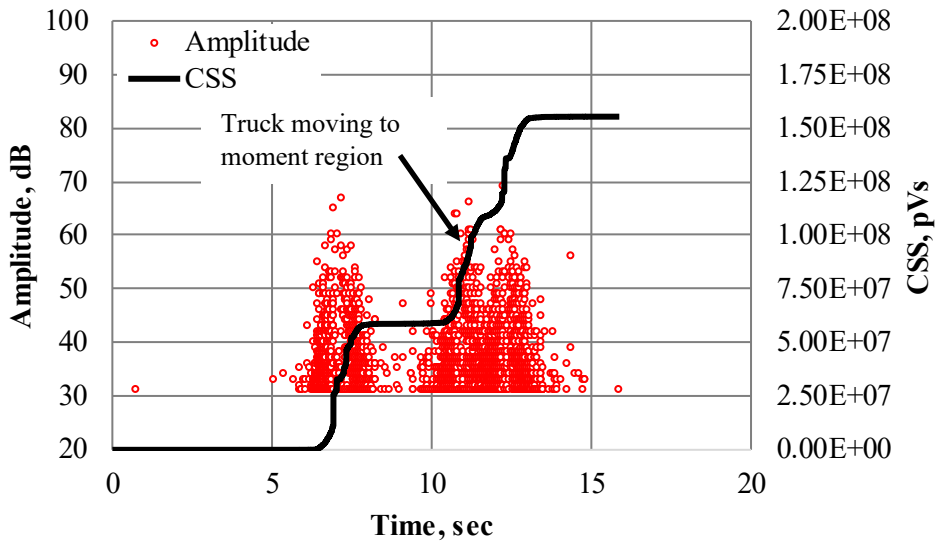

Figure 6.18. AE data for Slab B, single truck moving at constant speed (two ft from bridge rail)

Figure 6.19 is presented to demonstrate relationships between strain and acoustic emission data for the moment region of slabs B and C and bent cap 2. Because acoustic emission is a direct measure of damage (crack extension) there is no direct relationship between acoustic emission and strain, displacement, or similar measures. This figure illustrates this point and again the continuation of acoustic emission activity during the load hold periods for Slab B should be noted. **Figure 6.20** addresses the case of a moving single truck and the associated acoustic emission response. In this case it is of interest to note the continuing activity through the truck movement and it the amount of data recorded, which is more significant for slab B than Slab C due in part to the position of the truck.

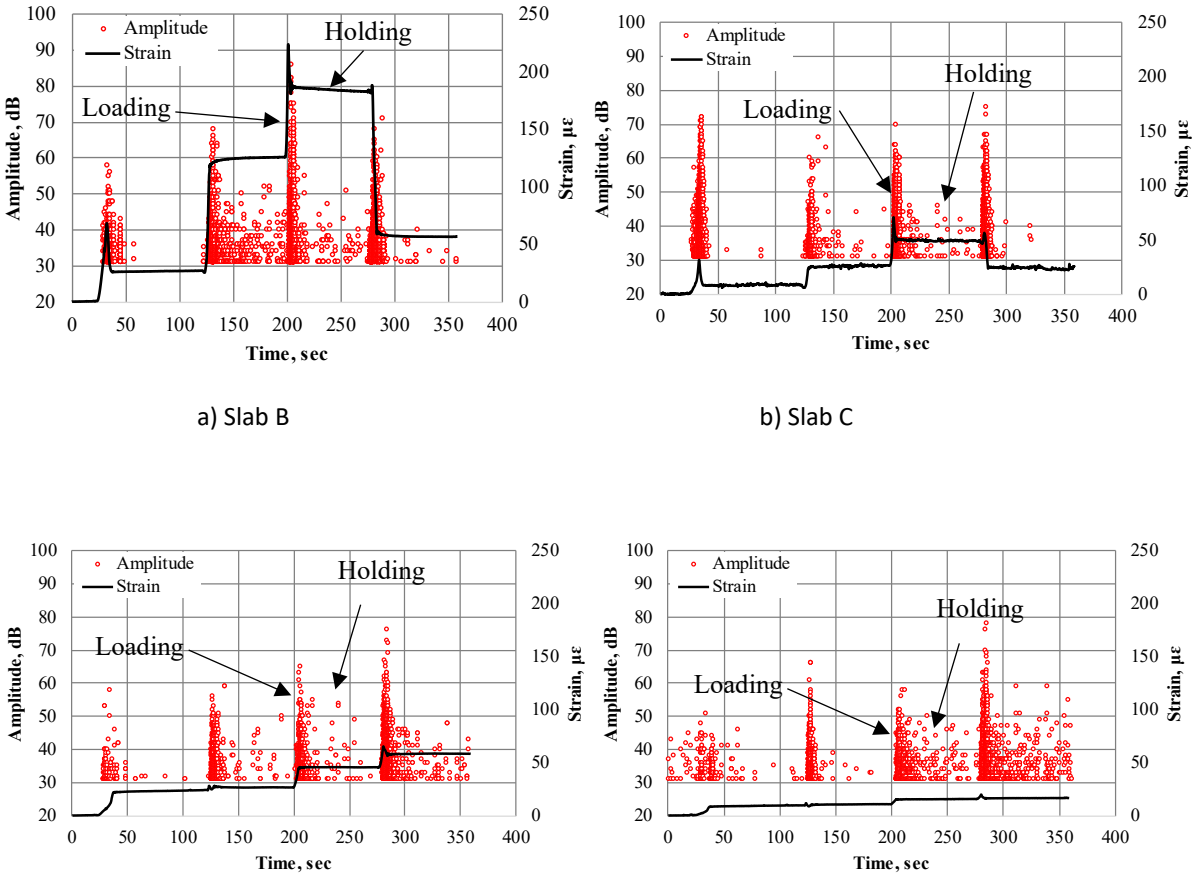

a) Slab B

b) Slab C

c) Bent cap 2, exterior span

d) Bent cap 2, interior span

Figure 6.19. AE data and strain, single truck (two ft from barrier)

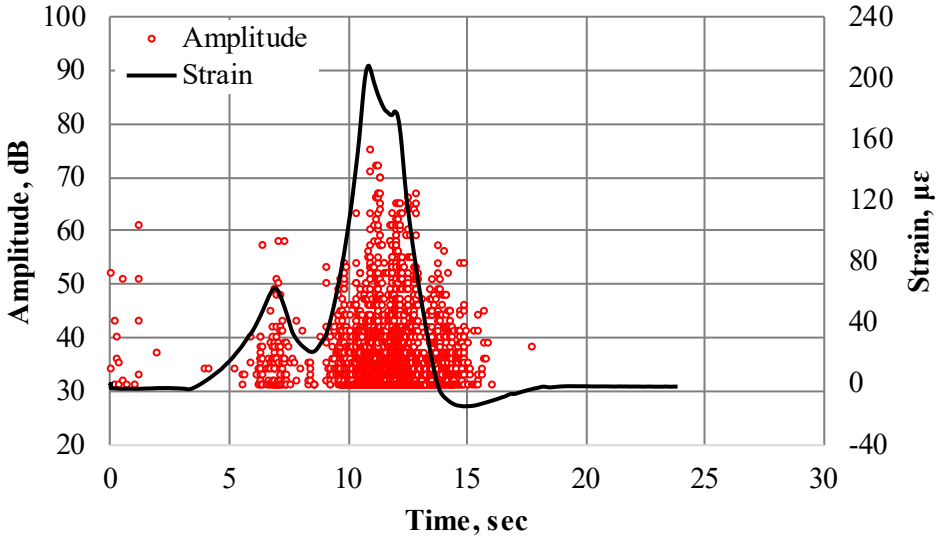

a) Slab B

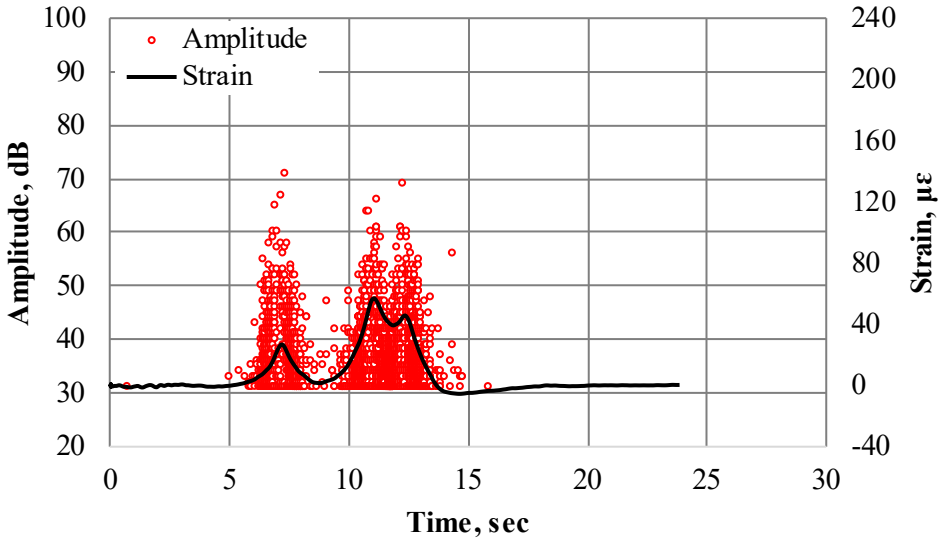

b) Slab C

Figure 6.20. AE data and strain, single truck at constant speed (two ft from barrier)

6.3. Discussion

The first bridge subjected to live load testing, US-221 over Hard Labor Creek, is a reinforced girder bridge. This bridge demonstrated better than expected performance which is attributed to boundary conditions that differ from those often assumed in a beam line analysis. The second bridge, S-97 over Johnson Creek, is a reinforced concrete slab bridge. This bridge demonstrated poor joint efficiency and load distribution. This behavior is attributed to joint deterioration and other factors that have occurred with the passage of time. Acoustic emission monitoring supported this conclusion as emission continued throughout load holds for all instrumented slabs. Furthermore, acoustic emission indicated that the bent caps may also warrant further investigation.

Acoustic emission differs from strain and displacement monitoring as acoustic emission is a measure of crack extension. One potentially promising aspect of acoustic emission monitoring is that regular traffic loading can be used obtain characteristic damage response of a given bridge type, bypassing the need for controlled load testing. This potential approach, however, assumes that a significant number of bridges of similar type can be instrumented and acoustic emission data recorded over a significant period of time.

7. Cost Benefit Analysis

Yearly cost for equipment and cost per inspection for the equipment are based on an hourly rate where the charged use of the equipment after five years is equal to the cost of the equipment. This is contrary to a more traditional “machine-use cost” method, due to unknowns in the expected machine lifetime, as figures vary widely.

Cost estimation for person-hours is set at $100/hr to account for salary, training, insurance, and supporting staff.

7.1. Bridge Inspections

There will be four separate considerations looked to for the cost benefit analysis of drone systems in the application of visual inspections. SCDOT-internal drone inspections, outsourcing drone inspections to contractors, the current baseline cost of tactile inspections using a bridge inspection boom truck, and the option of renting boom trucks/trailers for inspections.

7.1.1. Bridge Inspection Boom Trucks and Trailers

The bridge inspection truck and trailer platforms are commonly used for allowing inspectors to access the underside of bridges to perform visual and tactile inspections of decks, piles and other structural members and components. The equipment typically costs between $300,000 and $650,000 dollars. These systems may also be rented from suppliers to reduce the initial cost and prevent the necessity of SCDOT maintenance, however, these costs are built into the price, and for the volume of bridge inspections done in the state of South Carolina, is not a financially beneficial alternative to state-owned equipment. If one inspection is conducted in south Carolina on a bridge for eight hours per-day (a conservative estimate) the cost per year of equipment rental would be between $400,000 and $600,000 per year, and if we then add the cost of the two inspectors and driver, the price increases by an additional $600,000. Making the yearly cost of the rental equipment and operation on the order of $1,000,000 to $1,200,000 a year.

Comparing to the yearly cost of operation of a single boom truck or trailer to be between $60,000 and $120,000. Adding the cost of two inspectors and driver comes to between $660,000 and $720,000. This estimate does not include the maintenance costs covered by the SCDOT, however, the infrastructure to support maintenance already exists for the other large SCDOT equipment.

Drawbacks to the inspection truck systems in general are the inherent safety risks to inspectors as well as the public impact resulting from lane closures. Additionally, the initial cost is high and the fleet would require a maintenance schedule. Lane closures require crews to man signage as well as direct traffic which adds an additional $400,000 per year in inspection costs, bringing the total cost per year of inspecting bridges with boom trucks to $1,060,000 to $1,120,000 for SCDOT owned boom trucks, and $1,400,000 to $1,600,000 for rented equipment.

7.1.2. Drone systems

The systems being considered in this section are the Parrot Anafi, The DJI Matrice 210, and the Flyability Elios drone. The Elios was not present during the demonstrations but is a strong candidate due to its abundant use by inspection service contractors and its consideration by the CBA.

Drone operations at the very least require a single certified pilot operator which typically costs (including overhead) between $100-$150 per hour. Certification costs $150 and presents a low up-front cost for the SCDOT. The drone systems themselves are a wide range of costs as they are on opposite spectrums of the market segment. The Parrot Anafi costs $700, the DJI Matrice 210 costs $15,000-$35,000 depending on options, and the Flyability Elios costs $25,000.

Using the same methods employed for the boom truck and trailers section, assuming a single bridge inspection per day (8 hours/day) and the previously stated hourly rate for the drone pilot, the cost per year for inspection with the Parrot Anafi is $210,000, the DJI Matrice 210 is $340,000, and the Flyability Elios is $330,000. Adding a single inspection engineer to review the collected images and conduct evaluations off-site, the price per year for inspections increases to approximately $420,000, $550,000, and $540,000 for the Anafi, Matrice 210 and Elios respectively. Additionally, drone inspections do not require the use of a crew to shut down lanes, so the added cost of crew and equipment is not present.

7.1.3. Outsourcing Drone Inspections

Inspection services conducted by contractors is becoming more common as the market continues to grow and the need is recognized. Local companies were contacted to determine the average price of an inspection and many were reluctant to share figures due to the variability in price based on the customer needs. However, one company, Exelon Clearsight, shared some rough numbers for comparison purposes.

Based on the estimated costs provided by Exelon Clearsight, inspections would cost roughly $6,000 per day. This includes, two operators, a project manager, manual data analysis, delivery and their internal UAS support. Bringing these numbers on the scale of the other values presented here, for a full year of bridge inspections, using an external service, the cost would be approximately $1,570,000. This does not include travel expenses, which must be calculated on a case by case basis and are billed at actual cost plus 10%.

7.1.4. Drone Systems Cost Benefit Analysis Conclusions

From Table 7.1 a cost benefit of a state-owned fleet of drone systems and operators can be seen to be approximately 55% over the current method of tactile inspections with state-owned boom trucks.

Table 7.1. Cost for drone systems and alternative methods

Method	Average Yearly Cost	Cost/Inspection	Additional Cost	Savings
Rental Boom Truck	$1,500,000	$5,747	N/A	-36%
State-owned Boom Truck	$1,100,000	$4,215	Maintenance	Baseline
State-owned Drone Systems	$500,000	$1,916	Storage	55%
Drone Inspection Contractors	$1,570,000	$6,015	N/A	-42%

Implementation would likely be a combination of boom trucks utilized for in depth investigations of defects, and drones for visual inspection and identification of defects. Which would shift savings from 55% to approximately 40-50% depending on the frequency of boom truck use. Additionally, the added safety of using a drone system in place of tactile inspections cannot be quantified monetarily here, as data is not available.

There are some drawbacks associated with drone use in bridge inspections such as restrictions regarding drone use near power lines, and over traffic, as well as the need for certified drone pilots to conduct flight operations. Other potential drawbacks are associated with the management of the large quantity of data (images and video) that are collected, which must be analyzed and stored.

7.2. Culvert Inspections

7.2.1. Crawler Robots

Crawler robots are already used extensively in industry and other state departments of transportation in culvert inspections by using closed circuit television (CCTV) systems for qualitative analysis (Piratla, et al. 2016). Culvert inspection procedures were implemented by the SCDOT in 2011 and primarily rely on visual inspection from the inlet, and outlet of the culvert with flashlights and binoculars (Piratla, et al. 2016). This is a cost effective method for evaluating culverts when compared with crawler robots as they would not reduce the number of person-hours associated with an inspection, nor would their implementation reduce the overall cost of equipment used. Instead, the implementation crawler robots would be a means to increase the effectiveness of inspections, and better identify and track defect development. As such there is no foreseeable cost benefit to implementing a crawler system, save for potential early identification of defects that would not be identifiable through currently employed techniques. While this is a foreseen benefit of these crawler systems, instances of defects going unnoticed through currently employed techniques is not available and does not allow for evaluation of these factors.

Table 7.2. Cost for crawler robots and traditional culvert inspection

Method	Average Yearly Cost	Cost/Inspection	Additional Cost	Savings
Traditional Inspection (3 per day)	$416,000	$533	N/A	Baseline
Crawler Robot Inspection (3 per day)	$417,800	$536	Maintenance	-0.4%
Crawler Robot Inspection (2 per day)	$417,800	$803	Maintenance	-50.6%

The cost analysis presented in Table 7.2 shows the minimal impact that crawler robots would have on inspection cost if the same inspection rate is achieved. If the inspection rate is reduced due to the increased time necessary for a thorough culvert inspection with a crawler robot, the cost per inspection increases by 50%. This does not include the cost of maintaining the crawler systems and supporting hardware.

7.3. Scour Evaluation

There are multiple technologies presented during the literature review as supplementary sensor equipment to increase the effectiveness, accuracy, safety and relative ease of the scour evaluation process. Currently, scour evaluation is outsourced by the SCDOT to contractors. Information regarding the frequency of evaluation and the costs associated with outsourcing the task were not provided, so estimates were developed based on similar assumptions used for the bridge inspection section. Methods explored are SCDOT conducted scour evaluation, contractor conducted scour evaluation, outsourced diver inspections, supplemental sensor equipment, and autonomous system deployment. Additional hardware such as a boat and corresponding safety equipment are not considered as they would be necessary for all other manned inspection methods, and the autonomous kayak system would come with supporting hardware costs as well.

7.3.1. SCDOT Scour Evaluation

SCDOT “person-hours” associated with a typical scour evaluation operation are calculated based on a three-person crew and an eight-hour workday where one thorough evaluation is conducted per day.

7.3.2. Outsourced Scour Evaluation

Outsourced scour evaluation cost is based on the same crew size, hours, and pay as the SCDOT, but with additional associated costs for overhead and profit. Another additional cost associated with contractor hire is travel and per-diem, which would be determined on a case by case basis and is not accounted for here.

7.3.3. Outsourced Diver Evaluations

Diver inspection costs were determined through reaching out to multiple service providers to generate an average cost per inspection. Travel and per-diem are not accounted for here as it is calculated per inspection.

7.3.4. SCDOT Supplementary Sensor Equipment

The cost of implementing sonar and supporting hardware is estimated at $8,000, which is based on the SOLIX 15 CHIRP MEGA SI+ G2, a high-resolution sonar imaging system and display. This system allows the operators to map the depth of the bed near piles and other features. A drawback to such a system is the proprietary nature of the software and the difficulty of merging depth data with CAD software. These systems can be integrated into the existing fleet of boats and can reduce the crew member needs of each inspection. During the cost analysis, it is assumed that the supplementary sensor equipment would reduce crew member needs by one person.

7.3.5. Autonomous Data Collection

This section uses cost figures provide by Dr. Rekleitis and his team at the University of South Carolina who demonstrated the autonomous kayak system with onboard sonar equipment. Autonomous kayak deployment rate is specified in three cases in the cost comparison table. These cases are specifying the relative inspection percentage against “SCDOT 3-Person Inspections”. As an example: In “Autonomous Kayak 10%”, cost is evaluated for the case where 90% of scour evaluations are conducted by SCDOT 3-person inspection, and 10% are conducted via autonomous kayak. This highlights the ability to save cost even with slow initial implementation and continue to see savings as autonomous kayak use increases.

7.3.6. Scour Evaluation Cost Benefit Analysis and Conclusions

From the cost analysis conducted in Table 7.2, it is clear that nearly every alternative option is expected to decrease the cost of scour evaluation relative to the chosen baseline. The only case which showed an increase in cost relative to outsourcing the scour evaluations would be to conduct diving operations for every scour evaluation, which would not be necessary in many cases.

Based on the cost benefit, the most significant short-term savings in scour evaluation would be to implement SCDOT conducted scour evaluations while using supplemental sensory equipment.

Table 7.3. Cost for scour evaluation methods

Method	Expected Yearly Cost	Cost/Inspection	Additional Cost	Savings
SCDOT Scour Evaluation	$624,000	$2,400	N/A	17%
Outsourced Scour Evaluation	$748,800	$2,880	Travel	Baseline
Outsourced Diver Evaluation	$780,000	$3,000	Travel	-4%
SCDOT Supplemental Sensor Equip	$417,600	$1,606	N/A	44%
Autonomous Kayak 10%	$571,600	$2,198	N/A	24%
Autonomous Kayak 20%	$509,200	$1,958	N/A	32%
Autonomous Kayak 40%	$384,400	$1,478	N/A	49%

8. Summary and Implementation

8.1. Summary

Condition evaluation of bridges and culverts most commonly relies upon visual and tactile inspections. For the case of bridges inspections are extensive, whereas for culverts only the ends are normally inspected. While visual and tactile inspection procedures have provided satisfactory results in most cases, they are time-consuming, inadequate for the identification of hidden defects, and expensive in terms of human resources. Furthermore, they can be unsafe if adequate traffic control or complete traffic closure is not provided.

To address these limitations, a variety of evaluation techniques were investigated to save money and increase safety for the inspection and assessment of bridges and culverts. This chapter addresses both robotic methods of assessment (such as unmanned aerial systems and robotic crawlers) for bridges and culverts as well as in-situ load testing for bridges.

Robotic Systems for Bridge Inspection

Robotic systems can often extend and improve upon the sensory capabilities of human evaluators. Robotic systems can potentially aid in the visual, and to a lesser degree tactile, inspection of bridge superstructure and substructure elements and also assess scour, or conditions which may lead to scour. Three broad categories of robotic systems for bridge inspection were evaluated – unmanned aerial systems (aerial drones); robotic crawlers; and semi-autonomous jetyaks (engine-propelled kayaks).

Unmanned aerial systems (aerial drones): Extension of and improvement upon sensory capabilities is arguably most obvious for this type of robotic system, with optical capabilities far exceeding those of human inspectors. For example, 30x optical zoom and infrared sensing are widely available at reasonable cost. These capabilities are combined with tremendous ease of access to the underside of bridges and also from above (when inspecting from above, FHWA and FAA guidelines must be considered and observed for safe operation). One challenge for bridge inspection with aerial drones is the current requirement for tactile inspection. Aerial drones are limited in capabilities for tactile inspection, such as tapping of questionable areas with a coin or hammer.

Among the nine evaluated consumer, custom, and industrial grade drones, the Parrot Anafi and the Matrice 210 offer a cost-effective, compact, and high-quality camera option. Importantly, the Parrot Anafi can be stable with and without GPS. The Matrice 210 is widely used in many industries that rely on infrastructure inspection and has a more robust and customizable solution for industrial applications.

Robotic crawlers: These systems offer advantages in terms of contact sensing, thereby approaching the capabilities of tactile inspection. Though most systems have yet to be outfitted in this way, it is not difficult to imagine systems that could utilize impact echo or other ‘touch like’ inspection methods for concrete structural components. The systems investigated here were more aligned with inspection of steel

components and were capable of being outfitted with ultrasonic transducers to address such inspections. With this type of sensor, the remaining thickness of corroded steel girders could potentially be assessed as could the extent of fatigue cracks.

Among the systems investigated, the MRI device from Robotic Technologies of Tennessee seems to be promising for NDE of bridges, however, the tethered nature of the system limits its application. A wireless version of the device could be developed to increase the ease of application in the field.

Marine robotics: Jetyaks and similar systems allow for either semi-autonomous or fully autonomous inspection of bridge substructure elements (above the waterline) and provide reasonable potential for assessing scour or the precursors leading to scour. These systems can also serve as a platform the re-charging of aerial drones which is important for the inspection of longer bridges over larger bodies of water. For jetyaks and similar platforms, it is important to consider the current, with a current over 4 knots likely exceeding the capabilities of most platforms.

Jetyaks provide the capability to look beneath the surface of the water, and for this type of application Sonar systems such as the Kongsberg MS 1171 and the multibeam sonars designed by Teledyne and Kongsberg are recommended for scour monitoring due to their multiple features and supporting software.

Robotic Systems for Culvert Inspection

Culverts are not inspected to the same level of detail as bridges. In most cases only the inlet and outlet are subject to visual inspection regardless of the length of the culvert. However, if more detailed inspection is desired it can be achieved with robotic systems. For detailed inspection of culverts, the Super Droid SCT-32-W Inspection Robot and the Super Droid MLT-42 W Water-tight Compact Inspection Robot are recommended for further consideration. These devices have desirable features such as a 360-degree camera, water-tightness, and supporting software.

Bridge Live Load Testing

Two bridges were selected for live load testing. The first is a reinforced concrete girder bridge, US-221 over Hard Labor Creek Bridge, having National Bridge Inventory (NBI) condition ratings of six for the deck and superstructure, and four for the substructure. The second is a reinforced concrete slab bridge, S-97 over Johnson Creek, having NBI condition ratings of five for the deck and superstructure and four for the substructure. The bridges were instrumented with a variety of sensors including crack opening displacement; vertical displacement; surface mounted strain; and acoustic emission.

Results indicated that the performance of US-221 over Hard Labor Creek was better than expected. The reason may be attributed to boundary conditions that differ from those assumed in a beam line analysis combined with the stiffening effect of the guardrail system. The second bridge, S-97 over Johnson Creek, demonstrated poor joint efficiency and load distribution. This behavior was attributed to joint

deterioration and other factors that have occurred with the passage of time. Acoustic emission monitoring supported this conclusion as emission continued throughout load holds for all instrumented slabs.

Furthermore, acoustic emission data indicated that the bent caps may also warrant further investigation. Live load testing involves positioning of heavy trucks of known weight on the bridge while simultaneously measuring girder surface strains and deflections using strain transducers and wire potentiometers. The deflections and surface strains can be used to evaluate transverse load distribution in the bridge system and ultimately determine load distribution factors. Acoustic emission data is fundamentally different as it is generated by and is extremely sensitive to crack extension, which is closely associated with damage. Owing to this characteristic of acoustic emission, one potentially promising application is evaluation of shear regions and other regions that demonstrate very small strain response during loading. A second benefit is that regular traffic loading (sometimes referred to as ambient loading) can be used to obtain characteristic damage response of a given bridge type, obviating the need for detailed analysis and controlled live load testing. This potential approach assumes that a significant number of bridges of similar type can be instrumented and acoustic emission data recorded over a significant period of time.

8.2. Implementation

The following recommendations for implementation are provided for Robotic Systems for Bridge Inspection; Robotic Systems for Culvert Inspection; and Bridge Live Load Testing.

Robotic Systems for Bridge Inspection

Unmanned aerial systems (aerial drones): The benefit cost analyses related to this category indicated that aerial drones could significantly reduce the annual inspection cost of bridges. This was particularly the case if SCDOT personals were trained to operate the devices, as opposed to outsourcing the inspections. These devices can be employed for bridge components which are difficult to access and can enhance the safety of inspection crews. Ideally, aerial drones for bridge inspection should have an upward-facing high-resolution camera, small size to easily move between girders or other bridge components, a collision avoidance system, propeller guards to get close to bridge components, long battery life, extra payload capacity for attaching more sensors or cameras, and low price. The Matrice 210 and Parrot Anafi have some of the mentioned characteristics and are recommended for widespread implementation.

One of the considerations when using aerial drones is data management and data analysis. Although collecting pictures and movies using drones is very easy, data management and analyzing a large number of pictures and movies can be challenging. Automated algorithms for damage identification, such as convolution neural networks, when used in conjunction with carefully thought out data management can resolve the issues. While experience is being gained with aerial drone inspection, it is recommended that a data management planning be conducted in parallel with the collection of aerial drone-based video and image capture.

Implementation: Aerial drones should be placed into widespread use in parallel with visual inspections as soon as possible. Drone based images should be placed alongside handheld camera

based images in bridge inspection reports. Digital images should be embedded in the inspection reports alongside handheld images. The handheld and drone based images themselves (stored as *.jpeg or other suitable extension) should be collected along with the inspection reports. This will enable progress in data based image analysis.

Robotic crawlers: The tethered nature of the systems investigated limited their widespread implementation.

Implementation: Robotic crawlers should be implemented on a case by case basis, for example where difficult to access areas for ultrasonic inspection are a consideration.

Marine systems: Benefit cost analysis indicated that semi-autonomous and autonomous jetyak systems may provide substantial savings for assessment of scour. However, these systems are not widely commercially available.

Implementation: Systems such as jetyaks with multibeam sonar (or commercially available fish finder platforms) should be implemented on a case by case basis, for example in parallel with scour investigations for bridges with difficult access.

Robotic Systems for Culvert Inspection: Because inspection of culverts is generally limited to both ends of the culvert, it is difficult to imagine a system that could reduce cost of inspections.

Implementation: In the event that more detailed inspection of culverts is desired, the commercially available systems offer potential due to desirable features such as a 360-degree camera, water-tightness, and supporting software. Such systems should be implemented on a case by case basis in the event that detailed inspections of particular culverts are desired.

Bridge Live Load Testing

Widespread live load testing in South Carolina is ongoing and is effective for the estimation of transverse load distribution and the functionality of joints in bridge superstructures. When combined with calibrated numerical analysis (diagnostic load testing) this type of load testing can be effective in assessment of bridge superstructure performance. It can be used as an evaluation method to investigate individual bridges or classes of bridges with the ultimate goal of informing load rating decisions. It is not generally possible to assess failure modes or ultimate capacity through live load testing.

Acoustic emission data differs from data collected through strain gages or other displacement based sensors. Acoustic emission data is caused by crack formation and extension and therefore is a more direct measure of damage progression. Strain and other displacement-based information can be relatively compared to numerical simulations whereas this is not the case for acoustic emission-based data, where the sensors are sensitive to very small out of plane displacements caused by crack formation or extension (on the order of 10^{-12} meters). For these reasons, acoustic emission is well suited to monitoring of shear regions and other regions with small strain, and has the potential to evaluate the performance of bridges under regular traffic loading (ambient loading), thereby reducing the costs and risks associated with live load testing.

Implementation: Live load testing should be continued in South Carolina. Material property data should be collected where practical. In addition to conventional live load testing, selected bridges that are taken out of service be tested to failure to gain an understanding of failure modes and ultimate capacity.

Acoustic emission data should be gathered on a case by case basis. Such cases include assessment of shear regions for girders with unknown reinforcement or questionable shear capacity. This type of data requires specialized equipment and approaches to data analysis.

8.3. Future Research

A technological shift toward 'electrical and automated everything' has occurred, led by self-driving trucks and cars with unmanned urban lift close behind. This shift has been driven by military needs and enabled by very significant investments from venture capital. Evaluation the transportation infrastructure can greatly benefit from these investments.

Challenges ahead are of both a regulatory and technical nature. The regulatory challenges are well founded in the need to maintain safety for motorists from aerial drones and the need to assure that robotic technologies can affordably meet or exceed the capabilities of trained human inspectors.

The technical challenges include the development of 'robot on' technologies to enable 'tactile' inspection approaches such as light tapping of degraded areas. Such systems are in research and development phase at this time. Other challenges will include the capability to rapidly and autonomously differentiating between visual features of interest, such as hairline cracking, and features of marginal or no real interest, such as spiderwebs. Challenges associated with positioning and automatic mapping of brides and bridge components will also need to be resolved, particularly in GPS denied areas such as the underside of bridges.

The preceding discussion relates to inspection, which differs markedly from evaluation. For automated bridge evaluation acoustic emission data provides one potential path forward as this type of data is closely related to damage progression. Future challenges include simulation of acoustic emission data, the gathering of significant data sets for certain families of bridges, and identification of suitable damage assessment algorithms enabled through advances in artificial intelligence.

References

AASHTOnews (2019), Survey Finds State DOTs Hiring Next-Gen Workforce to Run Drone Operations. Retrieved from http:/./aashtonews.wpengine.com/2019/05/20/survey-finds-state-dots-hiring-next-gen-workforce-to-run-drone-operations/

Boone, S. (2019), *BDI Final Report: Project No. 1804009-CO*

Digital Aerolus (2019), Retrieved from https:/./digitalaerolus.com/aertos120/

DJI (2019a), Retrieved from https:/./www.dji.com/mavic/info#specs

DJI (2019b), Retrieved from https:/./www.dji.com/matrice100/info#specs

DJI (2019c), Retrieved from https:/./www.dji.com/matrice-200-series/info#specs

Edgetech (2017a), Retrieved from, https:/./www.edgetech.com/wpcontent/uploads/2017/04/2000_series_brochure-04-25-17.pdf

Edgetech (2017b), Retrieved from https:/./www.edgetech.com/wp-content/uploads/2017/04/2400-4-26-17.pdf

Edgetech (2016), Retrieved from https:/./www.edgetech.com/wp-content/uploads/2016/03/3300-brochure-022916.pdf

FreeFly (2019b) ,Retrieved from https:/./freeflysystems.com/alta-8/specs

FreeFly (2019a), Retrieved from https:/./freeflysystems.com/alta-6/specs

Hummingbird (2020), Retrieved from https:/./humminbird.johnsonoutdoors.com/fish-finders/solix/solix-15-chirp-mega-si-g2

Hummingbird, (2020), Retrieved from https:/./humminbird.johnsonoutdoors.com/fish-finders/solix/solix-15-chirp-mega-si-g2

Infrastructure Preservation Corporation, Thayer, D. (2018), Robotic Bridge Inspections & Infrastructure Inspections to Improve Transportation Infrastructure. Retrieved from https: /./www.infrastructurepc.com/robotic -bridge-inspections-infrastructure- inspections-to-improve-transportation-infrastructure/

Kongsberg (2019b), Retrieved from https:/./www.km.kongsberg.com/ks/web/nokbg0397.nsf/AllWeb/EFEA421E27C221B6C1257599002C4E3C/$file/GeoAcoustics-GeoSwath-Plus-Compact-data-sheet.pdf?OpenElement

Kongsberg (2019c), Retrieved from https:/./www.km.kongsberg.com/ ks/web/nokbg0397.nsf/AllWeb /38E3552DFE3BAE3C1257AF5004118FE/$file/369468_EM2040c_product_specification.pdf?OpenElemet

Kongsberg (2019d), Retrieved from https:/./www.km.kongsberg.com/ks/web/nokbg0240.nsf/AllWeb/ DAEF2D14D18B9603C1257B1F0036EF22?OpenDocument

Kongsberg (2019e), Retrieved from https:/./www.km.kongsberg.com/ks/web/nokbg0240.nsf/AllWeb /5A 7D7B55523C022FC1257B1F003586FC?OpenDocument

Kongsberg(2019a) , Retrieved from https:/./www.km.kongsberg.com/ks/web/nokbg0397.nsf/AllWeb /890 339D0ABD5187EC125805000277707/$file/922-20017901-1-4-M3-Sonar-500m.pdf?OpenElement

Lin, Y. B., Lai, J. S., Chang, K. C., Chang, W. Y., Lee, F. Z., & Tan, Y. C. (2010), Using MEMS sensors in the bridge scour monitoring system. *Journal of the Chinese institute of engineers*, *33*(1), 25-35

Lovelace, B., and Zink, J. (2015), Unmanned aerial vehicle bridge inspection demonstration project. *Research Project. Final Report*, *40 pp.*

Masada, T., Riley, P., and de Haag, M. U. (2017), Evaluation of new or emerging remote inspection technologies for conduits ranging from 12" to 120" spans, (No. FHWA/OH-2017-46)

Melo, M., Pascual, A., Camps, I., Del Campo, Á., & Ata-Ali, J. (2017), Caries diagnosis using light fluorescence devices in comparison with traditional visual and tactile evaluation: A prospective study in 152 patients. *Odontology*, *105*(3), 283-290.

Minnesota DOT (2016), Retrieved from http:/./www.dot.state.mn.us/research/projects/hive/Culvert Vehicle.pdf

Nexxis (2019a), Retrieved from https:/./nexxis.com.au/product/versatrax-vt450/

Nexxis (2019c), Retrieved from http:/./www.nexsens.com/pdf/Guide_Scour_Monitoring.pdf

Nexxis (2019b), Retrieved from https:/./nexxis.com.au/wp-content/uploads/2016/03/InuktunVT450 SpecSheet-4.pdf

Parrot (2019), Retrieved from https:/./www.parrot.com/global/drones/Anafi

Piratla, K. R., Pang, W., Jin, H., & Stoner, M. (2016, November), Best practices for assessing culvert health and determining appropriate rehabilitation methods. Retrieved January 2020, from https:/./ www.scdot.scltap.org/wp-content/uploads/2017/04/SPR-718-Final-Report-Revised.pdf

Ross, B. (2019), Phone conversation with Hummingbird Technical Support Department".

Sahs, S. (2000, June), Climbing techniques for bridge inspection. In Proc., 8th Int. Bridge Management Conf.

Seatronics (2019a), Retrieved from http:/./seatronics-group.com/equipment-sales/geophysical/side-scan-sonars/edgetech-2205-auvrov-sonar

Seatronics (2019b), Retrieved from http:/./seatronics-group.com/equipment-sales/geophysical/sub-bottom-profilers/edgetech-3100-portable-sub-bottom-profiler

Seatronics (2019c), Retrieved from http:/./seatronics-group.com/equipment-sales/geophysical/sub-bottom-profilers/edgetech-3200-high-penetration-sub-bottom-profiler

senseFLY (2018), Retrieved from https:/./www.sensefly.com/app/uploads/2018/05/albris_EN.pdf

SuperDroid Robots (2019a), Retrieved from https:/./www.robotictechtn.com/?page_id=665

SuperDroid Robots (2019a), Retrieved from https:/./www.superdroidrobots.com/shop/item.aspx/sst-tracked-inspection-robot-with-pan-and-tilt-camera/2365/

SuperDroid Robots (2019b), Retrieved from http:/./www.robotictechtn.com/?page_id=64

SuperDroid Robots (2019b), Retrieved from https:/./www.superdroidrobots.com/shop/item.aspx/ptw-42-l-4wd-inspection-and-surveillance-robot-with-scissor-lift-and-ptz-camera/1525/

SuperDroid Robots (2019c), Retrieved from https:/./www.superdroidrobots.com/shop/item.aspx/sct-32-w-adjustable-treaded-waterproof-pipe-and-duct-inspection-robot/2448/

SuperDroid Robots (2019e), Retrieved from https:/./www.superdroidrobots.com/shop/item.aspx/mlt-42-w-watertight-compact-inspection-robot-with-ptz-camera/2231/

SuperDroid Robots (2019d), Retrieved from https:/./www.superdroidrobots.com/shop/item.aspx/mlt-42-compact-inspection-robot-with-ptz-camera/1927/

Teledyne Marine (2019a), Retrieved from http:/./www.teledynemarine.com/Lists/Downloads/SeaBat%20IDH%20T20%2050-R%20Product%20Leaflet.pdf

Teledyne Marine (2019b), Retrieved from http:/./www.teledynemarine.com/SeaBat-IDH-T20-50-R

Teledyne Marine (2019c), Retrieved from http:/./www.teledynemarine.com/blueview-motion-scan/

Teledyne Marine (2019d), Retrieved from http:/./www.teledynemarine.com/blueview-3d-multibeam-scanning-sonar?ProductLineID=5

Teledyne Marine (2019d), Retrieved from http:/./www.teledynemarine.com/BlueViewT2250-360_Tunnel_Profiler

Wells, J., and Lovelace, B. (2017), *Unmanned aircraft system bridge inspection demonstration project phase II final report* (No. MN/RC 2017-18). Minnesota. Dept. of Transportation. Research Services & Library

Youngblood, D. (2017), *Enhanced culvert inspections-best practices guidebook* (No. MN/RC 2017-16). Minnesota. Dept. of Transportation. Research Services & Library (pg. 27)